NASA TECHNICAL NOTE

NASA TN D-7310

NASA TN D-7310

PILOT MODEL EXPANSION TUNNEL TEST FLOW PROPERTIES OBTAINED FROM VELOCITY, PRESSURE, AND PROBE MEASUREMENTS

by Wilfred J. Friesen and John A. Moore

Langley Research Center
Hampton, Va. 23665

NATIONAL AERONAUTICS AND SPACE ADMINISTRATION • WASHINGTON, D. C. • NOVEMBER 1973

1. Report No.	2. Government Accession No.	3. Recipient's Catalog No.
NASA TN D-7310		

4. Title and Subtitle	5. Report Date
PILOT MODEL EXPANSION TUNNEL TEST FLOW PROPERTIES OBTAINED FROM VELOCITY, PRESSURE, AND PROBE MEASUREMENTS	November 1973
	6. Performing Organization Code

7. Author(s)	8. Performing Organization Report No.
Wilfred J. Friesen and John A. Moore	L-8846
	10. Work Unit No.
9. Performing Organization Name and Address	502-27-02-01
NASA Langley Research Center Hampton, Va. 23665	11. Contract or Grant No.
	13. Type of Report and Period Covered
12. Sponsoring Agency Name and Address	Technical Note
National Aeronautics and Space Administration Washington, D.C. 20546	14. Sponsoring Agency Code

15. Supplementary Notes

16. Abstract

Velocity-profile, pitot-pressure, and supplemental probe measurements have been made at the nozzle exit of an expansion tunnel (a modification of the Langley pilot model expansion tube) for a nozzle inlet condition of a nitrogen test sample with a velocity of 4.5 km/sec and a density 5×10^{-3} times the density of nitrogen at standard conditions, both with the nozzle initially immersed in a helium atmosphere and with the nozzle initially evacuated. The purpose of this report is to present the results of these measurements and some of the physical properties of the nitrogen test sample which can be inferred from the measured results. The main conclusions reached are that: the velocity profiles differ for two nozzle conditions; regions of the flow field can be found where the velocity is uniform to within 5 percent and constant for several hundred microseconds; the velocity of the nitrogen test sample is reduced due to passage through the nozzle; and the velocity profiles do not significantly reflect the large variations which occur in the inferred density profiles.

17. Key Words (Suggested by Author(s))	18. Distribution Statement
Velocity profile Pitot probe Expansion tunnel	Unclassified – Unlimited

19. Security Classif. (of this report)	20. Security Classif. (of this page)	21. No. of Pages	22. Price*
Unclassified	Unclassified	106	Domestic, $4.25 Foreign, $6.75

*For sale by the National Technical Information Service, Springfield, Virginia 22151

Page Intentionally Left Blank

CONTENTS

PILOT MODEL EXPANSION TUNNEL TEST FLOW PROPERTIES OBTAINED FROM VELOCITY, PRESSURE, AND PROBE MEASUREMENTS

By Wilfred J. Friesen and John A. Moore
Langley Research Center

SUMMARY

Velocity-profile, pitot-pressure, and supplemental probe measurements have been made at the nozzle exit of an expansion tunnel (a modification of the Langley pilot model expansion tube) for a nozzle inlet condition of a nitrogen test sample with a velocity of 4.5 km/sec and a density 5×10^{-3} times the density of nitrogen at standard conditions, both with the nozzle initially immersed in a helium atmosphere and with the nozzle initially evacuated. The purpose of this report is to present the results of these measurements and some of the physical properties of the nitrogen test sample which can be inferred from the measured results. The main conclusions reached are that: the velocity profiles differ for two nozzle conditions; regions of the flow field can be found where the velocity is uniform to within 5 percent and constant for several hundred microseconds; the velocity of the nitrogen test sample is reduced due to passage through the nozzle; and the velocity profiles do not significantly reflect the large variations which occur in the inferred density profiles.

INTRODUCTION

A theoretical description of the expansion tube and an analysis of the expansion tunnel are given in references 1 and 2, respectively. These reports suggest the possibility of accelerating a small portion of a test gas, by means of shocks and expansions to a large velocity and obtaining a gas flow of short duration, with physical properties (velocity, density, and temperature) in a range comparable with the properties expected in planetary entry. Reference 2 compared the advantages and disadvantages of expansion tunnel operation with those of expansion tube operation. A description of an experimental study made in the Langley pilot model expansion tube is given in reference 3. One of the results of this study indicated that test flow times of the order of 100 μsec to 400 μsec could be obtained in this expansion tube.

The pilot model expansion tunnel at the Langley Research Center is a modification of the Langley pilot model expansion tube in which a 10° half-angle, conical scoop-type nozzle was added to the expansion tube to expand the expansion tube test flow. The expansion tunnel test flow is derived from the short test flow slug of the expansion tube. The test slug moves supersonically with respect to the nozzle entrance, and its length is comparable with the nozzle length. Some of the more apparent operational advantages to be gained from expanding the flow include an increase in flow-field diameter, a reduction in the impulse load on models due to the arrival of the dense driver gas, and the possible avoidance of model damage due to particles in the expansion tube flow by locating the model off the tunnel axis.

The purpose of this report is to present the results of some velocity-profile, pitot-pressure, and supplemental probe measurements which were made in the test flow at the nozzle exit of the pilot model expansion tunnel. From these measured results, some of the physical properties of the test gas slug are inferred.

For a hypersonic test facility, the uniformity of the free-stream flow velocity and the density is important in any experiment. In hypersonic flow, the pitot-pressure (stagnation pressure) probe responds primarily to the product of the density and the square of the free-stream flow velocity. If a uniform profile of pitot pressure is not observed in a test flow field, then the profiles of one or both of these flow properties are not uniform. A theoretical analysis of steady supersonic flow in conical nozzles with supersonic inlet flow (ref. 4) indicates that the flow in the conical nozzle may be complicated by an embedded shock structure.

Previous investigations in the pilot model expansion tunnel have considered a number of geometric configurations of the facility and several initial conditions for the tunnel nozzle. An electrically operated diaphragm (ref. 5) was also under development during these investigations. The investigations were mainly survey in nature and, similar to the approach followed in reference 3, were concerned with examining the shocks, interfaces, expansion waves, and test time within the theoretical framework of references 1 and 2. During these exploratory investigations, the observed pressure histories were often different for probes located on or off the tunnel axis.

The work presented in this report is limited in scope and represents only a small portion of the main general experimental program. The results presented are limited to one operating condition of the expansion tube portion of the facility and to two initial conditions for the tunnel nozzle. For one initial condition, the nozzle was isolated from the acceleration chamber with an electrically operated diaphragm (ref. 5) and the nozzle region was evacuated. For the other initial condition, no isolating diaphragm was used; therefore, the nozzle was immersed in the helium acceleration gas.

The velocity measuring technique was adapted from the photoionization technique employed for the velocity-profile measurements made in the expansion tube and reported in reference 6. In order to approximately locate the velocity measurements within the nitrogen test flow, the location of the helium-nitrogen interface was inferred from comparisons of various probe signal histories obtained from some additional tunnel runs.

The measurements presented herein represent the first measurements of velocity profile for the pilot model expansion tunnel. The manner in which the velocity profile develops from the start of flow was observed for the no-nozzle-diaphragm operating condition.

The measured results obtained at the nozzle entrance and exit are presented in tables I, II, and III for the convenience of the interested reader.

No other expansion tunnel studies are known to the authors with which the present measurements can be compared.

SYMBOLS

A,B,c,k,γ,σ	constants used in equations of appendix C
a	velocity of sound
a_o	velocity of sound in a gas at standard conditions
B.P.	band pass
D	optical density
E	exposure
M	Mach number
m	molecular mass
n	number of observations (expansion tunnel runs)
p_t	pitot pressure
p_w	flat-plate pressure, or tube wall pressure

R	nozzle exit radius
R'	universal gas constant
S	standard deviation from the mean
$\overline{S}$	estimated variance of the mean
T	temperature
T_o	standard temperature, 273 K
Δt_1	time after helium flow arrival at nozzle exit
Δt_2	time between ionization and detection
u	velocity (axial component)
u_c	velocity at nozzle exit on tunnel center line
u_i	velocity of interface in expansion tube
u_l	limiting velocity for expansion tube
u_m	measured velocity at nozzle exit
x	distance parallel to tunnel center line
y	distance above tunnel center line
θ	flow direction with respect to tunnel center line
ρ	density
ρ_o	density of nitrogen at standard conditions, 1.25 kg/m^3

Subscript:

i condition at nozzle entrance

A bar over a symbol indicates the arithmetic mean.

DESCRIPTION OF APPARATUS

A schematic drawing of the pilot model expansion tunnel is shown in figure 1(a). The flow facility consisted of the Langley pilot model expansion tube (ref. 3) which provided the entrance test flow to a conical scoop-type nozzle. The nozzle flow exited as a free jet into a large dump tank. The expansion tube flow external to the nozzle entrance area was diverted into a separate dump tank. The nozzle consisted of a 10° half-angle truncated cone with an entrance diameter of 5.08 cm and an exit diameter of 35.6 cm. The leading edge of the cone was sharpened to an approximate radius of 0.003 cm. An electrically operated diaphragm (ref. 3) was located 1.51 m upstream of the nozzle entrance.

During the measurements, the shock velocity in the intermediate chamber was routinely monitored. The microwave technique described in reference 3 was used to measure the helium-nitrogen interface velocity upstream of the nozzle entrance. The short stub antenna (indicated in fig. 1(a)) protruded radially into the flow at the expansion tube exit, outside the entrance area of the nozzle. Good microwave tracking of the helium-nitrogen interface in the acceleration chamber was not obtained routinely since the antenna was in an unfavorable location in order to avoid disturbance of the flow at the nozzle entrance. For the evacuated nozzle, a pressure gage in the tube wall just upstream of the electrically opened diaphragm was monitored. If the helium shock arrived prior to the opening of the diaphragm, a reflected shock was sensed by this gage.

Shown in figure 1(b) are the relative locations of the end of the expansion tube wall and the entrance to the nozzle. Also shown in the figure are the approximate locations of two pitot-pressure probes that were used to examine flow properties at the nozzle inlet but were removed for the velocity measurements. The extension to the expansion tube wall, indicated by the dashed lines, was added during the measurements to insure isolation of the flow entering the nozzle from any effects of the annular outer flow. No significant differences in the nozzle exit flow were noted as a result of the tube wall extension.

The velocity measuring technique was the same as that described in reference 6. The components of the apparatus were adapted to be compatible with the tunnel operation. The velocity-profile measurements surveyed 0.8 of the nozzle exit radius. A tunnel run was required for each measurement of a velocity profile.

The positions of the electrodes and a reference marker relative to the exit of the nozzle are shown in figure 2. The photoionization source and detector electrode were located inside the dump tank. Sharp leading edges were used for all parts exposed to the flow. The detector electrode consisted of a nylon insulator with a thin metal strip which was exposed to the flow. A rectangular splitter plate was attached to the upper part of the source holder to reduce the effect of the bow shock in the region between electrodes. A thin-film heat-transfer gage was mounted in the upper surface of the splitter plate. The arrival of flow at the exit of the nozzle was sensed by this gage. The signal from the heat-transfer gage, after a preselected delay, initiated the sequence of photoionization and detection of a column in the flowing gas.

The source and detector were located in a plane which included the axis of the nozzle. The distance between the source and detector electrode was about 23 cm. The exit hole of the source collimator was located about 7.9 cm below the nozzle axis and about 5.5 cm downstream of the exit plane of the nozzle.

A reference position marker (fig. 2), which could be remotely moved to a fixed position just downstream of the source and detector electrode, was located within the tunnel enclosure. The reference marker was pivoted out of the region for the run.

The detected displaced ionized column was photographed on film through a window (shown in fig. 1(a)) in the dump tank wall. An open shutter camera was used with an aperture of f/2 at a magnification of 0.23. A photomultiplier, which viewed the region of the nozzle exit through the dump tank window, was used to determine the time interval between ionization and detection.

Pitot-pressure measurements were made at the nozzle entrance and exit. Piezoelectric transducers were used in the pressure probes. For the single pitot-pressure probes, the transducers were encased in baffled housings. For a four-probe pitot-pressure rake and in a flat-plate probe, the transducers were coated with a thin heat-resistant coating and operated without a shield.

The single-probe data were taken from a separate tunnel run for each pitot-pressure measurement. The measurements of the pitot-pressure probe located off the center line at the nozzle entrance (fig. 1(b)) were recorded in conjunction with some of the single-probe pitot-pressure measurements.

The four-probe pitot-pressure rake was located at the nozzle exit in a plane containing the nozzle axis. Two tunnel runs were made with the evacuated nozzle. Between the two runs, the rake was rotated 180° in order to confirm the response of the individual gages.

Several types of probes were used at the nozzle exit to obtain information supplemental to the velocity-profile and pitot-pressure measurements. The types of probes

used were a flat-plate pressure probe, a photomultiplier which viewed the flow stagnation region of a pitot-pressure probe, a rake consisting of six 0.317-cm-diameter plastic rods, and a flow stagnation ion probe. The ion probe was located below the splitter plate. (See fig. 2.) For the flat-plate pressure probe, the transducer was mounted flush with the surface on the center line and 8.9 cm back of the leading edge of the plate. The plate was 12.7 cm wide and had a sharp leading edge. The plane of the flat plate was inclined to the axis of the tunnel so that the plane included the apex of the nozzle cone. With regard to the direction of the flow at the nozzle exit, measurements of flow direction indicated that the plane of the plate was inclined about 1^{o} leeward to the direction of the flow.

The photomultiplier, using a 931-A tube, was outside the dump tank window and the field of view was limited to the stagnation region of the pitot-pressure probe. For some runs, a 3920 ± 20 Å band-pass filter was inserted in the optical path to limit the response of the photomultiplier to a spectral region where light emitted from excited N_2^+ ions could be observed.

Data for estimating the flow direction and Mach number as a function of radial position were obtained by inserting a rake of plastic rods, displaced slightly from the plane containing the nozzle axis, into the flow field. The bow shock envelopes about the plastic rods were made visible when an electrical discharge was produced in the flow field. Sample data films are shown in figure 3.

TUNNEL OPERATING CONDITIONS

One initial operating condition of the expansion tube portion of the facility was used in obtaining the data presented in this report. The driver chamber was pressurized with room temperature hydrogen to a self-burst pressure of about 9.7 MN/m^2. The intermediate chamber was filled with nitrogen to a pressure of 6.66 kN/m^2. The acceleration chamber was filled with helium to a pressure of 133 N/m^2.

The difference between the two initial conditions of the nozzle was as follows: For the no-nozzle-diaphragm case, the helium acceleration gas filled the entire nozzle region and dump tanks. For the evacuated-nozzle case, a diaphragm was installed upstream of the nozzle entrance, and the entire region of the nozzle and dump tanks was evacuated to a pressure of less than 0.1 N/m^2. A signal derived from the shock arrival in the intermediate chamber was used, after an appropriate delay, to trigger the operation of the electrically opened diaphragm just prior to the arrival of the helium shock at the diaphragm.

DEFINITIONS

In this section a statement is made of some terms and assumptions which are used in presenting the results. The measurement uncertainties and the manner in which the arrival of the flow boundaries were estimated are discussed in appendixes A, B, and C.

A distance-time diagram of the expansion tunnel operating cycle is given in figure 4(a). It is essentially the same as the expansion tube cycle given in reference 3 except for the addition of a third diaphragm and a nozzle expansion. More detailed diagrams are shown in figure 4(b) for the tunnel without the third diaphragm and in figure 4(c) for the tunnel with the evacuated nozzle.

The helium shock, the residual-gas—helium interface, the helium-nitrogen interface, and the expansion fan, which are indicated in figures 4(b) and 4(c), were assumed to exist.

The arrival of helium flow at either the nozzle entrance or nozzle exit is designated flow arrival. Flow arrival corresponds to the arrival of the helium shock for the no-nozzle-diaphragm initial condition and to the arrival of the residual-gas—helium interface for the evacuated-nozzle initial condition. For the evacuated nozzle, the very-low-density residual-gas flow was not considered to be detectable by the gages that were used to indicate flow arrival.

The nitrogen test time (as used in this report) is defined as the time interval between the arrival of the helium-nitrogen interface and the arrival of the expansion fan. (See figs. 4(b) and 4(c).)

At the nozzle exit, the quantities referred to as measured are velocity, pressure, time interval, flow direction, and a lower bound of Mach number. At the nozzle entrance, the quantities referred to as measured are velocity, pressure, and time interval.

The word "velocity" in this report refers to the component of velocity parallel to the tunnel axis.

The quantities referred to as derived quantities were derived from the measured quantities presented in this report.

The gas density ρ normalized by the density of nitrogen at standard conditions, $\rho_o = 1.25\ kg/m^3$, was derived from the following relation:

$$\frac{\rho}{\rho_o} = \frac{p_t}{\rho_o u^2}$$

The gas temperature T was derived by using the following relations:

$$T = \frac{T_o u^2}{a_o M^2}$$

$$T = \frac{p_w u^2 M}{p_t R'}$$

$$T = \overline{T}_i \left(\frac{\rho}{\overline{\rho}_i} \right)^{0.4}$$

The standard deviation from the mean S is the uncertainty presented with the mean value of a quantity, unless a statement is made to the contrary. Where an estimate of the variance of the mean $\overline{S}$ is presented, the estimate was obtained from the relation $\overline{S} = S/\sqrt{n}$, where n is the number of observations. No uncertainty is presented for a quantity which is based on a single tunnel run with the exception of flow direction for the no-nozzle-diaphragm case.

The uncertainties which are presented with the derived quantities were obtained by propagation of the uncertainties presented for the measured quantities.

RESULTS AND DISCUSSION

Nozzle Entrance

Flow velocity.- The nitrogen test flow velocities in the acceleration chamber for the no-nozzle-diaphragm and evacuated-nozzle cases were assumed to be the same as the velocity of the helium-nitrogen interface. The average velocity obtained for 14 runs was 4.48 ± 0.22 km/sec. It was assumed that the velocity profile was uniform over the diameter of the nozzle entrance on the basis of a gross extrapolation of the trend of uniform velocity core diameter with increase in initial helium pressure, as indicated in reference 6.

Pitot pressure.- Shown in figure 5 are pitot pressures obtained at the nozzle entrance. The results indicate that the pitot pressure differs by as much as a factor of 2 between the center and the edge of the nozzle during the passage of the test flow. If the velocity profile is assumed to be uniform, the test flow density is a factor of 2 larger at the center than at the edge of the nozzle entrance. For the probe located off the center

line, the large decrease in pressure following the test flow is possibly due to the growth of the tube wall boundary layer.

Test flow duration.- The test flow time is the time interval between the arrival of the helium-nitrogen interface and the arrival of the expansion fan. The test flow duration is estimated to be of the order of 200 μsec. The accuracy of this value is limited by the difficulty of estimating the arrival of the expansion fan, as can be seen in figure 5.

Wall pressure.- The tube wall pressure was assumed to be the same as the free-stream static pressure. A wall pressure of 4.5 kN/m^2 was measured 1.6 m upstream of the nozzle entrance. The wall pressure was nearly constant during the passage of the helium and test portion of the flow.

Derived quantities.- The nitrogen test flow density, temperature, entrance Mach number, and test slug length were derived from the relationships between the measured quantities for the nozzle entrance.

Due to the differences observed on and off the tube center line, the pitot pressure and the quantities derived from it are presented as a range of values estimated by averaging the quantity over the test flow time interval at each of the two probe positions. Within this range of conditions, the properties of the test flow interval are considered to be the same for the two nozzle conditions. A quantity designated by the word "average" represents the weighted average of that quantity over the test slug volume which is defined by the nozzle entrance diameter and the test slug length. Estimates of the nozzle inlet flow conditions are as follows:

Flow velocity, u_i	4.5 ± 0.2 km/sec
Pitot pressure, $p_{t,i}$	100 to 200 kN/m^2
Average pitot pressure, $\bar{p}_{t,i}$	133 kN/m^2
Test flow duration	200 μsec
Tube wall pressure, $p_{w,i}$	4.5 ± 1 kN/m^2
Normalized density, ρ_i/ρ_o	3.95×10^{-3} to 7.9×10^{-3}
Normalized average density, $\bar{\rho}_i/\rho_o$	5.27×10^{-3}
Temperature, T_i	3000 K to 1500 K
Average temperature, $\overline{T}_i$	2250 K
Mach number, M_i	4.1 to 5.8
Test slug length	0.9 m

Nozzle Exit – No Nozzle Diaphragm

Center-line velocity.- The velocity on the tunnel center line as a function of time after the arrival of flow is shown in figure 6. A maximum in the velocity occurs about 400 μsec after flow arrival. During the first 100 μsec, the velocity increases from

70 percent to 95 percent of the maximum velocity. From Δt_1 = 400 μsec to 1350 μsec, there is a gradual decrease in velocity to about 83 percent of the maximum velocity.

The velocities measured at the nozzle exit are lower than the interface velocity at the nozzle entrance. The ratio of the exit velocity to the interface velocity at the nozzle entrance ranges from 0.66 ± 0.05 to 0.93 ± 0.07.

The rather low value of the flow velocity (2.95 km/sec) observed approximately 5 μsec after flow arrival might be expected as a result of the strong attenuation of the helium shock as it traverses the nozzle. The center-line helium shock velocity is reduced from a value of 4.7 km/sec at the nozzle entrance to about 2.3 km/sec at the nozzle exit. Shown in figure 7 are the arrival times of the helium shock at positions on the nozzle axis downstream of the nozzle entrance. The traverse of the helium shock through the nozzle was obtained from seven tunnel runs. A single pitot-pressure probe was located at a different position along the tunnel axis for each tunnel run.

Since the presence of nitrogen in the flow field was not directly identified, it was not possible to determine how soon after flow arrival that the helium-nitrogen interface arrived at the nozzle exit.

The rapid increase in flow velocity following flow arrival at the exit, shown in figure 6, indicates that the velocity of the helium shock on the center line is reduced more than the velocity of the helium-nitrogen interface due to passage through the nozzle. On the basis of this reasoning, the helium-nitrogen interface might be expected to arrive, at the nozzle exit on the center line, during the first 50 μsec after flow arrival.

Velocity profile.- The velocity as a function of radial position is shown in figure 8 for nine values of Δt_1. The flow starts as a central velocity core which increases in diameter from about 0.2 to 0.7 of the nozzle exit diameter during the first 400 μsec; this is followed by a decay of the central core pattern and a decrease in velocity.

In figure 9, velocity profiles (flow velocity normalized by the velocity at the center line) are presented for the nine values of Δt_1 in figure 8. Velocities within the central velocity core lie within 5 percent of the center-line velocity for the measurements between Δt_1 = 100 μsec and 250 μsec. The most uniform velocity profile was observed 150 μsec after flow arrival. Shearing or other discontinuities may be present in the velocity core, as indicated by large apparent steps in velocity.

Flow direction.- In figure 10, the effect of radial position on the flow direction is shown for Δt_1 = 100 μsec. The results are compared with the flow direction expected for an isotropic point source at the nozzle apex. Compared with a point source flow, the results indicate a slightly less divergent flow for radial positions between the center line and $y/R = 0.5$ and a slightly more divergent flow between $y/R = 0.5$ and $y/R = 0.8$ but, within the uncertainties of the measurements, only the result obtained between the

center line and $y/R = 0.2$ can be significantly distinguished from a point source flow. The results were obtained from a single tunnel run and the estimated uncertainties are the standard deviations from the mean of four data interpretations of the flow direction at each radial position.

Pitot pressure.- The pitot pressures at five radial positions are shown in figure 11. Common to each radial position is the appearance of a large pressure pulse. The arrival of the pressure pulse occurs at progressively later times after flow arrival with an increase in y/R. The pulse arrives about 250 μsec after flow arrival at $y/R = 0.69$. The pulse duration increases from about 30 μsec at $y/R = 0$ to about 200 μsec at $y/R = 0.69$. A decrease in the pulse amplitude and an increase in pressure level following the pulse are also observed with an increase in y/R.

Density.- In figure 12 is shown the radial distribution of density at various times after flow arrival. In the range from $\Delta t_1 = 50$ μsec to 400 μsec, the density profiles show a peak in density which starts on the center line and proceeds radially outward as time progresses. This behavior can be described by a dense shell of gas of somewhat conical shape, possibly caused by a nonstationary shock system, moving down the tunnel axis. A thickness of the order of 10 cm can be estimated for the shell near the tunnel axis, from the pitot-pressure pulse duration and the velocity. After passage of the dense shell, the flow density drops to a value which is as much as an order of magnitude lower than that of the shell. At $\Delta t_1 = 950$ μsec the density has increased, especially along the center line. At $\Delta t_1 = 1350$ μsec the center-line pressure became too oscillatory to estimate a pressure value from which to derive the density.

Indicated in figure 12 is a value of the center-line density, $\rho/\rho_0 = 0.5 \times 10^{-4}$, which was estimated by using the method of reference 4, an entrance Mach number of 5, and the average density of the nitrogen test slug at the nozzle entrance. This estimated density compares reasonably well with the observed center-line densities in the range from $\Delta t_1 = 100$ μsec to 400 μsec after flow arrival.

Comparison of results at 100 μsec after flow arrival.- In figure 13(a), the profiles of the velocity, pitot pressure, and Mach number (lower bound) are presented. In figure 13(b), the profiles of the density and temperature, derived from the results of figure 13(a), are presented. The results show that from the center line to $y/R = 0.55$ the velocity is essentially constant as compared with the variations occurring in pitot pressure, Mach number, density, and temperature.

The measured quantities from which the temperatures were derived are indicated within parentheses in figure 13(b). It was assumed that the gas at the nozzle exit was nitrogen. The temperatures derived from the Mach number are upper bounds, and it is possible to infer only that within the velocity core there are temperatures less than 30 percent of the temperature of the nitrogen test flow at the nozzle entrance. Tempera-

tures at two positions in the flow were also estimated by assuming an adiabatic expansion from the average density and average temperature of the test slug at the nozzle entrance to the density observed in the flow field. The uncertainties shown for these temperatures reflect only the uncertainties in the observed densities at the nozzle exit. The inferred temperature obtained by the two methods indicate an increase in temperature for the larger values of y/R.

Nozzle Exit – Evacuated Nozzle

Center-line velocity.- The velocity on the tunnel center line as a function of time after flow arrival is shown in figure 14. The velocity-profile measurements indicate a probable decrease in velocity between $\Delta t_1 = 250$ μsec and 350 μsec. The helium-nitrogen interface is assumed to arrive within this time interval. A nearly constant velocity (±4 percent) is indicated for the time interval between $\Delta t_1 = 350$ μsec and 800 μsec, which includes the nitrogen test flow.

The nitrogen flow velocities measured at the nozzle exit are lower than the helium-nitrogen interface velocity at the nozzle entrance. The ratio of the nitrogen flow velocity to the interface velocity at the nozzle entrance lies in the range from 0.91 ± 0.05 to 0.82 ± 0.05.

Indicated in figure 14 are the estimated arrivals of the helium-nitrogen interface and the expansion fan. These estimates were inferred from comparisons of several types of probe signals which were observed during several supplemental tunnel runs. These comparisons are discussed in appendix A.

Attempts to obtain velocity-profile data in the helium flow for times earlier than $\Delta t_1 = 250$ μsec were unsuccessful. The cause is thought to be primarily related to a low production of ions in the photoionized column due to the combined effects of a high ionization potential and a low density in the helium flow.

The trend of the helium exit velocity can be inferred from the average nozzle transit velocities (fig. 14) of the residual-gas—helium interface and helium-nitrogen interface. The nozzle transit times of these interfaces traveling from the nozzle entrance to exit were obtained by correlating the pitot pressures recorded by the probe located off the center line at the nozzle entrance (fig. 1(b)) and a probe located on the center line at the nozzle exit. On the basis of the assumption of constant acceleration of the flow through the nozzle, the exit velocities of the residual-gas—helium interface and the helium-nitrogen interface were estimated from the average transit velocities and are also shown in figure 14. The estimated exit velocity of the residual-gas—helium interface is 8.7 ± 1.1 km/sec which is about a factor of 2 larger than the helium shock velocity in the expansion tube. The exit velocity of the helium-nitrogen interface estimated from average transit velocity is 4.0 ± 0.4 km/sec, which agrees within the uncertainties of the

measurements with the velocity of 4.06 ± 0.23 km/sec measured 250 μsec after flow arrival.

Velocity profile.- The velocity as a function of radial position is shown in figure 15(a) for five values of Δt_1. The velocities presented are average velocities of repeat runs except those for $\Delta t_1 = 800$ μsec. The general trend of the velocity with increasing time over most of the radial interval is a decrease in velocity between 250 μsec and 350 μsec after flow arrival with a nearly constant velocity for the interval between $\Delta t_1 = 350$ μsec and 800 μsec.

Figure 15(b) shows the average velocities for repeated tunnel runs normalized by the average center-line velocities. The velocities appear to be the least reproducible for the two runs at $\Delta t_1 = 250$ μsec. In general, the velocities are reproducible to within ±5 percent of the average velocity for a given radial position. For $\Delta t_1 = 450$ μsec, the velocities are significantly more reproducible in the region from about 0.3 to 0.8 of the nozzle exit radius than in the central portion of the flow.

Figure 15(c) shows the estimated variance of the mean for the profiles shown in figure 15(b). For $\Delta t_1 = 350$ μsec, 450 μsec, and 550 μsec, the results indicate that, near the center line, the average velocity is from 2 to 8 percent lower than the maximum observed at larger values of y/R.

Figure 15(d) shows the average velocity and the normalized average velocity of the 14 velocity profiles obtained between 350 μsec and 550 μsec after flow arrival. A standard deviation from the mean velocity of about ±120 m/sec characterizes the reproducibility of the tunnel operation in this time interval. The estimated variance of the mean velocity is shown with the normalized average velocity profile in figure 15(d). The average velocity on the tunnel center line is 5 ± 1 percent lower than the maximum average velocity in the average velocity profile.

Figure 15(e) shows velocity profiles obtained 350 μsec after flow arrival for a nozzle diaphragm opened by the flow and a nozzle diaphragm electrically opened. The significant differences in velocity occur at the larger values of y/R for these two conditions.

In figure 16, individual velocity profiles normalized by the center-line velocity are presented for values of Δt_1 from 250 μsec to 800 μsec. Indicated in the figure are those profiles for which the nozzle diaphragm was only partially open upon the arrival of the helium flow at the diaphragm. The steps in velocity seen in many of the profiles imply that discontinuities or shocks are embedded within the flow field. The variations in velocity observed for any individual profile can be included within a range of 10 percent. With the exception of one profile at $\Delta t_1 = 250$ μsec, the variations in velocity are within ±5 percent of the average velocity in the radial interval from the center line to $y/R = 0.8$.

Flow direction.- In figure 17, the effect of radial position on the flow direction of the evacuated nozzle is shown for a time 550 μsec after flow arrival. The flow is less divergent than expected for an isotropic point source flow at the nozzle apex.

Pitot pressure.- In figure 18(a), the pitot pressures at four radial positions of the bare-gage pressure rake are shown. Common to all radial positions is a very low pressure level during the first 200 to 250 μsec of flow. For times after flow arrival greater than 200 μsec, the pressure increases with an increase in radial position. As a point of interest, compare the pressure trace for the evacuated-nozzle case at $y/R = 0.75$ in figure 18(a) with that for the no-nozzle-diaphragm case at $y/R = 0.69$ in figure 11 and note the similarity in the shapes of the traces. Also note the absence of any large pressure pulses for the evacuated-nozzle case at the two positions nearest the center line. The pressure rises observed by the four probes about 200 to 250 μsec after flow arrival suggest that the helium-nitrogen interface emerges as a nearly plane surface for the evacuated-nozzle case, as compared with a highly curved surface indicated by the time of arrival of the large pressure rises for the no-nozzle-diaphragm case (fig. 11). This assumes that these pressure rises for both nozzle cases correspond to the arrival of the helium-nitrogen interface. (See appendix A for further discussion.)

In figure 18(b), the results obtained with single pitot-pressure probes are shown for $y/R = 0$ and $y/R = 0.214$. For $\Delta t_1 > 400$ μsec, the pressures are larger than the pressures observed with the bare-gage rake at $y/R = 0$ and $y/R = 0.25$ (fig. 18(a)).

For the two tunnel runs for which the bare-gage rake was used, a sudden shift to a lower indicated pressure level was observed, about 580 μsec after flow arrival, for the pressure gage located on the tunnel center line. The direction of the shifts in indicated pressure level would be expected for these gage elements if they were heated significantly due to a particle impact. The center-line probe was the only probe in the four-probe rake for which a visible sign of particle impact was apparent from an inspection of the rake after the tunnel run. For the three bare-gage probes located outside the projected nozzle entrance area (fig. 18(a)) and the center-line single probe, for which the gage element was protected from particle impacts (fig. 18(b)), no sudden shift of signal level corresponding to that obtained for the bare center-line gage was observed. These were the only data available from which to estimate the earliest arrival of particles in the flow cycle and at least qualitatively assess their possible effect on the pitot-pressure measurements.

Density.- In figure 19(a), the radial distribution of the density derived from the rake pitot-pressure data is presented for various times after flow arrival. The results indicate, that along the tunnel center line, the density remains at a low value throughout the range of Δt_1 observed. The densities off the tunnel center line range from 2 to 10 times larger than those along the center line. This difference in density indicates that the major

portion of the mass flow is located within a ring or cylindrical shell, since the velocity is nearly constant with radial position.

In figure 19(b), the radial distribution of the density derived from the single-probe pitot-pressure data is presented for the same values of Δt_1 as in figure 18(a). After $\Delta t_1 = 350$ μsec, the densities are considerably larger than those in figure 19(a), but the trends of the density with radial position are the same.

Indicated also in figure 19 is the center-line density, $\rho/\rho_0 = 0.5 \times 10^{-4}$, estimated by using the method of reference 4. This value lies within the range of the observed center-line densities. A value of ρ/ρ_0 of 1.1×10^{-4} is obtained by dividing the average density of the nitrogen test slug at the nozzle entrance by the area ratio of the nozzle; this value is the density at the nozzle exit that would be expected for a uniform steady expansion of the test slug with no change in axial velocity. These two estimated densities bracket the observed densities on the tunnel center line for $\Delta t_1 = 350$ μsec, 450 μsec, and 550 μsec shown in figure 19(a) and $\Delta t_1 = 350$ μsec and 450 μsec shown in figure 19(b).

For steady nozzle flow and an entrance Mach number of 5, reference 4 predicts that a standing oblique shock system would intersect the exit plane of the nozzle in the vicinity of $y/R = 0.4$. For hypersonic flow, an oblique shock wave provides a mechanism for obtaining a relatively large change in density for a correspondingly small change in axial velocity as compared with a normal shock wave for which significant changes in both density and velocity occur. Direct evidence of an oblique shock system in the flow field was not obtained during this investigation, but the velocity profiles shown in figure 15 and the density profiles shown in figure 19(a) are consistent with the existence of a standing oblique shock wave system which intersects the exit plane of the nozzle between $y/R = 0.25$ and $y/R = 0.5$.

Comparison of results at 550 μsec after flow arrival.- In figure 20(a), the profiles of the velocity, pitot pressure, and Mach number are presented. In figure 20(b), the profiles of the density and temperature, derived from the results shown in figure 20(a), are presented. The results show that in the range from the center line to $y/R = 0.8$ the velocity is essentially constant as compared with the variations occurring in pitot pressure, Mach number, density, and temperature.

The measured quantities from which the temperatures were derived are indicated within parentheses in figure 20(b). The gas at the nozzle exit was assumed to be nitrogen. The temperatures derived from the Mach number and flat-plate pressure are upper bounds and agree within the uncertainties of the measurements. It can be inferred that near the center line the temperatures are less than 30 percent of the temperature of the nitrogen test flow at the nozzle entrance. Temperatures estimated for an assumed adiabatic expansion from the average density and average temperature of the test slug at the nozzle

entrance to the density observed in the flow field are also shown. The uncertainties shown for these temperatures reflect only the uncertainties in the observed densities at the nozzle exit. The temperatures estimated from the Mach number and the adiabatic expansion indicate the same trend with radial position. The inferred temperatures in the denser gas shell are about a factor of 2 larger than those for positions near the tunnel center line.

Test Flows for No Nozzle Diaphragm and Evacuated Nozzle

In figure 21 are presented the velocity and density profiles for the no-nozzle-diaphragm and evacuated-nozzle cases. For each nozzle case, the profiles sample a 200-μsec flow interval which approximately corresponds to the passage of the assumed nitrogen test flow at the nozzle exit. The velocities are normalized by the helium-nitrogen interface velocity at the nozzle entrance and the densities are normalized by the average density of the nitrogen test slug at the nozzle entrance divided by the area ratio of the nozzle. It can be seen that the evacuated-nozzle case provides a much more uniform velocity and density flow field during the passage of the nitrogen test flow slug as compared with the no-nozzle-diaphragm case. For the no-nozzle-diaphragm case, a central region is observed where the velocity is reasonably constant with radial position and time, but a large excursion in density is indicated at any position in the flow field during the passage of the nitrogen test flow slug.

SUMMARY OF RESULTS

Velocity-profile measurements of the axial component of the free-stream velocity and some pitot-pressure and supplemental probe measurements have been made at the exit of the 10° half-angle, conical scoop-type nozzle of the pilot model expansion tunnel, a modification of the Langley pilot model expansion tube. The velocity-profile measurements surveyed 0.8 of the nozzle exit radius. An initial nozzle condition in which the nozzle was immersed in the helium acceleration gas of the expansion tube portion of the facility and an initial nozzle condition in which the nozzle region was evacuated were examined for one nozzle inlet test sample condition.

The incident nitrogen test slug, which was provided by the expansion tube portion of the facility, had the following approximate properties near the nozzle entrance: a helium-nitrogen interface velocity of 4.5 km/sec and a geometric shape consisting of a 5.08-cm-diameter cylinder (defined by the nozzle entrance) with a length of 0.9 m. The inferred radial distribution of mass and temperature in the test slug depends on the velocity profile that is assumed, but the physical properties of the test slug can be approximately bounded, as follows: If the velocity profile is uniform, then the properties on the axis and at the circumference of the test slug, respectively, are densities of 8×10^{-3} and

4×10^{-3} times the density of nitrogen at standard conditions and temperatures of 1500 K and 3000 K. If the velocity profile is not uniform but the velocity decreases radially to about 70 percent of its axial value, then the physical properties of the test slug are uniform with a density of 8×10^{-3} times the density of nitrogen at standard conditions and a temperature of 1500 K.

Concerning the properties of the nitrogen test slug that emerges at the nozzle exit, the following general results were obtained:

1. The flow velocity was smaller than the helium-nitrogen interface velocity at the nozzle entrance.

2. The velocity profiles were an order of magnitude more uniform than the corresponding density profiles.

The following results were obtained for the no-nozzle-diaphragm case:

3. During the first 400 μsec after flow arrival, a higher density pulse was observed at the tunnel exit. This pulse, possibly incorporating a moving embedded shock system, may be characterized as a dense, conically shaped shell moving past the test location. The density in the shell was about a factor of 10 larger than those for positions interior to the cone near the tunnel center line. The shell has a thickness of about 10 cm near the tunnel center line upon emergence from the nozzle.

4. Velocity profiles for the nitrogen test slug were uniform to within 5 percent from the center line to a radial position y/R of 0.5 in the time interval between 100 μsec and 250 μsec after flow arrival.

5. The center-line velocity reached a maximum, which was 93 percent of the helium-nitrogen interface velocity at the nozzle entrance, about 400 μsec after flow arrival at the nozzle exit. The velocity increased to within 5 percent of the maximum velocity in the first 100 μsec of flow. After the maximum velocity was reached, the velocity decreased gradually to about 83 percent of the maximum velocity in the next 950 μsec.

6. At 100 μsec after flow arrival, the test flow was less divergent than a point source flow up to $y/R = 0.5$.

7. The temperatures in the nitrogen test slug at 100 μsec after flow arrival were less than 30 percent of the temperature of the nitrogen test slug at the nozzle entrance.

The following results were obtained for the evacuated-nozzle case:

8. The helium-nitrogen interface emerged as a nearly plane surface between 250 μsec and 350 μsec after flow arrival.

9. The mass distribution, or shape, of the emerging nitrogen test slug was similar to a thick cylindrical shell. The densities within the shell were two to four times larger than those for positions interior to the cylinder near the tunnel center line.

10. Velocity profiles for the nitrogen test slug were uniform within about 5 percent. The average flow velocity on the center line was 5 percent lower than that in the denser shell.

11. Between 350 μsec and 800 μsec after flow arrival, the center-line velocity was constant within ±4 percent with a value of 82 percent of the helium-nitrogen interface velocity at the nozzle entrance.

12. At 550 μsec after flow arrival, the test flow was less divergent than a point source flow in the radial interval from the center line to 0.75 of the nozzle exit radius.

13. The temperatures in the nitrogen test slug at 550 μsec after flow arrival were smaller than the temperature of the nitrogen test slug at the nozzle entrance. Temperatures in the denser shell were less than 60 percent and temperatures near the center line were less than 30 percent of the temperature of the nitrogen test slug at the nozzle entrance.

Langley Research Center,
National Aeronautics and Space Administration,
Hampton, Va., July 6, 1973.

APPENDIX A

FLOW SEQUENCE AND FLOW REGION BOUNDARIES

Model of Flow Sequence

A number of papers have been published on the starting processes in the nozzle of a hypersonic shock tunnel. Smith (ref. 7) reports experimental and theoretical studies of a reflected shock tunnel. Glick, Hertzberg, and Smith (ref. 8) give an analysis of the non-reflected shock tunnel as do Henshall and Gadd (ref. 9). The flow in these facilities is shown in the following sketch:

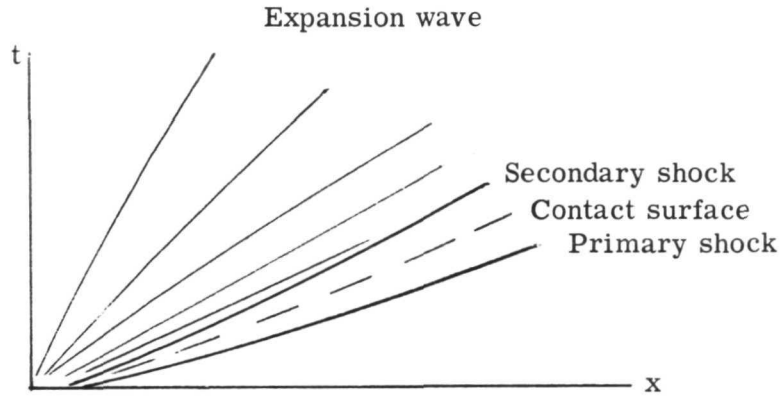

Sketch (a) – Wave diagram of unsteady flow in a diverging nozzle

In this sketch, a secondary upstream facing shock follows the primary shock and contact surface through the nozzle. This upstream facing shock adjusts the conditions behind the primary shock to the conditions in the gas that was originally processed by the shock in the shock tube and is now in the nozzle.

The test time in the reflected shock tunnel and that in the nonreflected shock tunnel are modified by the loss in time due to the passage of the secondary shock and expansion wave through the nozzle.

In the expansion-tube-driven tunnel of the present investigation, the flow described by Smith (ref. 7) takes place in the helium gas for the no-third-diaphragm case and in the residual gases for the evacuated-nozzle case. The passage through the nozzle of the helium-nitrogen interface and the tail of the expansion fan which follows the test gas (fig. 4) affects the loss of test time in the expansion tunnel. A treatment of this process is given in reference 2.

A simple comparison of the loss of test time in the test gas was made between the prediction of reference 2 and the present nozzle. For an entering flow of $M = 5$, an axial Mach number distribution was calculated by using the method of reference 4. From these calculations, the local values of velocity and speed of sound were determined. The time t of passage through the nozzle of the $u + a$ characteristic and the $u - a$ characteristic was determined by using the following expression:

$$t_{\pm} = \int_0^x \frac{dx}{u \pm a}$$

The traverse time for the $u - a$ characteristic, corresponding to the leading edge of the test gas, was 206 μsec; the traverse time for the $u + a$ characteristic, corresponding to the tail of the expansion fan at the trailing edge of the test gas, was 166 μsec. These values compare with values of 198 μsec and 165 μsec, respectively, using the method of reference 2 for the initial Mach number M_i of 5 and the final Mach number M_f of 16. The experimental data indicate that the traverse time of the acceleration-gas—test-gas interface was about 225 μsec and of the expansion fan, which is much more difficult to detect, was roughly 200 μsec. The loss in test time for the nozzle, compared with that of the expansion tube, is then the difference between these two traverse times, and the experimental values are of the same order of magnitude as the calculated values.

Other factors that could affect the loss of theoretical test time are the upstream facing secondary shock in the no-third-diaphragm case and the expansion fan from the third diaphragm in the evacuated-nozzle case. (See figs. 4(b) and 4(c).) The effects of these disturbances could not be identified from the time histories of the total-pressure probe or other instrumentation used.

Relative Location of Flow Region Boundaries

Since the measurements of the physical properties of the nitrogen test flow region (defined in figs. 4(b) and 4(c)) were of primary interest, it was necessary to locate the test flow region relative to flow arrival. Flow arrival was indicated by the initial response of either a heat-transfer gage or a pitot-pressure probe used in the course of the measurements. The passage of the flow region boundaries (shock, interface, and expansion wave) were inferred from changes in the signals of several types of probes which were employed in several supplemental tunnel runs. In this section is indicated the type of data upon which the inferred locations of the flow boundaries were based.

Nozzle entrance.- At the nozzle entrance, the locations of the flow boundaries were based on changes in the response of pitot-pressure probes. The locations of the flow boundaries are indicated on the pressure data traces shown in figure 5. The probes were

located on the center line and 2.54 cm off the center line of the expansion tube near the nozzle entrance as shown in figure 1(b).

It was assumed that the first indication of pressure corresponds to the arrival of helium flow. For the no-nozzle-diaphragm case, flow arrival corresponds to the helium shock (fig. 4(b)). For the evacuated-nozzle case, flow arrival corresponds to the residual-gas—helium interface instead of the residual-gas shock (fig. 4(c)).

For the evacuated-nozzle case, it was estimated that, due to the very low density of the residual-gas flow in the expansion tube, the passage of the residual-gas shock would not be detectable at the pitot-pressure-probe sensitivity employed here. Also, due to an estimated temperature of about 6000 K for the residual-gas flow in the expansion tube, the residual gas might be expected to be largely ionized. On the microwave data record which was used to track the helium-nitrogen interface in the expansion tube, there was a brief indication of a rapidly moving (7.5 km/sec) ionized front just prior to its impingement on the microwave antenna (which was located near the nozzle entrance). This moving ionized front could possibly be interpreted to be the expected residual-gas shock indicated in figure 4(c). From the microwave data, it was not possible to locate the position of the ionized front with respect to the residual-gas—helium interface. Only the velocity of the front could be estimated.

The average velocity over the distance interval of 1.6 m was determined for the helium shock and the residual-gas—helium interface for the two initial nozzle conditions. The passage of the initial helium flow was detected by a wall pressure probe located 1.6 m upstream of the nozzle entrance and the pitot-pressure probe at the nozzle entrance. For the no-nozzle-diaphragm case, the average helium shock velocity obtained for six runs was 4.7 ± 0.1 km/sec. For the evacuated-nozzle case, the average residual-gas—helium interface velocity for three runs was 6.1 ± 0.5 km/sec. The larger average velocity obtained over this distance interval for the evacuated-nozzle case indicates that the residual-gas—helium interface is accelerated in the region between the nozzle diaphragm and the nozzle entrance as would be expected.

The velocity of the helium-nitrogen interface in the expansion tube acceleration chamber was determined from microwave tracking of an ionized region associated with the interface. This tracking technique is discussed in reference 3. The average velocity obtained for 14 runs was 4.48 ± 0.22 km/sec.

For the evacuated-nozzle case, the interface could only be tracked upstream of the nozzle diaphragm since the electrical noise associated with the opening of the diaphragm and the impingement of the residual-gas shock on the antenna masked the signal from the helium-nitrogen interface. Since the helium-nitrogen interface velocity could not be obtained in the distance interval between the nozzle diaphragm and the nozzle entrance, it could only be inferred that the change in the helium-nitrogen interface velocity in this

distance interval was small compared with the change in velocity experienced by the residual-gas—helium interface. This inference is based on a comparison, for the two initial nozzle conditions, of the average velocities of the helium shock and residual-gas—helium interface and the arrival times for the helium-nitrogen interface (fig. 5).

Nozzle exit – evacuated nozzle.- For the evacuated-nozzle case, the helium-nitrogen interface was inferred to arrive between 250 μsec and 350 μsec after flow arrival. The arrival of the helium-nitrogen interface was inferred from filtered photomultiplier data and ion-probe data. It was assumed that the filtered photomultiplier responded to the arrival of nitrogen in the flow field. The ion probe was assumed to respond to the arrival of residual ions from the ionized region located near the helium-nitrogen interface which was tracked by microwave in the expansion tube portion of the facility.

A rise in the pitot pressure was expected to occur during the passage of the helium-nitrogen interface due to an expected increase in density across the interface, but a change in pitot pressure could not be uniquely interpreted as a change in chemical composition.

Photomultiplier, pitot probe, flat-plate-pressure, and heat-transfer-gage responses: The locations of the residual-gas shock, the helium-nitrogen interface, and the expansion fan were based on interpreting the changes in the signal of a photomultiplier which viewed the stagnation region of a pitot-pressure probe. The locations of these flow boundaries relative to the residual-gas—helium interface (taken to be flow arrival) were obtained from correlation with the signals of the pitot-pressure probe, a pressure gage, and a heat-transfer gage which were mounted in a flat plate. The responses of the probes are shown in figure 22(a), 22(b), and 22(c). The data presented in each figure were obtained from a separate tunnel run and the first indication of the pitot-pressure-probe signal for each run was assumed to indicate flow arrival.

In figures 22(a) and 22(b), the photomultiplier has a 3920 ± 40 Å band-pass filter inserted in the optical path to limit the response to the spectral region where light emitted from excited N_2^+ ions could be observed. The N_2^+ ions might be expected to form in the flow stagnation region of the probe. The relative light level required for a given deflection of the photomultiplier traces is indicated in the figures. The markedly different photomultiplier responses shown in figures 22(b) and 22(c) tend to imply that the light observed in figure 22(b) lies within the band pass of the optical filter and is not just an attenuation of the light emitted outside the band pass of the filter. The light observed by the unfiltered photomultiplier in figure 22(c) was assumed to be primarily due to impurities in the gases.

The arrival of the residual-gas shock (figs. 22(b) and 22(c)) was indicated by the small initial response of the photomultiplier just prior to flow arrival.

The arrival of the residual-gas—helium interface, indicated by the initial response of the pitot-pressure probe, follows closely behind the residual-gas shock (figs. 22(b)

and 22(c). As shown in figure 22(a), the initial responses of the pressure gage and the heat-transfer gage, which were mounted in the flat plate, correlate with the initial response of the pitot-pressure probe.

The arrival of the helium-nitrogen interface was indicated by the first large deflection of the signal trace of the photomultiplier with the filter (fig. 22(b)).

The arrival of the expansion fan (figs. 22(a) and 22(b)) was indicated by the large deflection, after the helium-nitrogen interface, of the signal trace of the photomultiplier with the filter.

From the data presented in figure 22, the time sequences of the arrival of the flow boundaries (fig. 4(c)) with respect to flow arrival at the nozzle exit were approximately as follows:

	Δt_1
Residual-gas shock	-50 μsec
Residual-gas—helium interface	0
Helium-nitrogen interface	350 to 400 μsec
Expansion fan	600 to 650 μsec

Ion-probe and heat-transfer-gage responses: Shown in figure 23 are samples of data from the heat-transfer gage located in the source splitter plate and the ion probe located just below the leading edge of the plate. The locations of the heat-transfer gage and ion probe are shown in figure 2. The approximate radial position y/R of the gage and probe is -0.44.

The ion-probe data were obtained during the velocity measurements to see whether the arrival of nitrogen in the flow could be sensed by such a probe. The assumption that the arrival of nitrogen might be sensed by the probe is based on the much larger ionization potential of helium relative to nitrogen. In the flow stagnation region of the probe, a much lower level of ionization would be expected for pure helium flow than for nitrogen flow.

Two limitations of the ion probe are important in interpreting the data from the probe. First, the chemical identity of the ions cannot be distinguished by the probe. Second, ions existing in the flow cannot be distinguished from ions which are produced in the flow stagnation region of the probe.

The second limitation also applies to the filtered photomultiplier data presented in figures 22(a) and 22(b); that is, N_2^+ ions existing in the flow which are excited in the flow stagnation region of the probe cannot be distinguished from excited N_2^+ ions which are formed in the flow stagnation region of the probe.

As shown in figure 23(a), a peak in ionization is observed between 200 μsec and 400 μsec for the evacuated-nozzle case. After this peak is reached, the ionization drops to a low level which is followed by a broad peak between 600 μsec and 1500 μsec after flow arrival.

Note in figure 23(a) that the amplitude of the first ion peak is of the same order of magnitude as that of the following broad peak between 600 μsec and 1500 μsec. Comparison of the shapes of the signal traces of the ion probe in figure 23(a) and the filtered photomultiplier in figure 22(a) indicates that the amplitude of the first ion peak is far too large to be due to N_2^+ ions formed only in the stagnation region of the ion probe. These observations are consistent with the assumption that the first ion peak corresponds to an ionized region which exists in the free-stream flow. This ion peak was interpreted to correspond to the same ionized region, located near the helium-nitrogen interface, which was tracked by microwave in the expansion tube portion of the facility.

Interface arrival from ion-probe, filtered photomultiplier, and pitot probe responses: For the evacuated-nozzle case, the arrival of the ion peak with the arrival of N_2^+ ions detected by the filtered photomultiplier is indicated in figures 22(a), 22(b), and 23(a). A comparison of these figures indicates that the ion peak precedes the helium-nitrogen interface by approximately 50 μsec.

Indicated in figure 23(a) is the location of the pitot-pressure rise (obtained from fig. 18), which was interpreted to correspond to the helium-nitrogen interface, for a pitot-pressure probe at a radial position comparable with that of the ion probe. The location of the pressure rise indicates that the ion peak correlates with or slightly follows the rise in pitot pressure.

The arrival times of the ion peak, N_2^+ ions, and pitot-pressure rise were obtained from separate tunnel runs. Since there were not sufficient data available to estimate the run-to-run reproducibility of the arrival times of these phenomena, it was not possible to determine from the data whether the differences in arrival times of these phenomena are significant or reflect run-to-run variations in the arrival time of the helium-nitrogen interface.

In view of the preceding discussion, when comparisons are made involving different tunnel runs for the evacuated-nozzle case, the arrival time of the helium-nitrogen interface relative to flow arrival will be assumed to lie in the interval between 250 μsec and 350 μsec.

Nozzle exit – no nozzle diaphragm.- Since the presence of nitrogen in the flow field was not directly identified for the no-nozzle-diaphragm case, it was not possible to directly establish the arrival of the helium-nitrogen interface. An interpretation of the velocity, pitot-pressure, and ion-probe data, which appears to be consistent, is that the interface arrives during the first 50 μsec after flow arrival on the tunnel center line and

at progressively later times with increasing y/R. This behavior indicates that the interface may be a highly curved surface.

Center-line velocity: The arrival of the interface during the first 50 μsec after flow arrival was inferred from a consideration of the reduction of the velocity of the helium shock due to passage through the nozzle and the rapid increase in flow velocity, shown in figure 6, after the helium shock at the nozzle exit.

Pitot pressure: As shown in figure 11, the first pitot-pressure rise after flow arrival occurs at progressively later times with increasing y/R. A pressure rise does not uniquely identify the arrival of the interface, but the pitot-pressure rise associated with the interface for a position off the tunnel center line must at least arrive later than that for a position on the tunnel center line.

Ion probe: Samples of the ion-probe data are shown in figure 23. The extremes in level which were observed are indicated by the two signal traces shown in figure 23(a). Also indicated in figure 23(a) is the relative time location of the pitot-pressure rise, obtained from figure 11, corresponding to a radial position comparable to that of the ion probe. The location of the pitot-pressure rise correlates with the first ion peak. This correlation is consistent with the assumption that the pitot-pressure rise is associated with the arrival of the helium-nitrogen interface, but, as has already been mentioned, the ion peak does not uniquely identify the presence of nitrogen in the flow.

Flow visualization: Two discontinuities in the flow field, which were visualized as a result of the electrical discharge associated with the velocity measuring technique, can be seen in figure 24. Shown in figure 24 are the approximate profiles for the shapes of the helium shock and a following discontinuity labeled "Possible He-N_2 interface." The profile of the possible interface is consistent with the boundary of the emerging gas jet which is implied by the velocity profiles shown in figure 8. The location and shape of the discontinuity relative to the helium shock are approximately the location and shape of the interface which would be implied if it were assumed that the pitot-pressure rises, shown in figure 11, were associated with the arrival of the helium-nitrogen interface.

Heat-transfer-gage response: The primary use of the heat-transfer gage was to indicate flow arrival for which an increase in the resistance of the gage was always observed. No attempt was made to interpret the changes observed in the heat-transfer-gage signal in terms of helium and nitrogen flow. Since the gage was not tested for use in ionized flow, a reasonable doubt exists in the interpretation of any heat-transfer rates, from the gage response, when ionized flow is present. The thin-film platinum resistance element of the gage was coated with a thin glasslike insulating material, but the difficulty of obtaining such an insulating coating free from pin holes has been discussed in reference 10. For the gage used in this study, an increase in resistance of the gage indicates an increase in the gage temperature. If a shorting ion current is flowing parallel to the

gage current, the apparent resistance of the gage element is reduced and a reduction in the temperature of the gage is inferred.

In figure 23(b), the heat-transfer-gage responses are presented with the corresponding probe responses for the two initial nozzle conditions. A more rapid rise in gage temperature after flow arrival is indicated for the no-nozzle-diaphragm case as compared with that for the evacuated-nozzle case. For both initial nozzle conditions, there is a large apparent reduction in the heating rate in the time interval corresponding to the first peak in the ion-probe response, with the reduction being larger for the no-nozzle-diaphragm case. After the passage of the first ion pulse, the heating rates appear to be nearly equal and constant with time for the two initial nozzle conditions, and no significant reduction in the apparent heating rate corresponding to the second ion peak between 600 μsec and 1500 μsec is indicated. For the ion probe, ions existing in the free stream cannot be distinguished from ions produced in the flow stagnation region of the probe. Since the heat-transfer gage was located in a flat plate with a sharp leading edge instead of a flow stagnation region, the main distortion of the heat-transfer signal would be expected to be due to ions which exist in the free-stream flow.

APPENDIX B

METHOD OF DATA ANALYSIS AND UNCERTAINTIES

Velocity

The velocity measuring technique was the same as that described in reference 6 and the components were adapted to be compatible with the tunnel operation. Briefly, the principle of the flow-velocity measuring technique is as follows: a column of gas located at a known position in the flow field is identified (or tagged) and, after a known time interval, the displaced position of the identified column is detected. The method used to identify the gas column was to partially ionize the gas in the column by means of a pulsed (10^{-7} sec duration) beam of vacuum ultraviolet light. The method used to detect the identified column was to photograph the light emitted from molecules in the column which were excited by means of an electrical current pulse (10^{-7} sec duration) which was passed through the now electrically conducting column. Due to the very short lifetimes of those excited states from which the predominance of the photographed light was produced, the duration of the photographed light was essentially the same as the duration of the detecting current pulse; thus, it was possible to avoid the use of an elaborate camera shuttering technique.

The velocity was derived from the time interval Δt_2 between photoionization and detection of the ionized column and the displacement Δx of the ionized column during this time interval.

Uncertainty in velocity.- An uncertainty of about ±1.8 percent is estimated for the velocity by compounding the uncertainties in Δt_2 and Δx.

Δt_2: A nominal value for Δt_2 was 5 μsec with an estimated uncertainty of ±0.02 μsec.

Δx: Densitometer scans of the data films were used to locate the position of the detected ionized column with respect to the reference position marker (fig. 2). The films were scanned parallel to the tunnel axis at radial intervals of 0.646 cm. The scanning slit was rectangular with dimensions of 0.29 cm in the scan direction and 0.59 cm in the radial direction.

A nominal value for Δx was of the order of 2 cm with an estimated uncertainty of ±0.034 cm. The estimated uncertainty is based on consideration of the following observations:

(1) The standard deviation from the mean of eight determinations of the initial position of the ionized column was ±0.026 cm.

(2) The overall magnification of the optical system was obtained by photographing a calibrated grid that was placed at the nozzle exit. Over the field of view employed in the measurements, the magnification was found to be constant to within ±0.2 percent.

(3) Due to background density gradients present on the data films, a consistent method of estimating the position of the center of the detected column was required. The method used is discussed in appendix C. The uncertainty introduced in Δx due to the presence of the density gradients is estimated to be of the order of ±0.02 cm.

(4) The densitometer scan corresponding to the tunnel center line was repeated for each data film. The differences in Δx obtained from the two scans for the 28 runs were within ±1.0 percent of Δx.

(5) Since a current loop is formed during the detection of the ionized column, a displacement of the column due to the presence of the current loop might be anticipated. An order-of-magnitude estimate of this displacement was 10^{-5} cm. The estimate was based on an estimate of the detection current, pulse duration, mass of gas in the column, and the dimensions of the current loop. The location of the photoionizing light beam was determined experimentally and was found to agree with the position of the detected ionized column, obtained under static conditions, within 0.006 ± 0.017 cm.

Comparison of individual velocity measurements.- A tunnel run was required for each velocity-profile measurement. Since variations occur in the opening of the primary diaphragm, a method of comparing the velocities obtained from the different tunnel runs was required. The shock Mach number in the intermediate chamber was routinely measured and was assumed to characterize the energy of the intermediate chamber flow.

The velocity u at the nozzle exit was obtained from the following relation:

$$u = \frac{u_m \bar{u}_l}{u_l}$$

where u_m is the measured velocity at the nozzle exit, u_l is the limiting velocity, and $\bar{u}_l$ is the average limiting velocity for the tunnel runs used in measuring the velocity. The limiting velocity, which was computed from the shock Mach number, is a conceptual velocity and is described in reference 11. The average value of the limiting velocity for 29 tunnel runs was 6.89 ± 0.33 km/sec.

Partial opening of nozzle diaphragm.- During the velocity measurements for the evacuated-nozzle case, the pressure gage in the expansion tunnel wall just upstream of the nozzle diaphragm was monitored. If the diaphragm was not fully opened prior to the arrival of flow, a reflected shock was sensed by this pressure gage. Inadvertently, a run was made for which the electrical opening mechanism did not operate and the nozzle dia-

phragm was opened only by the flow. A strong reflected shock was indicated by a large pressure rise at the wall pressure gage. It was surprising that for this extreme nozzle diaphragm opening case, the resultant tunnel flow velocities were not significantly different from velocities obtained when the diaphragm was opened properly, except in the outer portions of the flow. A comparison of the velocity profile for this one accidental diaphragm opening with the velocity profiles for normally opened diaphragms is presented in figure 15(e).

A weak reflected shock with an associated wall pressure rise of about an order of magnitude smaller than that for the condition just described was observed during four tunnel runs. Differences were not apparent between the resultant velocity profiles obtained for these four runs and runs for which no reflected shocks were indicated. The nozzle diaphragm holder was examined after each of these runs and it was observed that for one of these runs the diaphragm wire protruded slightly from the tube wall. The velocity profiles for these four runs (labeled "Partially opened diaphragm") along with the individual velocity profiles of all the runs are presented in figure 16.

No reflected shocks from the nozzle diaphragm were indicated for the runs which were made to obtain pressure data at the nozzle exit.

Flow Visualization

Several types of variance may be rendered visible in low-density gases by an electrical discharge in the gas, such as acoustical waves, shock waves, variations in density, temperature, chemical composition, and ionization. To reduce the uncertainty in the interpretation of what has been visualized, it is usually necessary to correlate the phenomenon with some other measurement.

Flow direction.- Disturbances in the flow field, caused by the presence of the plastic rods (fig. 3), were rendered visible by the detector current pulse which passed through the flow field. The flow direction was obtained from the symmetry of the bow shock envelope in the range from 4 to 10 rod diameters downstream from the end of the rod. For small inclinations of the plastic rod axis with respect to the direction of the flow, the bow shock envelope should be symmetrical about the flow direction for envelope positions which are not too close to the rod. Several observations support this assumption. Two tunnel runs were made in which a straight length of insulated copper wire, having approximately the same diameter as the plastic rods, was located on the tunnel axis. For the first run, the wire was alined with the tunnel axis. For the second run, the wire was inclined 6^{o} with respect to the tunnel axis. The shocked flow was made visible by applying an electrical pulse between the wire and a ground plane downstream. The two bow shock envelopes were observed to be essentially the same with respect to the end of the wire and the direction of the tunnel axis for at least 14 wire diameters downstream from the end of the wire.

Mach number.- The Mach number was obtained from the reciprocal of the sine of the estimated Mach angle. The Mach angles were estimated from the disturbance envelopes about the plastic rods in the flow direction data photographs. The angle was estimated in the range from 4 to 10 rod diameters downstream from the end of the rod. It would be difficult to estimate an uncertainty for the Mach number obtained in this manner. The Mach number which is estimated in this manner is expected to be systematically low and, therefore, at least to represent a lower bound to the true Mach number.

For the evacuated-nozzle case, one flow-direction data film was obtained at $\Delta t_1 = 630$ μsec. The results from this data film have been included in the averaged results for flow direction and Mach number presented at $\Delta t_1 = 550$ μsec.

Pressure

The pressure values presented are based on the static calibration of the piezoelectric transducers. The uncertainty presented indicates only the reproducibility of the observed pressure for available repeated data. For the low pressures encountered at the nozzle exit, electronic noise and drift become important sources of uncertainty which are difficult to assess. Surface heating of the transducers, due to flow, can introduce a change in the gage signal which is difficult to assess from the results obtained in this study. The surface heating effect should be most pronounced for the measurements made with the bare-gage pitot-pressure rake. Differences in rake and single-probe data were observed for the late portions of the flow.

No corrections have been applied to the observed pitot-pressure data to account for any possible low-density aerodynamic effects. On the basis of the results presented in reference 12 and estimates of the range of possible Reynolds number at the nozzle exit, the observed pitot pressure may be as much as 20 percent larger than the actual pitot pressure for some of the lower densities encountered.

Time After Flow Arrival

For the velocity measurements, the time after flow arrival is the preset delay between the response of the heat-transfer gage (fig. 2) to the start of flow and the triggering of the photoionization source pulser. The inherent delay between triggering the photoionization source pulser and photoionization was about 3 μsec. An uncertainty of the order of ± 5 μsec in the flow arrival time is estimated due to variations in trigger level relative to the signal from the heat-transfer gage.

For the measurements obtained by the pitot-pressure rake, the flow arrival time was referenced to the same heat-transfer gage used in the velocity measurements. For the single-pitot-pressure-probe measurements the start of flow was taken to be the first

observable pressure increase, and an uncertainty of the order of ±5 μsec was estimated for the flow arrival time.

Derived Quantities

The uncertainties presented for the derived quantities were obtained by propagation of the uncertainties in the measured input quantities.

Density.- The gas density ρ normalized by the density of nitrogen at standard conditions, $\rho_o = 1.25$ kg/m^3, was derived from the approximate relation

$$\frac{\rho}{\rho_o} = \frac{p_t}{\rho_o u^2}$$

where p_t is the pitot pressure and u is the flow velocity.

This approximate relation requires only the pitot pressure and the flow velocity as measured input quantities. The density derived from this relation is lower than the true density for true input values, but the derived density should at least be within 10 percent of the true density for the hypersonic nitrogen flow conditions expected here.

Temperature.- The gas temperature T was derived from

$$T = \frac{T_o u^2}{a_o{}^2 M^2} \tag{B1}$$

where u is the flow velocity, M is the free-stream Mach number, $T_o = 273$ K, and a_o is the speed of sound in the gas at T_o. For nitrogen, $a_o = 332$ m/sec. For helium, $a_o = 1016$ m/sec.

The gas temperature was also derived from

$$T = \frac{p_w m}{\rho R'} = \frac{p_w u^2 m}{p_t R'} \tag{B2}$$

where p_w is the pressure observed by the flat-plate gage, p_t is the pitot pressure, R' is the universal gas constant, and m is the molecular mass of the gas. For nitrogen, $m = 28.01$ g/mol. For helium, $m = 4.003$ g/mol.

The gas temperature was also derived from

$$T = \overline{T}_i \left\{ \frac{\rho}{\bar{\rho}_i} \right\}^{0.4} = \left(\frac{p_{w,i} u^2 m}{\bar{p}_{t,i} R'} \right) \left\{ \frac{p_t / u^2}{\bar{p}_{t,i} / u_i^2} \right\}^{0.4} \tag{B3}$$

where $p_{w,i}$ is the expansion-tube wall pressure, $\bar{p}_{t,i}$ is the average pitot pressure at the nozzle entrance, and u_i is the flow velocity at the nozzle entrance.

The measured input quantities differ for the three relations with the flow velocity appearing as a measured input in each of the relations. The additional measured inputs are Mach number in the first relation and pressures in the second and third relations.

In applying these three relations, it is assumed that the gas is an ideal gas and the gas composition is pure molecular nitrogen. The temperature derived from the third relation is merely the temperature expected for an assumed adiabatic expansion from the average temperature and density of the nitrogen at the nozzle entrance to the density in the flow field at the nozzle exit.

The temperatures derived from these relations are expected to represent only upper bounds to the true temperature, even for the assumption of an ideal gas. For the first relation, only lower bounds to the Mach number were obtained from the measurements. The second relation is true only if the observed flat-plate pressure is equal to the free-stream static pressure. On the basis of the results presented in reference 13 and the possible correction to the pitot pressure already discussed, the ratio of the observed flat-plate pressure to the free-stream pressure should always be larger than the ratio of the observed pitot pressure to the actual pitot pressure for a plate alined perfectly with the free-stream flow direction.

The temperatures derived from any of these relations will be larger than the true temperature if the nitrogen is contaminated with helium. For example, if pure helium was erroneously assumed to be molecular nitrogen, the inferred temperature would be at least seven times larger than the true temperature.

APPENDIX C

LOCATION OF IONIZED COLUMN FROM DATA FILMS

Densitometer scans of the data films were used to determine the location of the displaced detected ionized column. Due to the presence of a spatially varying background exposure on the films, a consistent method of estimating the position of the detected column on the film was required. The method used and the model employed for the basis of the method are discussed in this appendix.

Assumed Model of Photographic Image

The following three assumptions were made concerning the model of the photographic image of the detected column, for a given radial position:

(1) The relation between exposure E and the optical density D for the film can be given by

$$D = \gamma \ln \frac{E}{E_f} + D_f \tag{C1}$$

where D_f is the film fog density (constant for any given film), E_f is an exposure corresponding to the fog density, γ is a constant for any given film.

(2) The exposure g of the detected column, centered at $x = 0$, as a function of position x in the scanning direction can be expressed as

$$g = Ae^{-\frac{x^2}{2\sigma^2}} \tag{C2}$$

where A and σ are constants. This function is symmetrical about its maximum value which occurs at $x = 0$.

(3) The background exposure b as a function of position x can be expressed as

$$b = Be^{kx} \tag{C3}$$

where B and k are constants.

The density D of the film as a function of position x can be obtained from equations (C1), (C2), and (C3) as

$$D(x) = D(g + b) + D_f$$

$$D(x) = \gamma \ln\left(\frac{Ae^{-\frac{x^2}{2\sigma^2}} + Be^{kx}}{E_f}\right) + D_f \tag{C4}$$

The function $D(x)$ is not symmetrical, except for $k = 0$ or $B = 0$. For the conditions where a peak exists in the range of x, the maximum of the peak occurs for values of $x < 0$ when $k < 0$ and $x > 0$ when $k > 0$.

For the values of $|x| >> \sigma$, equation (C4) approaches the function

$$D_b(x) = \gamma \ln\left(\frac{Be^{kx}}{E_f}\right) + D_f \tag{C5}$$

Equation (C5) is a linear function of x of the form

$$D_b(x) = \gamma kx + c \tag{C6}$$

where γ, k, and c are constants.

If equation (C5) is subtracted from equation (C4), the following equation is obtained:

$$D(x) - D_b(x) = \gamma \ln\left(1 + \frac{A}{B} e^{-\left(\frac{x^2}{2\sigma^2} + kx\right)}\right) \tag{C7}$$

This function is symmetrical about its maximum value which occurs at $x = -k\sigma^2$.

Application of Model to Data Films

Location of center of detected column.- The function $D(x)$, equation (C4), was used as the model for the observed density scan trace in the vicinity of the image of the detected column. Two points, D_1,x_1 and D_2,x_2 (see fig. 25), near the peak of the density trace were determined for which the values x_1 and x_2 are reflected images about the line of symmetry in the function $D(x) - D_b(x)$, equation (C7). The two points D_1,x_1 and D_2,x_2 were determined from the intercepts of the density trace and a line

drawn parallel to the estimated background density function $D_b(x)$, equation (C6). By using equations (C3), (C6), and (C7), the position of the center of the detected column x_c was found from

$$x_c = \frac{x_1 + x_2}{2} + k\sigma^2$$

$$x_c = \frac{x_1 + x_2}{2} + \frac{\sigma^2\left(D_2 - D_1\right)}{\gamma\left(x_2 - x_1\right)} \tag{C8}$$

Assumptions and uncertainties.- Equation (C1) is based on the linear portion of the characteristic curve of density as a function of the logarithm of exposure for photographic film (ref. 14). From densitometer data, taken for the type of film and developing procedure used for obtaining data films, the range of optical densities encountered in the data films was found to lie on the linear portion of the characteristic curve. From the densitometer data, a value for γ could be estimated to about ±30 percent.

Equation (C2) was assumed because it is a mathematically convenient symmetrical function which reasonably represents the shape of the density peak in the region of interest. A normalized sample density trace and a curve obtained from equation (C7) fitted at the half-amplitude points are compared in figure 26. From the data obtained, it was not possible to obtain a value for σ that was independent of an estimate of γ. The order of 1/2 of the percentage uncertainty in γ is reflected in estimates of σ. The value of σ, which was used in the computations, was estimated by using the estimated value of γ and the observed width of density peaks, for which the background density variation was small compared with the variation of the density due to the peak.

The use of equation (C3) assumed that in the vicinity of the density peak, the density which would be produced by the background exposure alone could be approximated by a linear function of x. The assumption could not be verified, since exposure due to the background discharge could not be produced independently of the discharge through the ionized column. Equation (C3) was assumed to be a reasonable, mathematically convenient interpolation of the character of the background density observed in regions away from the density peak.

In equation (C8), the term $\frac{\sigma^2\left(D_2 - D_1\right)}{\gamma\left(x_2 - x_1\right)}$ was considered a correction to the estimated position of the detected column due to the change in background exposure with position. The range of the magnitude of the correction term relative to the displaced distance

of the ionized column, encountered in the velocity measurements, was from 3 percent to zero with most of the correction terms less than 1 percent. The value of $\gamma \pm 30$ percent was used for computation since γ was not determined for the data films. The ratio σ^2/γ tends to be self-consistent for the model employed. Examination of equation (C4) indicates that for a zero background (that is, for $B = 0$), the ratio σ^2/γ is independent of γ.

Because of the somewhat arbitrary nature of the model presented herein and the lack of specific values of γ or σ^2/γ for each data film, the estimated uncertainty in the displaced distance of the ionized column due to variation in background density is of the order of 1 percent.

REFERENCES

1. Trimpi, Robert L.: A Preliminary Theoretical Study of the Expansion Tube, a New Device for Producing High-Enthalpy Short-Duration Hypersonic Gas Flows. NASA TR R-133, 1962.

2. Trimpi, Robert L.; and Callis, Linwood B.: A Perfect-Gas Analysis of the Expansion Tunnel, a Modification to the Expansion Tube. NASA TR R-223, 1965.

3. Jones, Jim J.; and Moore, John A.: Exploratory Study of Performance of the Langley Pilot Model Expansion Tube With a Hydrogen Driver. NASA TN D-3421, 1966.

4. Callis, Linwood B.: An Analysis of Supersonic Flow Phenomena in Conical Nozzles by a Method of Characteristics. NASA TN D-3550, 1966.

5. Weilmuenster, K. J.: A Self-Opening Diaphragm for Expansion Tubes and Expansion Tunnels. AIAA J., vol. 8, no. 3, Mar. 1970, pp. 573-574.

6. Friesen, Wilfred J.: Use of Photoionization in Measuring Velocity Profile of Free-Stream Flow in Langley Pilot Model Expansion Tube. NASA TN D-4936, 1968.

7. Smith, C. Edward: The Starting Process in a Hypersonic Nozzle. J. Fluid Mech., vol. 24, pt. 4, Apr. 1966, pp. 625-640.

8. Glick, H. S.; Hertzberg, A.; and Smith, W. E.: Flow Phenomena in Starting a Hypersonic Shock Tunnel. AEDC-TN-55-16 (AD-789-A-3), U.S. Air Force, Mar. 1955.

9. Henshall, B. D.; and Gadd, G. E.: Factors Affecting the Performance of the Nozzle of a Hypersonic Shock Tube. C.P. No. 293, Brit. A.R.C., 1956.

10. Vidal, R. J.; and Golian, T. C.: Heat Transfer Measurements With a Catalytic Flat Plate in Dissociated Oxygen. AIAA Paper No. 67-163, Jan. 1967.

11. Grose, William L.; and Trimpi, Robert L.: Charts for the Analysis of Isentropic One-Dimensional Unsteady Expansions in Equilibrium Real Air With Particular Reference to Shock-Initiated Flows. NASA TR R-167, 1963.

12. Bailey, A. B.; and Boylan, D. E.: Some Experiments on Impact-Pressure Probes in a Low-Density, Hypervelocity Flow. AEDC-TN-61-161, U.S. Air Force, Dec. 1961

13. Harvey, William D.: Effects of Leading-Edge Bluntness on Pressure and Heat-Transfer Measurements Over a Flat Plate at a Mach Number of 20. NASA TN D-2846, 1965.

14. Anon.: Kodak Plates and Films for Science and Industry. Publ. No. P-9, Eastman Kodak Co., 1962.

TABLE I.- MEASURED RESULTS AT NOZZLE ENTRANCE

[$He-N_2$ interface velocity, 4.5 ± 0.2 km/sec; $p_w = 4.5 \pm 1$ kN/m^2]

(a) Pitot pressure; no nozzle diaphragm; y = 0 cm; n = 2

Δt_1, μsec	$\bar{p}_{t,i}$, kN/m^2	$\bar{S}$, kN/m^2
0	0	± 0
10	5	0
20	8	1
30	9	1
40	10	1
50	11	1
60	11	1
70	12	2
80	12	2
90	12	2
100	16	5
110	33	10
120	69	12
130	121	33
140	168	35
150	204	39
160	220	34
170	232	26
180	235	18
190	257	0
200	296	3
210	279	24
220	266	25
230	298	25
240	315	13
250	274	10
260	294	20
270	252	4
280	249	7
290	263	17
300	279	13
310	268	± 8
320	255	57
330	255	17
340	287	34
350	281	39
360	292	33
370	321	47
380	338	41
390	358	48
400	345	30
410	351	22
420	340	0
430	330	2
440	337	1
450	338	26
460	328	50
470	326	16
480	333	8
490	353	12
500	362	44
510	345	56
520	363	35
530	338	30
540	367	11
550	393	16
560	360	15

TABLE I.- MEASURED RESULTS AT NOZZLE ENTRANCE – Continued

[$He-N_2$ interface velocity, 4.5 ± 0.2 km/sec; p_w = 4.5 ± 1 kN/m^2]

(b) Pitot pressure; no nozzle diaphragm; y = 2.54 cm; n = 2

Δt_1, μsec	$\bar{p}_{t,i}$, kN/m^2	$\bar{S}$, kN/m^2
0	0	± 0
10	2	0
20	4	0
30	6	1
40	7	1
50	8	1
60	8	2
70	9	1
80	9	2
90	10	1
100	12	1
110	18	1
120	32	0
130	49	2
140	78	4
150	91	7
160	104	10
170	120	18
180	129	20
190	131	18
200	135	20
210	140	19
220	141	17
230	129	21
240	116	22
250	106	24
260	95	20
270	82	17
280	67	14
290	56	11
300	47	6
310	38	± 3
320	35	2
330	37	9
340	37	15
350	30	16
360	22	15
370	21	16
380	26	9
390	25	0
400	21	2
410	20	5
420	24	18
430	18	20
440	17	20
450	24	17
460	33	7
470	32	3
480	28	1
490	33	1
500	38	3
510	37	8
520	35	10
530	35	4
540	35	3
550	38	5
560	50	5
570	59	1
580	58	9
590	52	7
600	43	1

TABLE I.- MEASURED RESULTS AT NOZZLE ENTRANCE – Concluded

[$He-N_2$ interface velocity, 4.5 ± 0.2 km/sec; p_w = 4.5 ± 1 kN/m^2]

(c) Pitot pressure; evacuated nozzle; y = 0 cm; n = 1

Δt_1, μsec	$\bar{p}_{t,i}$, kN/m^2
0	0
10	5
20	8
30	10
40	13
50	15
60	17
70	18
80	19
90	20
100	21
110	21
120	23
130	24
140	24
150	24
160	24
170	25
180	26
190	33
200	38
210	39
220	38
230	42
240	49
250	66
260	115
270	101
280	147
290	171
300	178
310	194
320	227
330	216
340	214
350	250
360	209
370	297
380	230
390	201
400	212
410	195
420	134
430	280
440	224
450	238
460	235
470	310
480	192
490	217
500	374
510	307
520	323
530	374
540	377
550	348
560	384
570	382
580	381
590	384
600	384
610	385
620	386
630	386
640	387
650	385
660	363
670	366
680	381

(d) Pitot pressure; evacuated nozzle; y = 2.54 cm; n = 1

Δt_1, μsec	$\bar{p}_{t,i}$, kN/m^2
0	0
10	2
20	4
30	6
40	7
50	9
60	10
70	12
80	13
90	15
100	17
110	20
120	24
130	26
140	27
150	27
160	27
170	27
180	29
190	31
200	33
210	34
220	36
230	39
240	43
250	48
260	53
270	60
280	77
290	102
300	111
310	132
320	140
330	146
340	150
350	154
360	162
370	148
380	143
390	158
400	157
410	138
420	132
430	140
440	126
450	94
460	85
470	100
480	90
490	100
500	100
510	84
520	102
530	100
540	87
550	110
560	87
570	75
580	108
590	114
600	93
610	77
620	78
630	91
640	110
650	121
660	113
670	98
680	104
690	150
700	140

TABLE II.- MEASURED RESULTS AT NOZZLE EXIT WITH NO NOZZLE DIAPHRAGM

(a) Flow velocity

y, cm	Velocity and variance at –									
	Δt_1 = 1 μsec n = 1	Δt_1 = 50 μsec n = 2		Δt_1 = 100 μsec n = 1	Δt_1 = 150 μsec n = 1	Δt_1 = 250 μsec n = 1	Δt_1 = 400 μsec n = 1	Δt_1 = 600 μsec n = 1	Δt_1 = 950 μsec n = 1	Δt_1 = 1350 μsec n = 1
	u, m/sec	$\bar{u}$, m/sec	$\bar{S}$, m/sec	u, m/sec	u, m/sec	u, m/sec	u, m/sec	u, m/sec	u, m/sec	u, m/sec
-2.58	2913	3817	±17	3944	4076	4117	4230	3770	3709	3432
-1.93	2937	3741	140	3965	4071	4143	4306	3783	3724	3476
-1.29	2898	3732	180	3947	4068	4142	4310	3791	3694	3512
-.65	2922	3815	200	3937	4061	4109	4253	3779	3631	3492
.00	2950	3790	220	3963	4065	4107	4183	3791	3636	3487
.65	2972	3778	250	3975	4059	4098	4223	3806	3636	3493
1.29	2828	3762	280	3973	4072	4076	4154	3886	3567	3417
1.94	2998	4033	28	4006	4040	4048	4068	3861	3527	3374
2.58	2950	3520	540	3979	4055	4028	4103	3856	3547	3285
3.23	2873	3902	190	3988	4028	4045	4015	3895	3505	3267
3.88	2613	3782	52	4015	4040	4081	4008	3809	3495	3194
4.52	2255	3824	6	3949	3990	3906	3971	3829	3509	3148
5.17	1928	3904	13	3924	4013	3934	3919	3832	3492	3152
5.81	1744	3955	26	4218	3983	4029	3882	3834	3466	3079
6.46	1558	3902	50	3747	3977	4047	3979	3848	3479	3132
7.11	1220	3691	43	3889	3935	4080	4023	3811	3375	3072
7.53	773	3611	8	3964	3940	4069	4122	3815	3372	3086
8.40	113	2996	250	3988	3936	4058	4135	3692	3293	3023
9.04	143	2443	230	3911	3955	3926	4101	3734	3271	3044
9.69	91	1569	32	3803	3981	3907	4011	3527	3176	2935
10.34	39	1257	58	3126	3998	3888	3990	3499	3141	2984
10.98	51	1133	6	2382	3872	3857	3992	3411	3095	2904
11.63	78	1397	270	1832	3511	3690	4006	3365	3070	2967
12.27	66	1359	300	1475	3161	3398	3842	3356	2894	2909
12.92	50	1522	200	1231	2414	2937	3602	3288	2840	2928
13.57	38	1585	134	1064	1948	2645	3121	3458	2733	2875
14.21	5	1567	110	1041	1677	2159	2803	3785	2633	2828

TABLE II.- MEASURED RESULTS AT NOZZLE EXIT WITH NO NOZZLE DIAPHRAGM – Continued

(b) Pitot pressure

y = 0 cm; n = 4

Δt_1, μsec	$\bar{p}_t$, N/m^2	$\bar{S}$, N/m^2
0	848	± 841
5	2614	1665
10	3837	2544
15	5468	3338
20	7592	3991
25	10467	3330
30	14172	4528
35	17838	6209
40	17497	6616
45	14262	5161
50	13010	4600
55	10530	3067
60	9051	2271
65	6586	1390
70	5364	1395
75	4740	1273
80	4292	1176
85	3741	994
90	3490	1003
95	3263	953
100	3117	940
110	2457	897
120	1975	809
130	1743	727
140	1594	664
150	1489	636
160	1423	619
170	1376	584
180	1402	512
190	1407	461
200	1381	438
210	1320	417
220	1196	436
230	1155	434
240	1128	429
250	1104	424
260	1110	427
270	1182	405
280	1231	390
290	1336	358
300	1531	291
310	1720	218
320	1839	185
330	1866	± 189
340	1849	194
350	1809	196
360	1696	214
370	1521	273
380	1420	330
390	1424	287
400	1341	275
410	1253	275
420	1189	268
430	1148	225
440	1191	162
450	1294	192
460	1304	363
470	1331	545
480	1341	639
490	1418	638
500	1528	596
510	1488	576
520	1437	588
530	1276	601
540	1174	533
550	1378	187
560	1664	192
570	1935	273
580	2244	398
590	2527	686
600	3506	960
610	3369	843
620	3356	863
630	3543	832
640	3820	757
650	4008	687
660	4132	768
670	4468	741
680	4708	701
690	5268	615
700	5542	585
710	5818	578
950	10750	---

TABLE II.- MEASURED RESULTS AT NOZZLE EXIT WITH NO NOZZLE DIAPHRAGM – Continued

(b) Pitot pressure – Continued

y = 5.08 cm; n = 3

Δt_1, μsec	$\bar{p}_t$, N/m^2	$\bar{S}$, N/m^2
0	184	± 147
10	1399	510
20	2390	895
30	3458	956
40	5335	926
50	6712	669
60	8370	1772
70	11676	4350
80	15129	5930
90	18151	6593
100	20800	6964
110	20412	6515
120	19426	5825
130	18026	4649
140	21918	1601
150	17918	2147
160	13913	804
170	10822	396
180	11110	1568
190	9918	2305
200	7558	2093
210	6507	1491
220	5661	653
230	4412	440
240	3158	766
250	2478	767
260	2030	863
270	1669	990
280	1472	1036
290	1391	1045
300	1396	1035
310	1372	1039
320	1309	1060
330	1255	1084
340	1253	1084
350	1274	1071
360	1361	1034
370	1439	1021
380	1528	1003
390	1636	985
400	1666	1009
410	1659	1054
420	1531	1168
430	1453	1257
440	1392	1354
450	1412	1398
460	1575	1357
470	1776	1298
480	1967	1211
490	2213	± 1085
500	2419	1001
510	2450	1035
520	2187	1214
530	2189	1244
540	2453	1194
550	2530	1221
560	2440	1264
570	2442	1272
580	2513	1262
590	2723	1246
600	3201	1137
610	3221	1166
620	3014	1336
630	2940	1486
640	2551	1736
650	2536	1828
660	2874	1738
670	3280	1618
680	3386	1656
690	3611	1597
700	4169	1353
710	4405	1293
720	4607	1257
730	4698	1283
740	4735	1333
750	4680	1395
760	4416	1524
770	4377	1563
780	4467	1539
790	4167	1706
800	3953	1829
810	3888	1877
820	3900	1925
830	3963	1951
840	4216	1906
850	4430	1874
860	4633	1850
870	4662	1911
880	4603	2012
890	4505	2085
900	4460	2043
910	4397	1997
920	4494	2082
930	4652	2162
940	4880	2196
950	5176	2155

TABLE II.- MEASURED RESULTS AT NOZZLE EXIT WITH NO NOZZLE DIAPHRAGM – Continued

(b) Pitot pressure – Continued

y = 8.89 cm; n = 2

Δt_1, μsec	$\bar{p}_t$, N/m^2	$\bar{S}$, N/m^2
0	248	± 202
10	2153	359
20	2455	511
30	1027	536
40	631	172
50	4	4
60	660	6
70	534	75
80	982	213
90	1082	252
100	1058	81
110	1216	153
120	1064	229
130	2397	701
140	4952	2896
150	6219	3806
160	4991	2538
170	4820	2378
180	5137	2576
190	5683	3399
200	6201	4200
210	7248	5915
220	7153	
230	7249	
240	8058	
250	9208	
260	9306	
270	9219	
280	9145	
290	10095	
300	10672	
310	10576	
320	10481	
330	10385	
340	10290	
350	10194	
360	10099	
370	10003	
380	9657	
390	9084	
400	8558	
410	8004	
420	7680	
430	7547	
440	7424	
450	6971	904
460	5909	9
470	5778	7
480	5719	59

Lower bound

Δt_1, μsec	$\bar{p}_t$, N/m^2	$\bar{S}$, N/m^2
490	5672	± 106
500	5633	160
510	5604	218
520	5578	271
530	5546	318
540	5516	367
550	5486	416
560	5369	331
570	5307	287
580	5263	262
590	5248	276
600	5276	355
610	5358	487
620	5450	580
630	5515	630
640	5524	619
650	5526	591
660	5496	531
670	5462	450
680	5448	389
690	5453	314
700	5503	271
710	5562	238
720	5629	219
730	5635	153
740	5620	80
750	5133	425
760	5035	524
770	5035	506
780	5065	433
790	5087	312
800	5155	144
810	5241	33
820	5332	196
830	5343	280
840	5257	267
850	5065	157
860	4873	47
870	4886	133
880	5074	383
890	5233	560
900	5344	670
910	5368	664
920	5373	639
930	5352	567
940	5352	517
950	5378	491

TABLE II.- MEASURED RESULTS AT NOZZLE EXIT WITH NO NOZZLE DIAPHRAGM – Continued

(b) Pitot pressure – Continued

y = 6.35 cm; n = 1

Δt_1, μsec	p_t, N/m^2
0	0
10	204
20	309
30	411
40	588
50	858
60	1114
70	1663
80	1966
90	2517
100	5366
110	8409
120	10308
130	12532
140	14082
150	18810
160	19386
170	19801
180	18877
190	19279
200	18673
210	18683
220	18599
230	17386
240	15971
250	13698
260	10672
270	8690
280	7588
290	6409
300	5900
310	5485
320	4680
330	4177
340	3715
350	3482
360	3401
370	3336
380	3345
390	3396
400	3385
410	3331
420	3361
430	3447
440	3532
450	3685
460	3889
470	4076
480	4246
490	4297
500	4348
510	4374
520	4399
530	4439
540	4479
550	4543
560	4632
570	4722
580	4812
590	4907
600	4967
610	4965
620	4964
630	4963
640	5040
650	5126
660	5211
670	5327
680	5446
690	5566
700	5555
710	5539
720	5564
730	5615
740	5718
750	5793
760	5810
770	5826
780	5847
790	5881
800	5914
810	5938
820	5936
830	5981
840	6134
850	6309
860	6546
870	6711
880	6817
890	6789
900	6776
910	6819
920	6863
930	6906
940	7169
950	7534

(b) Pitot pressure – Concluded

y = 12.19 cm; n = 1

Δt_1, μsec	p_t, N/m^2
0	0
10	512
20	819
30	716
40	401
50	274
60	275
70	301
80	326
90	326
100	335
110	395
120	426
130	403
140	324
150	314
160	290
170	290
180	255
190	210
200	138
210	77
220	62
230	102
240	145
250	208
260	383
270	548
280	882
290	1380
300	1949
310	2637
320	3740
330	4625
340	6316
350	9257
360	10079
370	10652
380	10825
390	11849
400	14268
410	14341
420	13327
430	12262
440	11409
450	10004
460	9926
470	12580
480	12526
490	11765
500	12263
510	12535
520	12535
530	10309
540	9843
550	11137
560	9970
570	10156
580	7227
590	7091
600	6623
610	6138
620	6591
630	6738
640	6721
650	6661
660	6550
670	6395
680	6278
690	6345
700	6501
710	6650
720	6949
730	7138
740	7206
750	7148
760	7056
770	6919
780	6729
790	6539
800	6503
810	6480
820	6480
830	6500
840	6584
850	6744
860	6940
870	7093
880	7011
890	6903
900	6753
910	6502
920	6149
930	6153
940	6248
950	6367

TABLE II.- MEASURED RESULTS AT NOZZLE EXIT WITH NO NOZZLE DIAPHRAGM – Concluded

(c) Flow direction

$[\Delta t_1 = 100\ \mu\text{sec};\quad n = 1]$

y, cm	θ, deg	Estimated error, deg
0	-0.32	±0.39
2.54	.16	±.47
5.08	2.0	±1.1
7.62	3.6	±1.1
10.16	6.5	±1.0
12.70	8.5	±1.9

(d) Mach number (lower bound)

$[\Delta t_1 = 100\ \mu\text{sec};\quad n = 1]$

y, cm	M
0	8.6
2.54	7.2
5.08	8.4
7.62	5.4

TABLE III.- MEASURED RESULTS AT NOZZLE EXIT WITH EVACUATED NOZZLE

(a) Flow velocity

y, cm	Velocity and variance at –									
	Δt_1 = 250 μsec n = 2		Δt_1 = 350 μsec n = 3		Δt_1 = 450 μsec n = 5		Δt_1 = 550 μsec n = 6		Δt_1 = 700 μsec n = 1	Δt_1 = 800 μsec n = 1
	$\bar{u}$, m/sec	$\bar{S}$, m/sec	$\bar{u}$, m/sec	$\bar{S}$, m/sec	$\bar{u}$, m/sec	$\bar{S}$, m/sec	$\bar{u}$, m/sec	$\bar{S}$, m/sec	u, m/sec	u, m/sec
-2.58	4183	±10	3644	±81	3823	±89	3658	±42	3626	3652
-1.93	4096	120	3613	81	3773	80	3675	53	3772	3664
-1.29	4152	160	3693	108	3837	71	3667	37	3684	3620
-.65	4004	14	3706	92	3808	65	3638	37	3724	3644
.00	4071	160	3730	88	3834	62	3680	38	3840	3716
.65	4101	180	3716	42	3859	33	3698	39	3773	3693
1.29	4167	180	3771	61	3917	65	3729	53	3843	3796
1.94	4101	210	3764	35	3907	80	3744	39	3724	3831
2.58	4008	130	3816	46	3913	77	3813	31	3739	3935
3.23	4000	130	3767	61	3934	77	3789	39	3702	3952
3.88	4142	140	3797	24	3939	59	3895	56	3743	3911
4.52	4191	230	3757	29	3937	62	3818	37	3681	3887
5.17	4185	190	3814	11	3938	68	3891	39	3692	3891
5.81	4081	68	3802	32	3917	80	3841	48	3580	3865
6.46	4082	19	3827	35	3967	43	3897	42	3627	3862
7.11	4078	160	3829	58	3956	37	3865	42	3609	3831
7.53	4100	160	3891	58	3954	26	3896	56	3633	3880
8.40	4145	160	3888	58	3944	37	3861	62	3640	3872
9.04	4172	146	3922	69	3942	31	3924	70	3696	3952
9.69	4190	110	3910	54	3901	34	3870	73	3730	3933
10.34	4261	88	3961	58	3893	34	3933	73	3758	3927
10.98	4188	54	3933	58	3862	43	3877	70	3734	3904
11.63	4230	24	3995	54	3867	49	3906	76	3690	3855
12.27	4060	100	4001	31	3806	40	3829	70	3669	3804
12.92	3651	590	4002	42	3804	43	3862	67	3700	3773
13.57	3832	310	3937	26	3733	26	3763	59	3762	3738
14.21	----	---	3942	127	3669	40	3751	96	3605	3526

TABLE III.- MEASURED RESULTS AT NOZZLE EXIT WITH EVACUATED NOZZLE – Continued

(a) Flow velocity – Concluded

y, cm	Velocity and estimated variance at –	
	Δt_1 = 350 μsec to 550 μsec n = 14	
	$\bar{u}$, m/sec	$\bar{S}$, m/sec
-2.58	3714	±44
-1.93	3697	41
-1.29	3733	41
-.65	3713	38
.00	3746	37
.65	3760	39
1.29	3805	40
1.94	3807	38
2.58	3850	33
3.23	3836	38
3.88	3890	33
4.52	3848	32
5.17	3892	31
5.81	3860	36
6.46	3907	27
7.11	3890	28
7.53	3915	28
8.40	3897	31
9.04	3930	33
9.69	3890	34
10.34	3924	34
10.98	3884	35
11.63	3911	38
12.27	3858	38
12.92	3871	38
13.57	3789	34
14.21	3762	55

TABLE III.- MEASURED RESULTS AT NOZZLE EXIT WITH EVACUATED NOZZLE – Continued

(b) Pitot pressure (bare rake probes)

y = 0 cm; n = 2

Δt_1, μsec	$\bar{p}_t$, N/m^2	$\bar{S}$, N/m^2
0	188	± 152
10	464	201
20	636	125
30	670	151
40	567	129
50	457	13
60	461	44
70	531	17
80	681	117
90	737	125
100	720	111
110	639	31
120	583	9
130	561	10
140	555	46
150	528	38
160	530	35
170	495	32
180	497	29
190	585	61
200	745	174
210	911	241
220	782	6
230	529	345
240	417	419
250	283	223
260	340	65
270	488	38
280	624	114
290	872	66
300	1046	117
310	1215	± 152
320	1294	164
330	1345	175
340	1453	186
350	1529	199
360	1611	220
370	1598	182
380	1660	192
390	1710	127
400	1680	144
410	1703	186
420	1743	397
430	1766	396
440	1589	91
450	1299	63
460	1192	82
470	1131	58
480	1022	45
490	968	30
500	951	117
510	783	7
520	753	2
530	813	67
540	802	45
550	838	10
560	891	18
570	994	8

TABLE III.- MEASURED RESULTS AT NOZZLE EXIT WITH EVACUATED NOZZLE – Continued

(b) Pitot pressure (bare rake probes) – Continued

y = 4.45 cm; n = 2

Δt_1, μsec	$\bar{p}_t$, N/m^2	$\bar{S}$, N/m^2
0	466	± 430
10	644	343
20	873	306
30	996	244
40	852	52
50	818	13
60	920	28
70	1028	62
80	1091	85
90	1127	95
100	1117	113
110	1054	131
120	1009	249
130	1067	330
140	1087	356
150	1008	360
160	797	200
170	805	269
180	756	298
190	426	50
200	490	272
210	690	361
220	999	346
230	1089	480
240	878	714
250	647	651
260	353	325
270	120	8
280	663	393
290	886	474
300	1154	327
310	1214	452
320	1142	638
330	1250	719
340	1374	696
350	1414	280
360	1599	216
370	1968	401
380	2251	542
390	2418	600
400	2498	540
410	2331	296
420	2164	146
430	2198	250

Δt_1, μsec	$\bar{p}_t$, N/m^2	$\bar{S}$, N/m^2
440	2205	± 437
450	1979	730
460	2108	902
470	2603	694
480	3081	393
490	2813	663
500	2372	919
510	2268	816
520	2262	756
530	2247	752
540	2226	796
550	2182	839
560	2088	874
570	2046	871
580	2202	703
590	2490	544
600	2593	734
610	2739	1057
620	3058	1254
630	3327	1310
640	3631	1247
650	3862	1142
660	4071	1048
670	4107	1043
680	4088	1008
690	4055	968
700	3905	1061
710	3745	1177
720	3911	1074
730	4129	1025
740	4128	1014
750	4025	1018
760	3934	995
770	3967	1024
780	4082	1122
790	4406	1015
800	4677	817
810	4816	599
820	4953	409
830	4995	324
840	4978	340
850	5239	77
860	5722	408

TABLE III.- MEASURED RESULTS AT NOZZLE EXIT WITH EVACUATED NOZZLE – Continued

(b) Pitot pressure (bare rake probes) – Continued

y = 8.89 cm; n = 2

Δt_1, μsec	$\bar{p}_t$, N/m^2	$\bar{S}$, N/m^2
0	166	± 129
10	278	140
20	387	161
30	341	212
40	248	138
50	213	22
60	184	153
70	152	149
80	146	33
90	265	199
100	436	373
110	436	297
120	209	65
130	93	3
140	88	4
150	121	26
160	174	77
170	219	120
180	212	103
190	264	37
200	412	110
210	719	326
220	1259	812
230	1959	1345
240	2541	1438
250	2226	549
260	2293	291
270	2594	484
280	3017	656
290	3234	756
300	3227	863
310	3218	874
320	3257	851
330	3410	757
340	3599	720
350	3796	616
360	4130	676
370	4608	898
380	5058	1052
390	5190	1047
400	5213	927
410	5281	708
420	5637	645
430	6133	767

Δt_1, μsec	$\bar{p}_t$, N/m^2	$\bar{S}$, N/m^2
440	6668	± 921
450	6988	1092
460	7092	1177
470	6826	1101
480	6423	1179
490	6462	1371
500	6800	1575
510	5867	458
520	5860	283
530	6051	418
540	6314	610
550	6432	683
560	6431	746
570	6694	1115
580	7070	1654
590	7245	1884
600	7190	1884
610	7034	1760
620	6918	1643
630	6810	1426
640	6684	1081
650	6750	911
660	6857	836
670	6891	804
680	6915	783
690	6912	749
700	6893	714
710	7156	756
720	7548	913
730	7705	1073
740	7514	1298
750	7365	1431
760	7499	1298
770	7593	1226
780	7599	1215
790	7400	1385
800	7336	1378
810	7432	1249
820	7643	1118
830	7833	1092
840	7885	1280
850	7842	1431
860	7657	1382

TABLE III.- MEASURED RESULTS AT NOZZLE EXIT WITH EVACUATED NOZZLE – Continued

(b) Pitot pressure (bare rake probes) – Continued

y = 13.34 cm; n = 2

Δt_1, μsec	$\bar{p}_t$, N/m^2	$\bar{S}$, N/m^2
0	495	± 43
10	477	22
20	441	17
30	439	21
40	423	40
50	404	56
60	371	24
70	372	26
80	361	16
90	328	6
100	296	37
110	265	71
120	229	110
130	251	91
140	226	28
150	254	34
160	320	58
170	310	69
180	282	97
190	214	88
200	121	49
210	7	6
220	14	14
230	89	86
240	181	175
250	470	314
260	961	524
270	1626	667
280	2396	1150
290	4021	656
300	4643	376
310	4590	538
320	4713	512
330	4758	554
340	4844	801
350	5157	658
360	5357	194
370	5976	418
380	6041	621
390	5877	897
400	6328	905
410	6922	869
420	6838	948
430	7061	75

Δt_1, μsec	$\bar{p}_t$, N/m^2	$\bar{S}$, N/m^2
440	6321	± 308
450	5962	15
460	5930	651
470	4438	614
480	4502	111
490	3681	161
500	3385	370
510	4067	839
520	4032	1094
530	4089	1049
540	4506	701
550	4713	812
560	5493	844
570	5334	1198
580	5047	994
590	4634	856
600	5392	606
610	5438	1011
620	5000	1278
630	5683	438
640	5021	1364
650	6102	814
660	5801	1150
670	5878	1122
680	6081	906
690	5591	1065
700	5441	623
710	5117	763
720	5140	1234
730	5205	1590
740	5442	1462
750	5297	1226
760	5077	1095
770	5108	693
780	4974	635
790	5083	533
800	4814	993
810	5070	1187
820	5565	1226
830	5366	1539
840	5172	1781
850	5602	1436
860	6008	1120

TABLE III.- MEASURED RESULTS AT NOZZLE EXIT WITH EVACUATED NOZZLE – Continued

(b) Pitot pressure (single probes) – Continued

y = 0 cm; n = 2

Δt_1, μsec	$\bar{p}_t$, N/m^2	$\bar{S}$, N/m^2
0	0	± 0
10	53	21
20	121	20
30	159	11
40	173	13
50	206	15
60	256	17
70	304	20
80	316	31
90	313	28
100	334	34
110	375	66
120	409	99
130	407	97
140	402	83
150	419	84
160	438	103
170	459	109
180	473	64
190	531	4
200	557	21
210	561	10
220	571	33
230	602	81
240	613	153
250	570	170
260	618	145
270	721	50
280	752	51
290	711	116
300	750	108
310	882	78
320	1033	44
330	1091	34
340	1126	13
350	1189	6
360	1253	35
370	1291	63
380	1325	35
390	1359	0
400	1384	17
410	1405	57
420	1353	34
430	1279	118
440	1519	± 49
450	1797	8
460	1904	66
470	2106	473
480	2355	654
490	2356	557
500	2214	570
510	2182	514
520	2208	384
530	2375	442
540	2606	567
550	2646	588
560	2423	713
570	2717	607
580	2895	640
590	2906	576
600	2714	414
610	2643	254
620	2786	238
630	2908	368
640	3233	744
650	3326	864
660	3323	659
670	3253	534
680	3541	705
690	3512	681
700	3429	648
710	3712	798
720	3943	1016
730	4011	1162
740	4069	1268
750	4406	863
760	4410	772
770	4520	693
780	4546	864
790	4690	1142
800	5166	1279
810	5318	1552
820	5484	1671
830	5602	1467
840	5718	1093
850	5602	1205
860	6126	1274

TABLE III.- MEASURED RESULTS AT NOZZLE EXIT WITH EVACUATED NOZZLE – Continued

(b) Pitot pressure (single probes) – Concluded

y = 3.81 cm; n = 4

Δt_1, μsec	$\bar{p}_t$, N/m^2	$\bar{S}$, N/m^2
0	0	± 0
10	74	19
20	200	40
30	301	53
40	392	58
50	472	67
60	571	71
70	655	70
80	708	60
90	779	64
100	845	59
110	911	50
120	965	38
130	1000	31
140	1005	27
150	1000	26
160	1017	25
170	1046	37
180	1054	38
190	1050	40
200	1035	42
210	1023	48
220	994	67
230	948	84
240	948	93
250	1032	91
260	1074	99
270	962	88
280	873	64
290	784	94
300	778	118
310	866	70
320	961	125
330	971	130
340	958	122
350	946	146
360	1109	114
370	1308	91
380	1496	111
390	1536	144
400	1602	213
410	1695	194
420	2019	298
430	2613	306

Δt_1, μsec	$\bar{p}_t$, N/m^2	$\bar{S}$, N/m^2
440	3098	± 393
450	3224	358
460	3240	237
470	3603	329
480	4067	358
490	4420	530
500	4578	641
510	4214	464
520	4284	504
530	4817	737
540	4849	729
550	4790	662
560	5259	736
570	5444	810
580	5271	766
590	5324	839
600	5736	585
610	6308	606
620	6852	706
630	7226	846
640	7064	720
650	7155	792
660	6972	647
670	6859	506
680	7079	662
690	7370	805
700	7837	952
710	7851	1125
720	7819	775
730	7873	339
740	8402	529
750	8787	454
760	8365	584
770	8003	480
780	8481	617
790	9644	669
800	10146	732
810	9416	530
820	8641	526
830	9092	613
840	9640	905
850	9541	1024
860	9696	1052

TABLE III.- MEASURED RESULTS AT NOZZLE EXIT WITH EVACUATED NOZZLE – Continued

(c) Flow direction

$[\Delta t_1 = 550\ \mu\text{sec};\ n = 5]$

y, cm	θ, deg	$\bar{S}$, deg
0	-0.45	±0.37
2.54	.54	±.43
5.08	.87	±.49
7.62	2.37	±.34
10.16	3.99	±.42
12.70	5.03	±.39

(d) Mach number (lower bound)

$[\Delta t_1 = 550\ \mu\text{sec}]$

y, cm	M	$\bar{S}$	n
0	8.53	±0.73	3
2.54	10.15	±.88	3
5.08	6.96	±.08	3
7.62	6.67	±.19	2
10.16	6.16	±.23	3
12.70	6.94	±.22	3

TABLE III.- MEASURED RESULTS AT NOZZLE EXIT WITH EVACUATED NOZZLE – Concluded

(e) Flat-plate pressure; y = 3.81 cm; n = 3

Δt_1, μsec	$\bar{p}_t$, N/m^2	$\bar{S}$, N/m^2
0	0	± 0
10	3	1
20	11	2
30	19	0
40	24	1
50	26	2
60	29	2
70	34	4
80	39	6
90	40	7
100	42	6
110	45	5
120	47	4
130	49	3
140	50	3
150	51	3
160	52	3
170	53	3
180	56	2
190	58	2
200	59	1
210	59	0
220	59	1
230	59	2
240	58	3
250	56	2
260	56	1
270	55	2
280	53	1
290	52	2
300	49	4
310	44	6
320	40	8
330	35	7
340	33	6
350	34	7
360	36	9
370	39	10
380	41	11
390	43	11
400	45	11
410	48	10
420	51	9
430	53	8
440	53	± 8
450	55	9
460	57	10
470	58	11
480	61	12
490	63	13
500	65	13
510	66	14
520	68	14
530	71	17
540	76	20
550	79	22
560	80	23
570	78	22
580	77	20
590	74	17
600	73	14
610	76	14
620	80	17
630	83	20
640	83	19
650	80	15
660	82	14
670	83	12
680	84	12
690	86	11
700	91	14
710	93	15
720	92	13
730	90	12
740	92	13
750	97	16
760	100	16
770	109	17
780	111	15
790	114	15
800	119	15
810	120	14
820	120	14
830	122	14
840	124	14
850	125	15
860	128	16

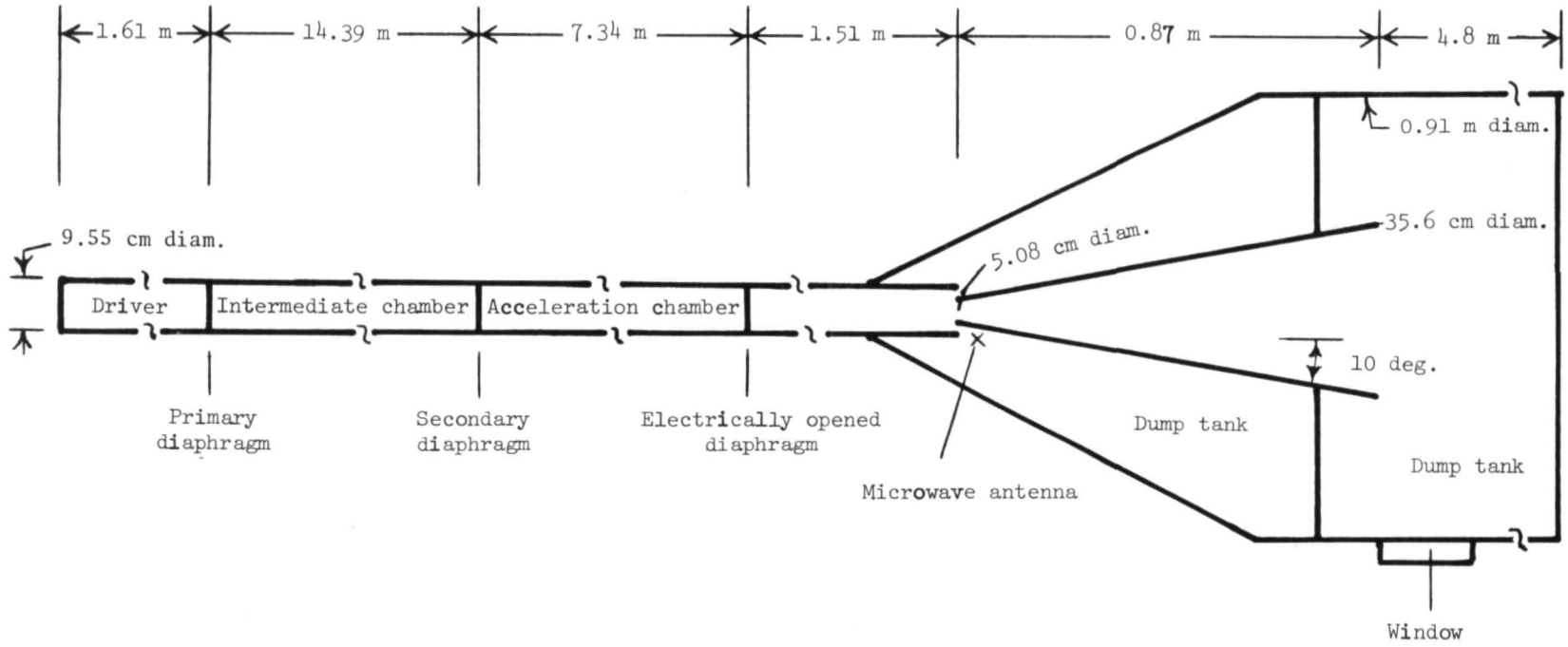

(a) Sketch of facility.

Figure 1.- Pilot model expansion tunnel.

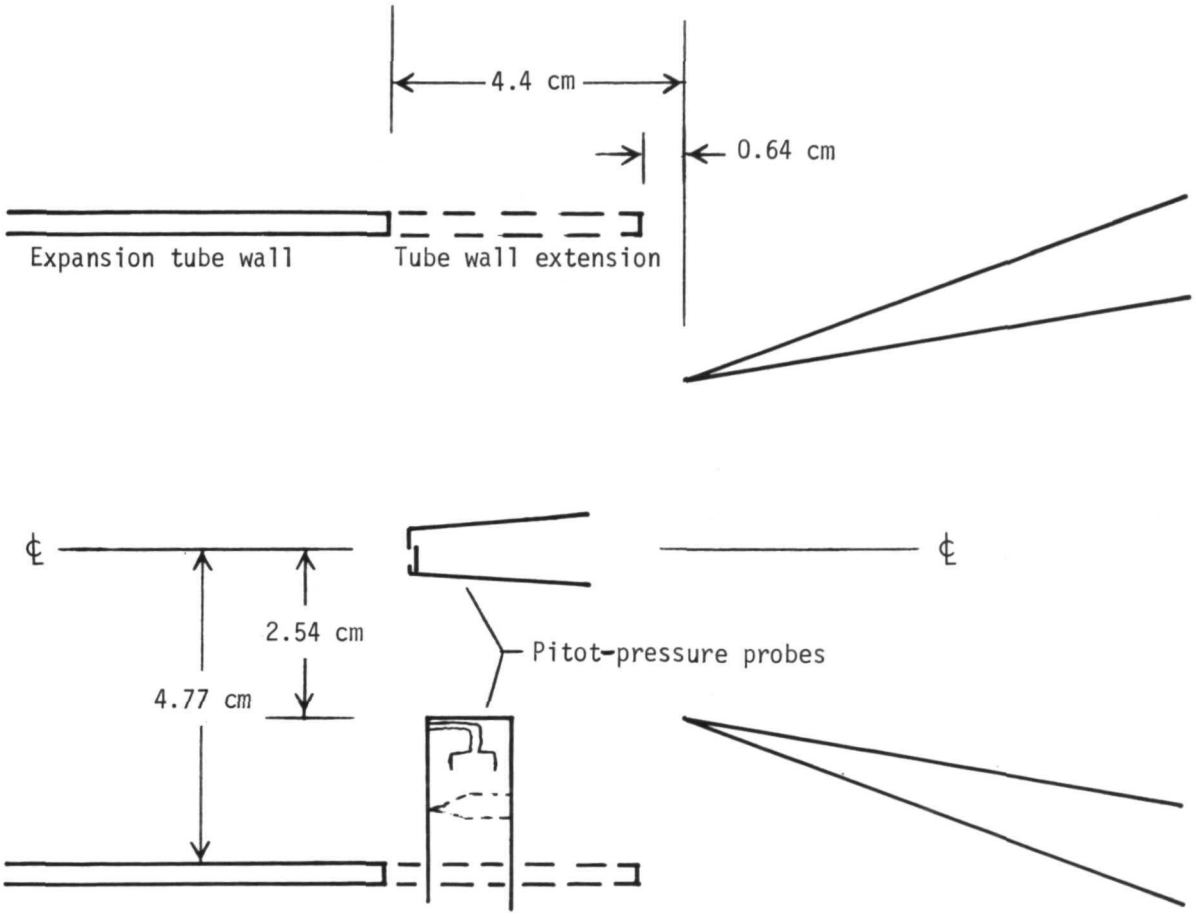

(b) Sketch of nozzle entrance.

Figure 1.- Concluded.

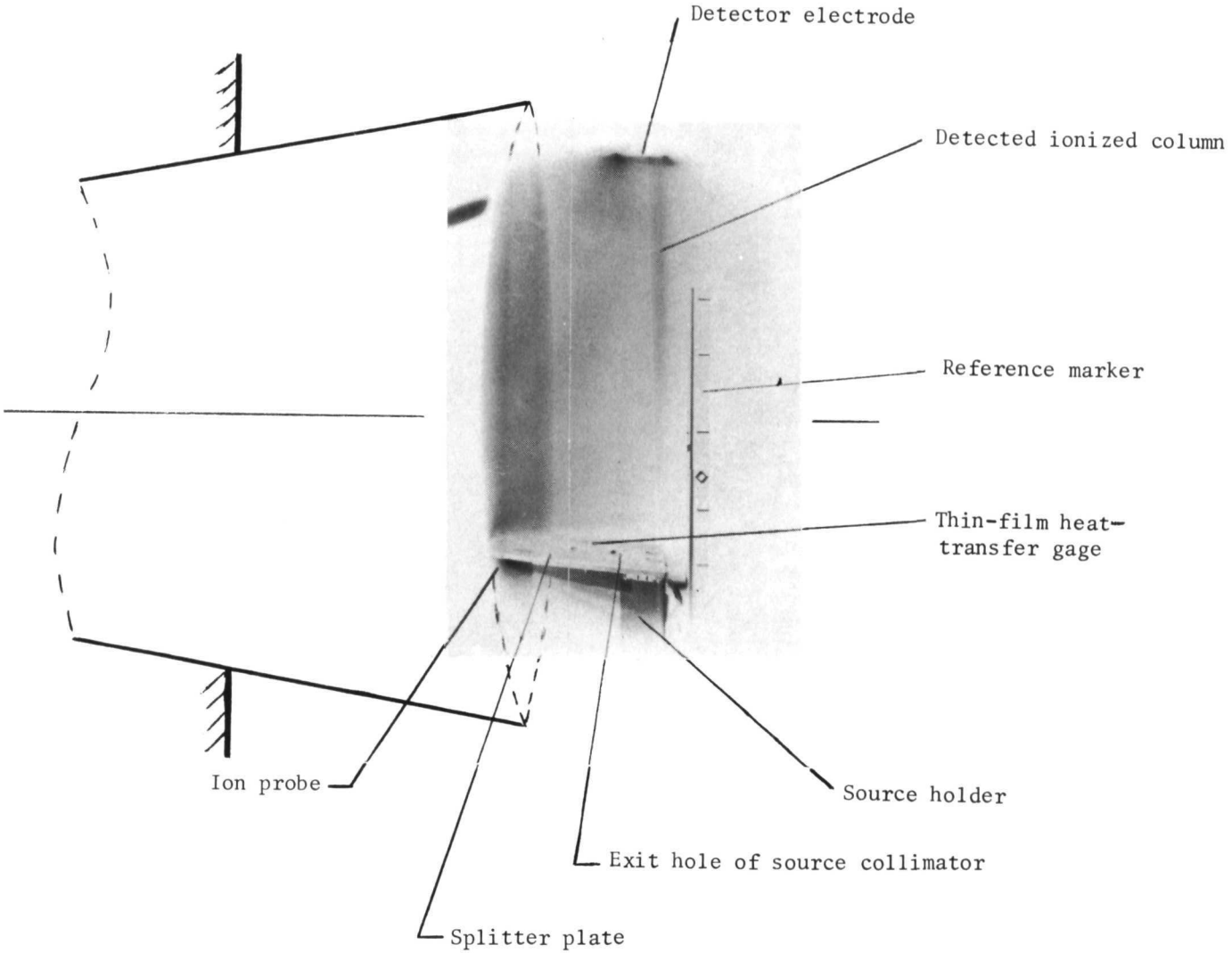

L-73-3099

Figure 2.- Sample velocity data photograph showing relative location of nozzle exit. Evacuated nozzle; Δt_1 = 450 μsec.

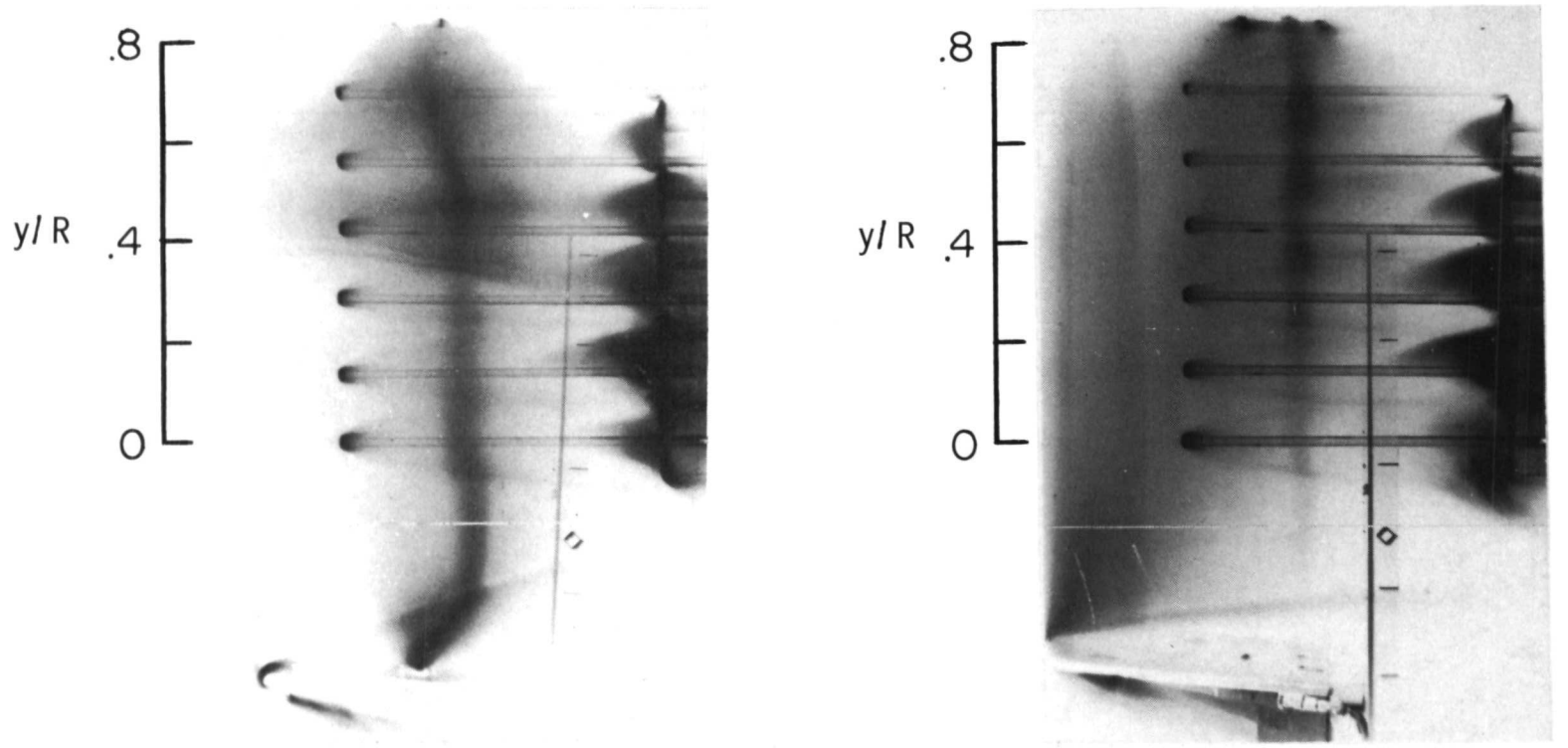

Δt_1 = 100 μsec

No nozzle diaphragm

Δt_1 = 550 μsec

Evacuated nozzle

L-73-3100

Figure 3.- Sample flow direction data.

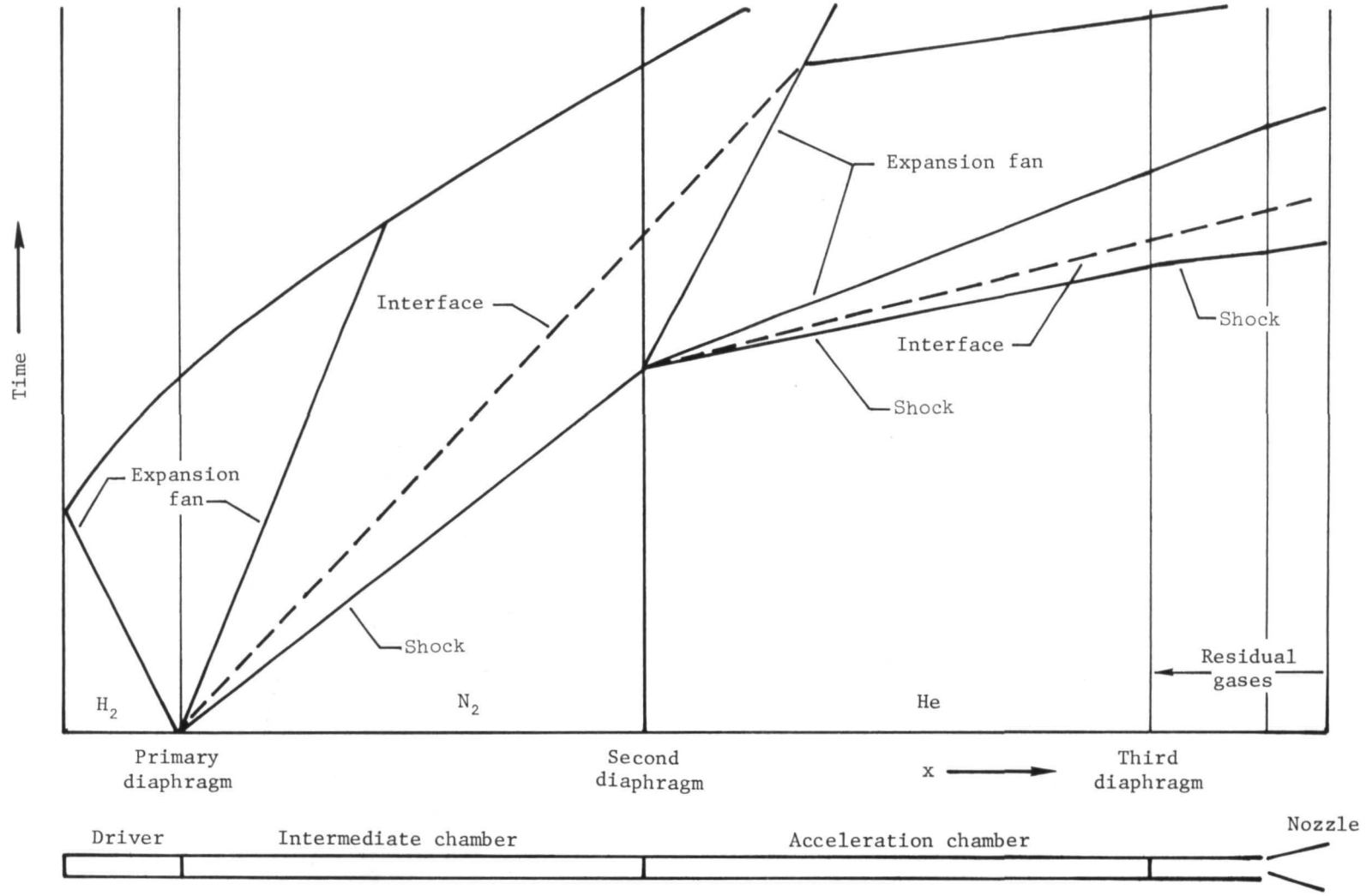

(a) Complete flow cycle.

Figure 4.- Operating flow cycle in expansion tunnel.

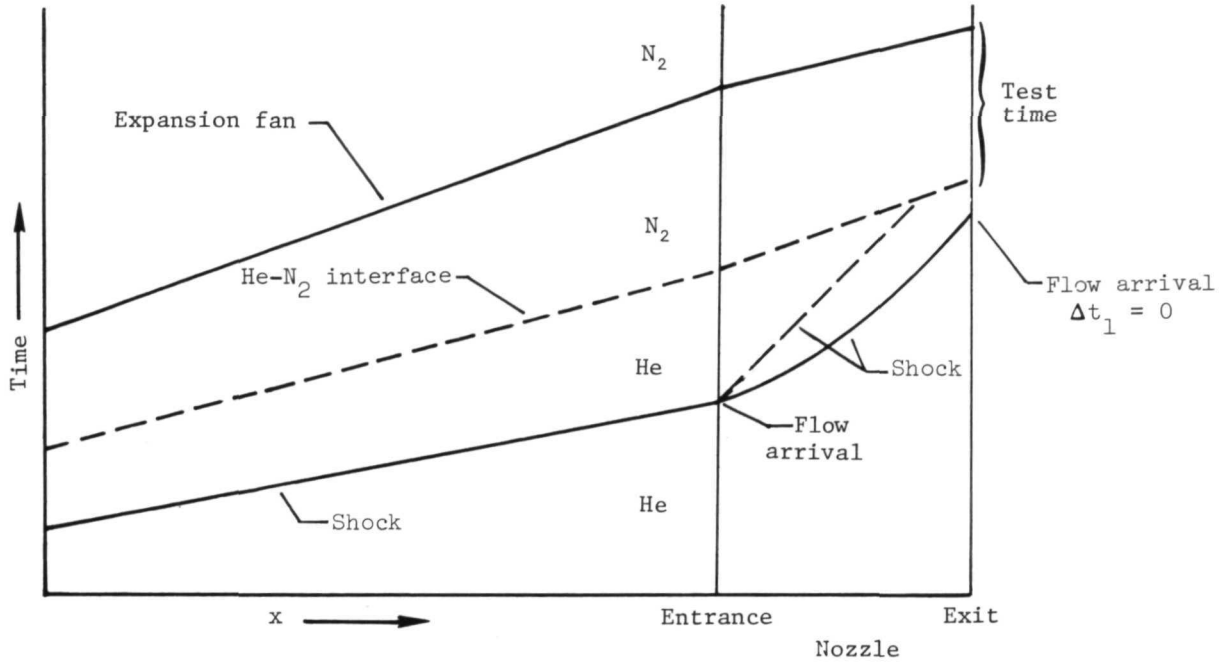

(b) Flow cycle for no-third-diaphragm case.

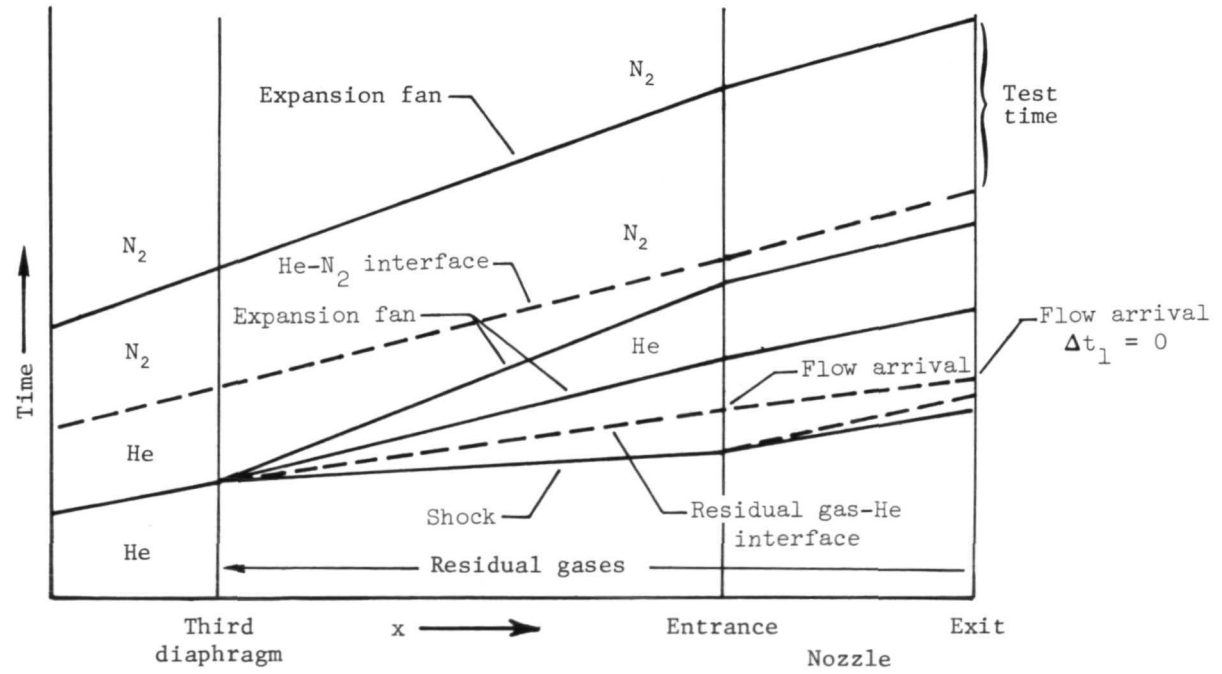

(c) Flow cycle for evacuated-nozzle case.

Figure 4.- Concluded.

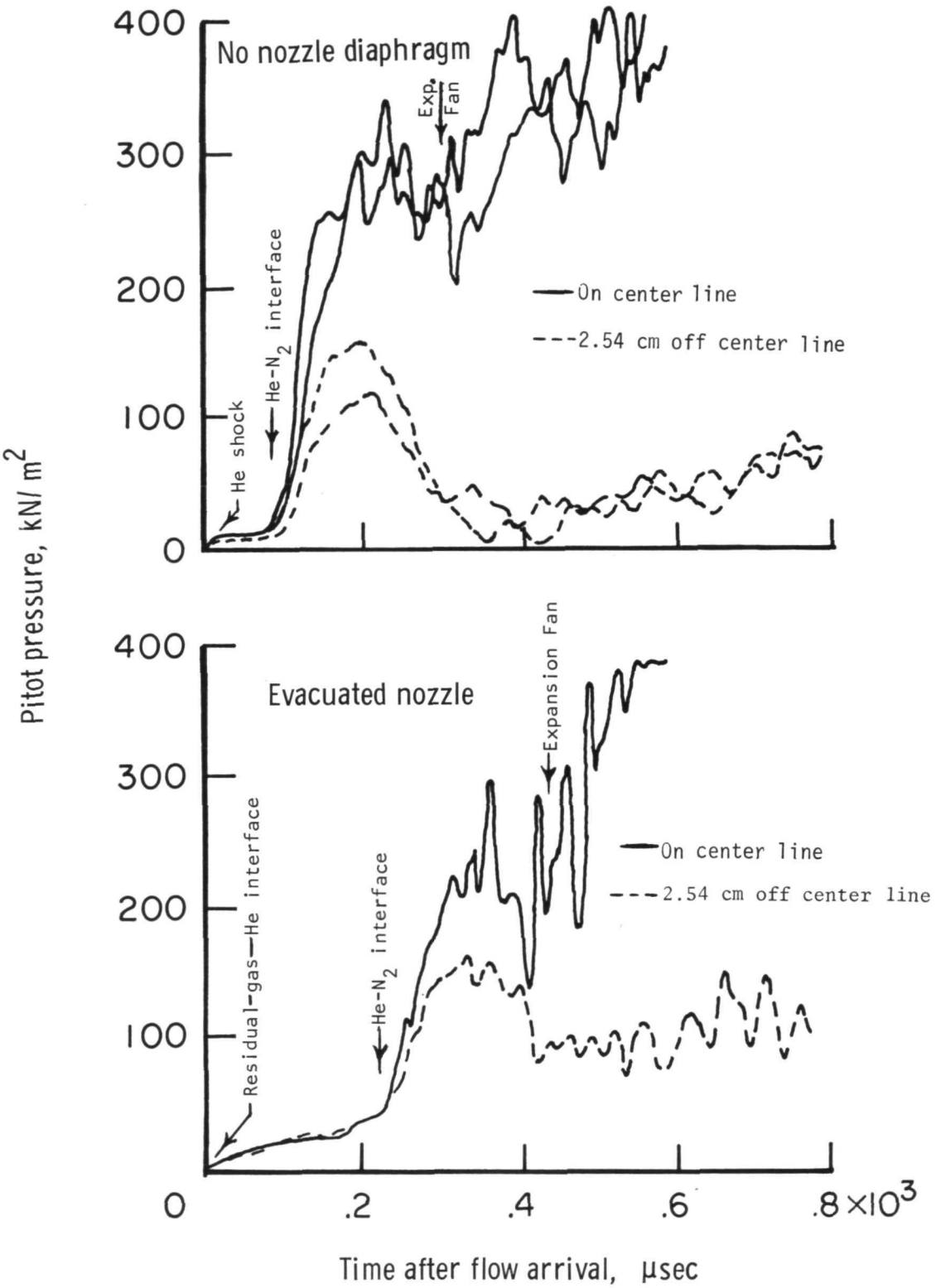

Figure 5.- Pitot pressure at nozzle entrance.

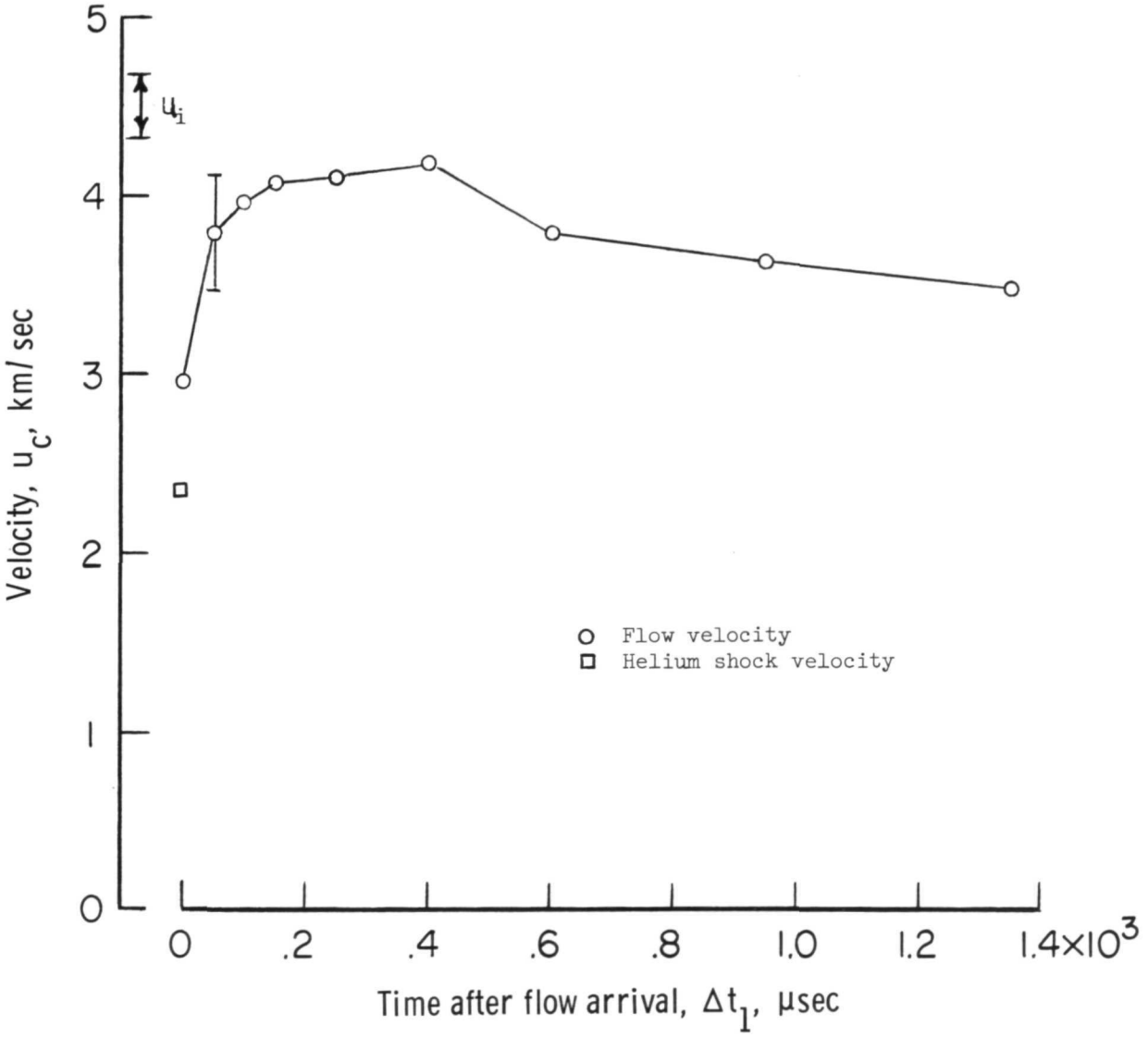

Figure 6.- Flow velocity on tunnel center line at nozzle exit. No nozzle diaphragm.

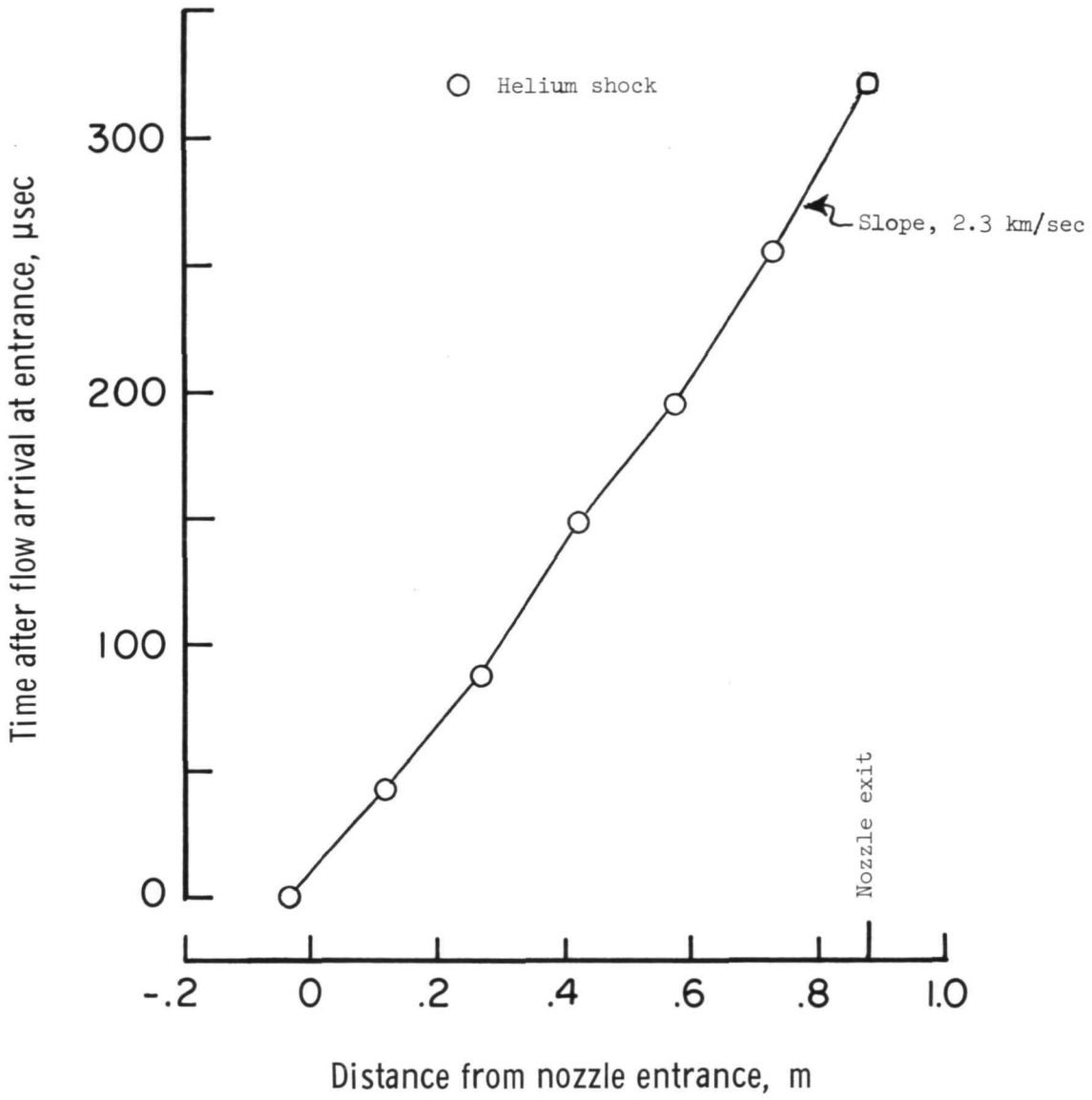

Figure 7.- Transit of helium shock through nozzle. No nozzle diaphragm.

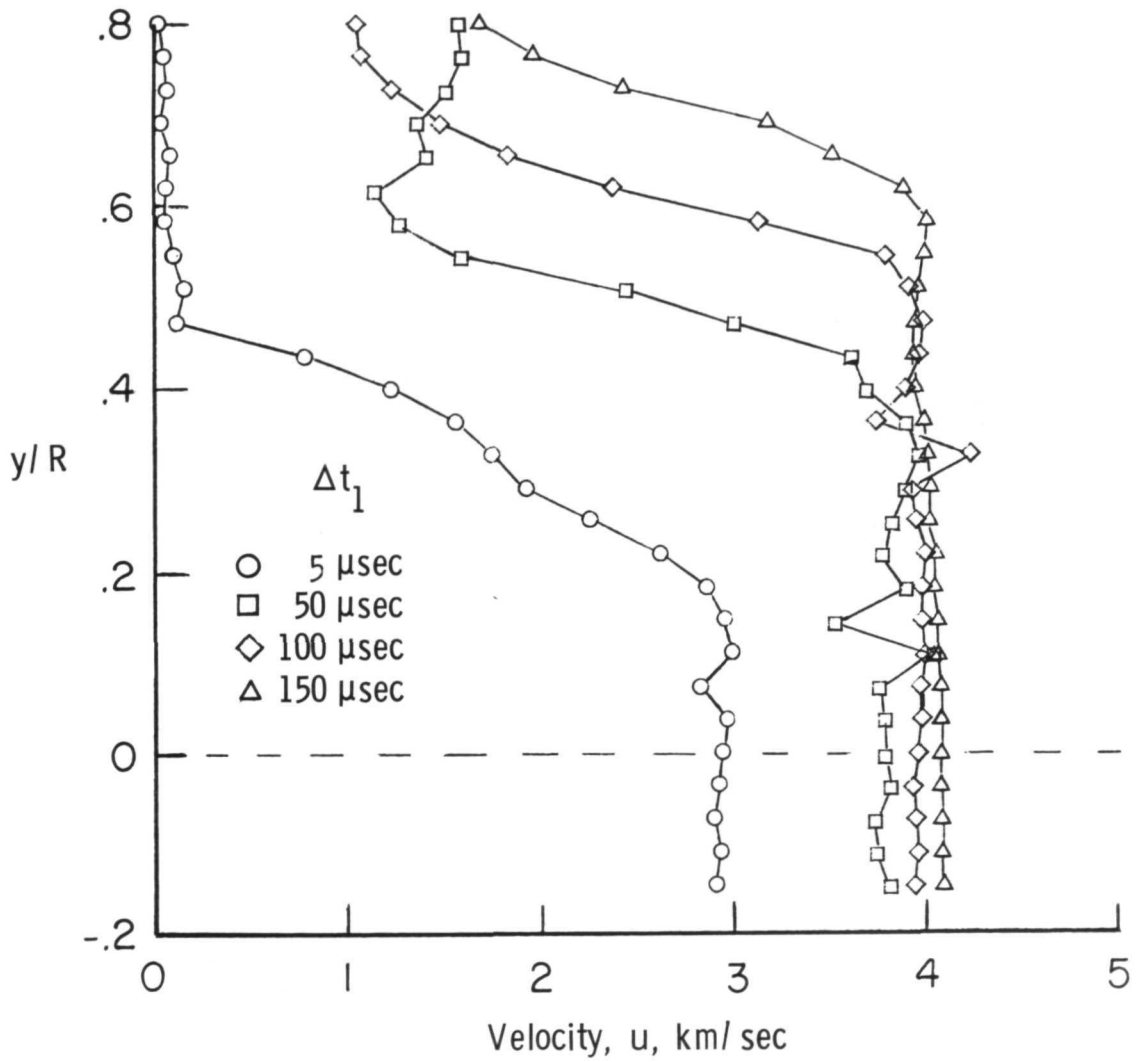

Figure 8.- Flow velocity. No nozzle diaphragm.

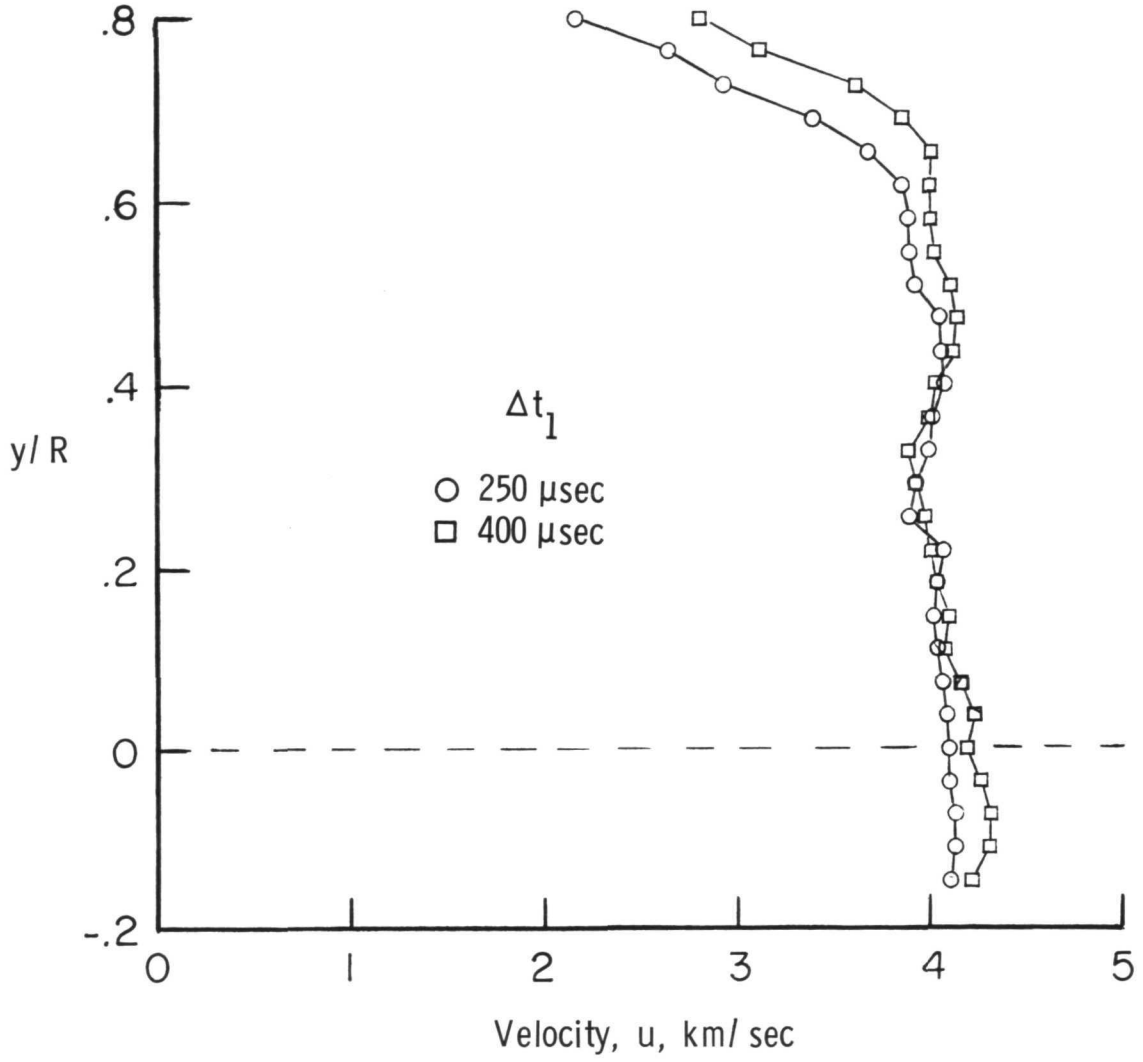

Figure 8.- Continued.

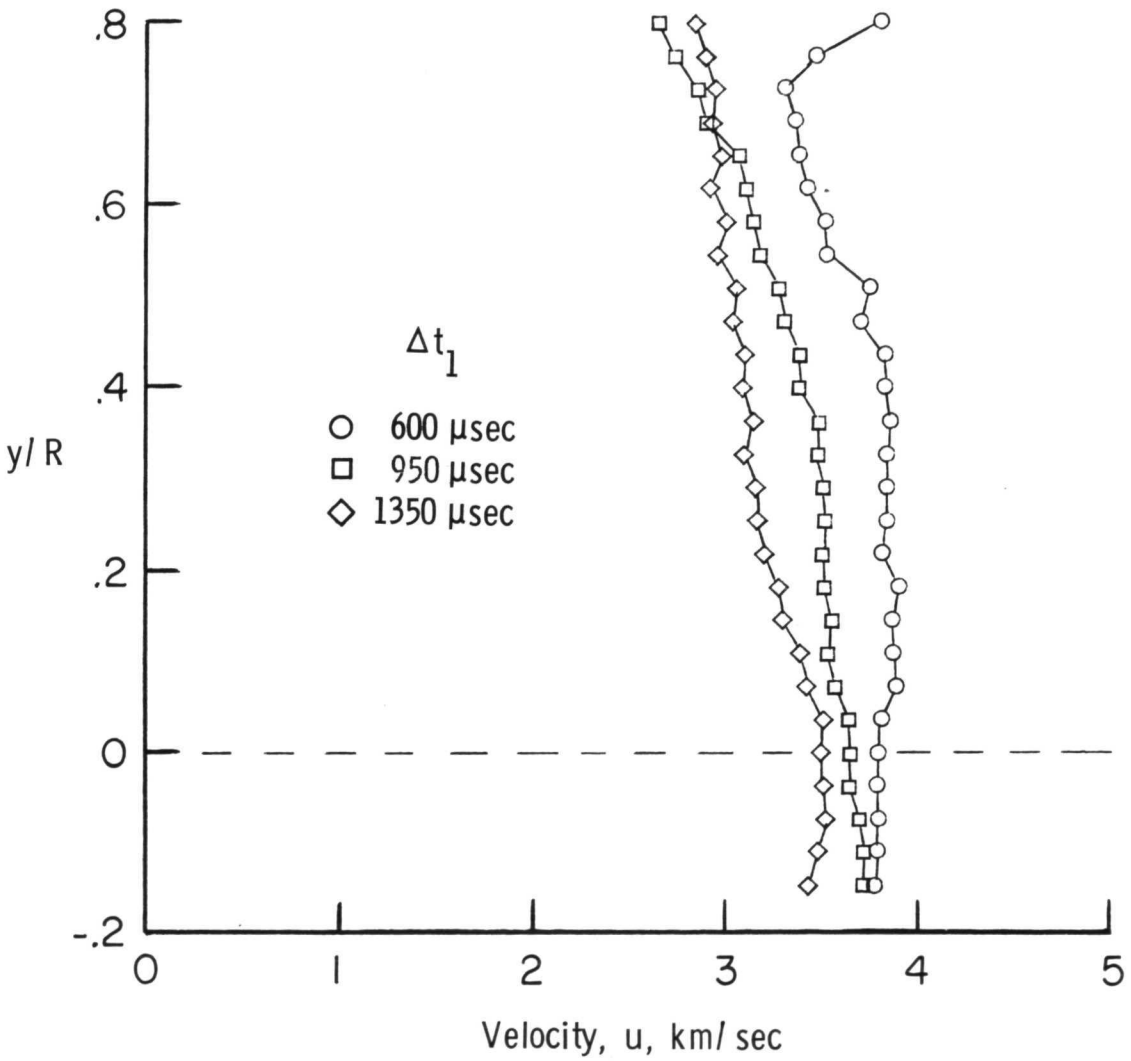

Figure 8.- Concluded.

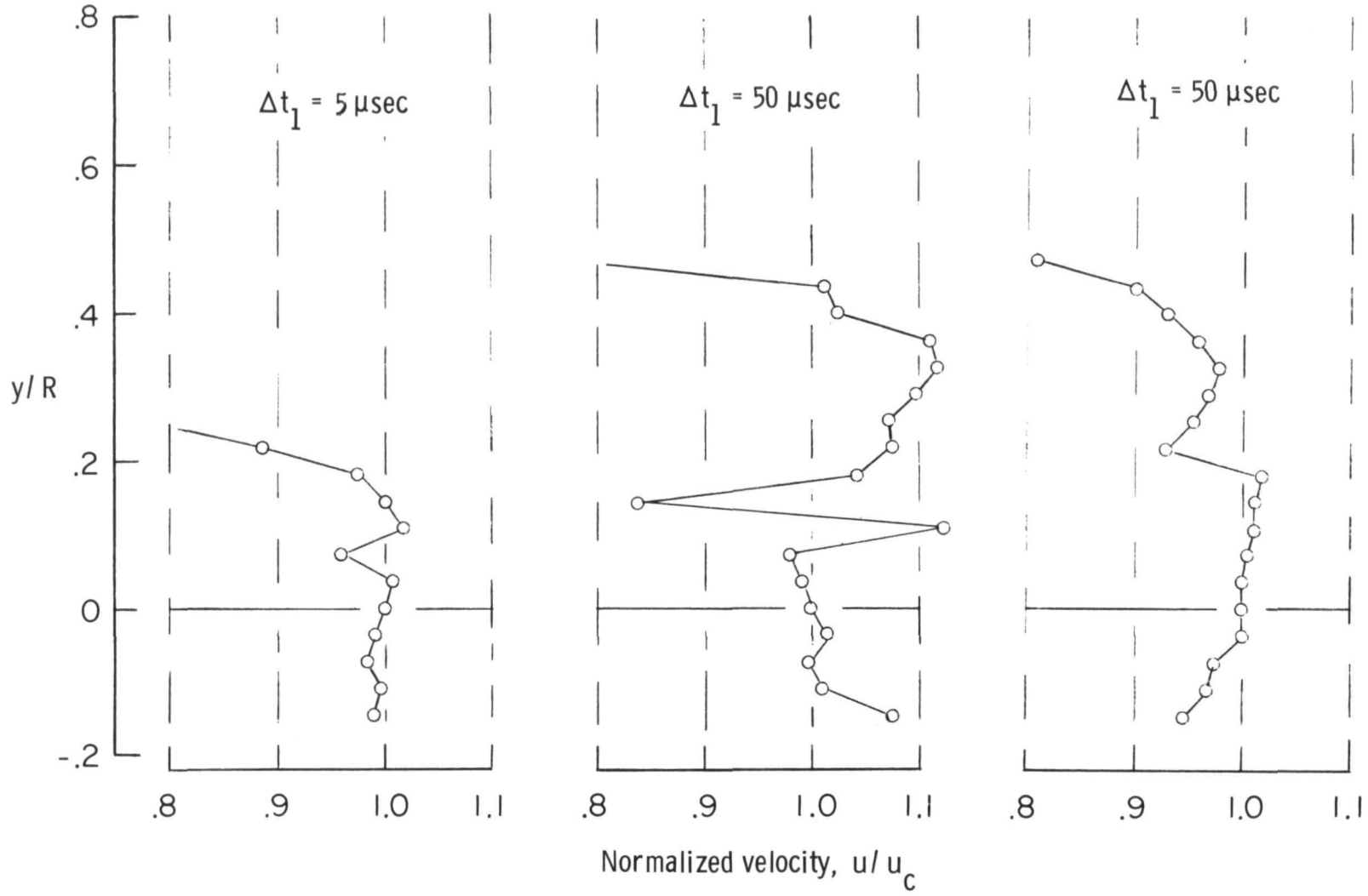

Figure 9.- Flow velocity profile. No nozzle diaphragm.

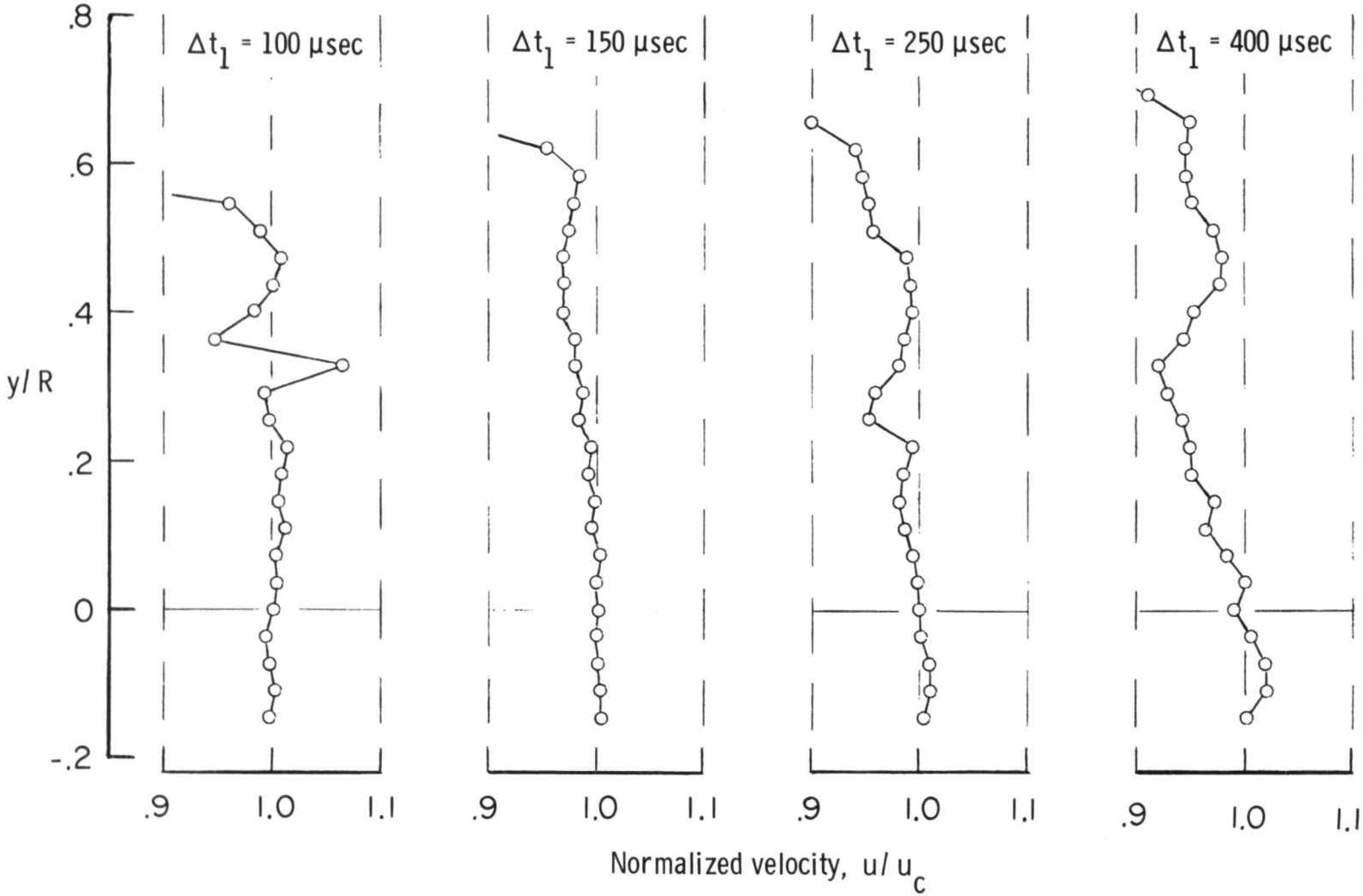

Figure 9.- Continued.

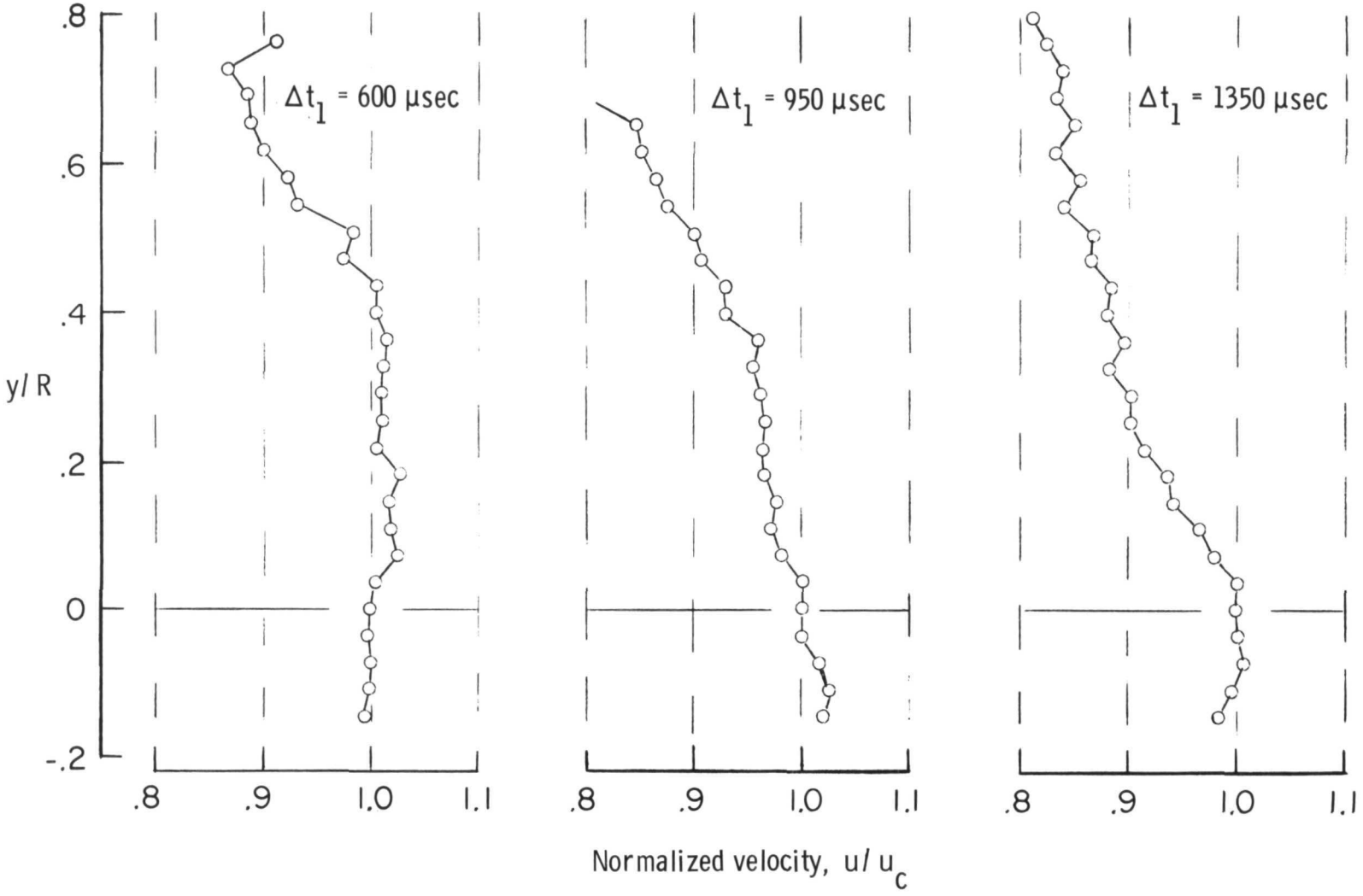

Figure 9.- Concluded.

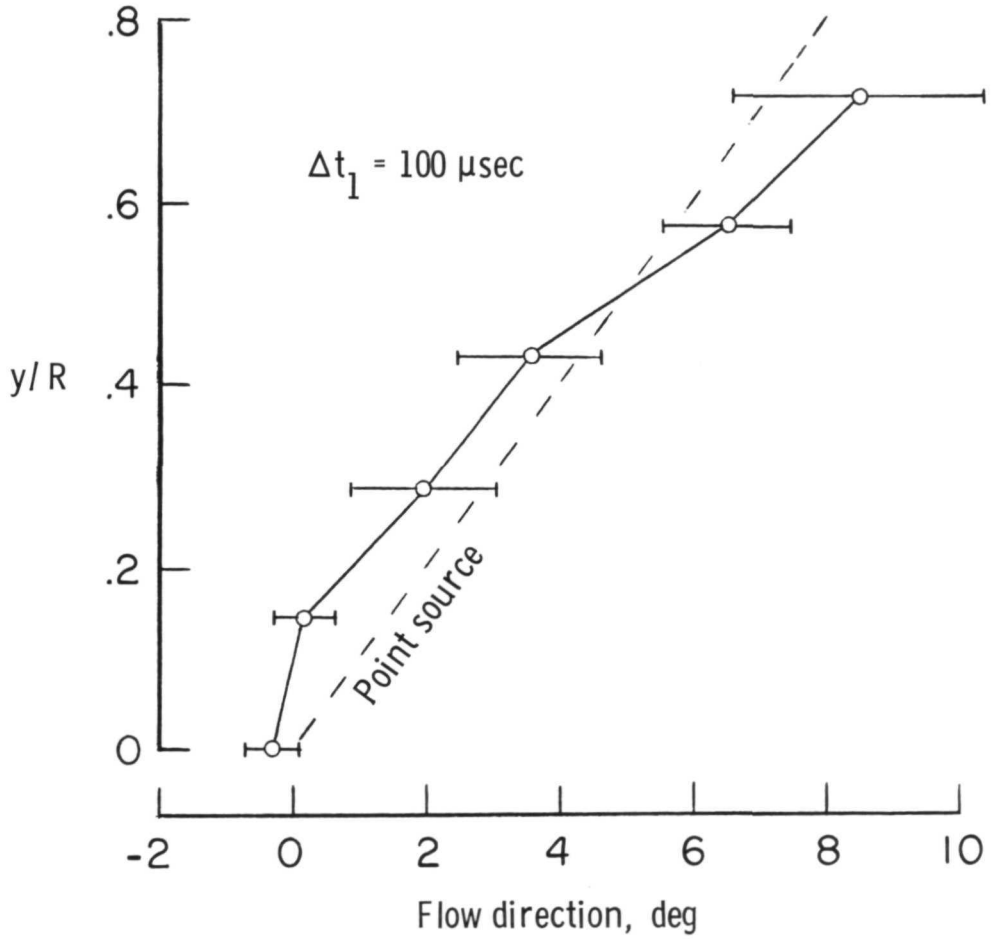

Figure 10.- Flow direction. No nozzle diaphragm.

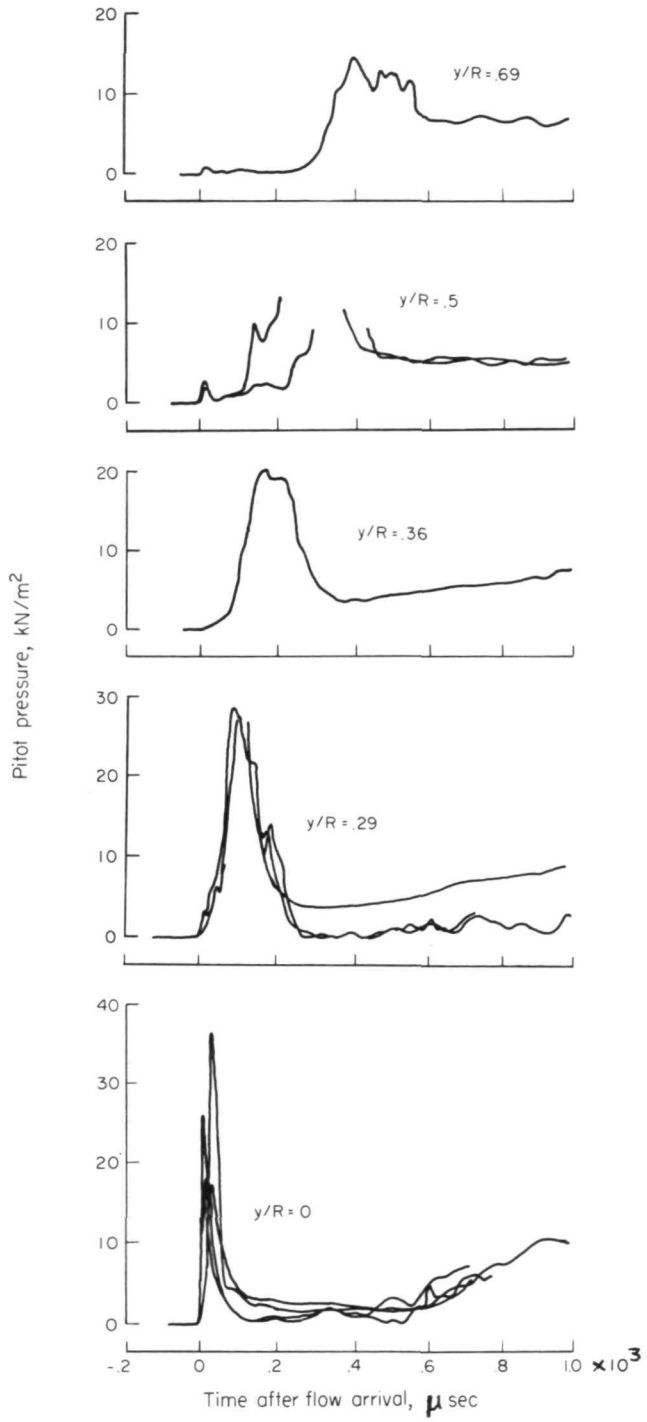

Figure 11.- Pitot pressure. No nozzle diaphragm.

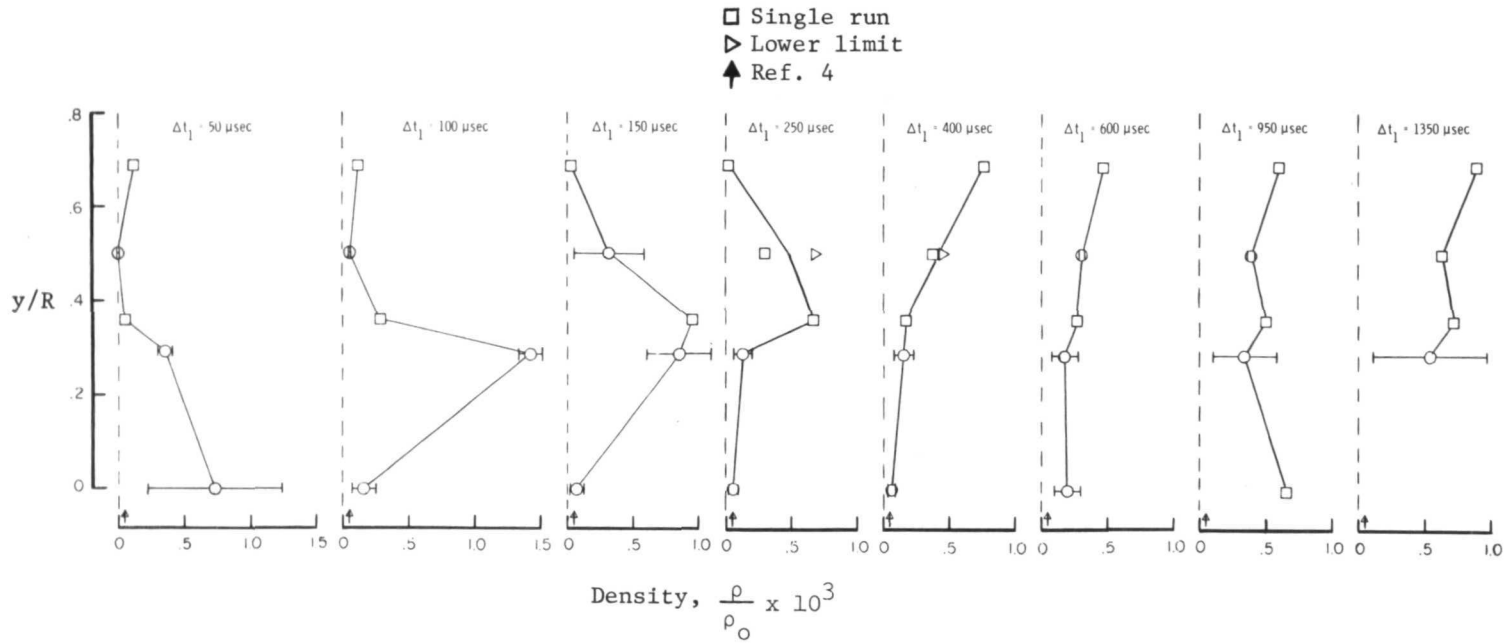

Figure 12.- Density. No nozzle diaphragm.

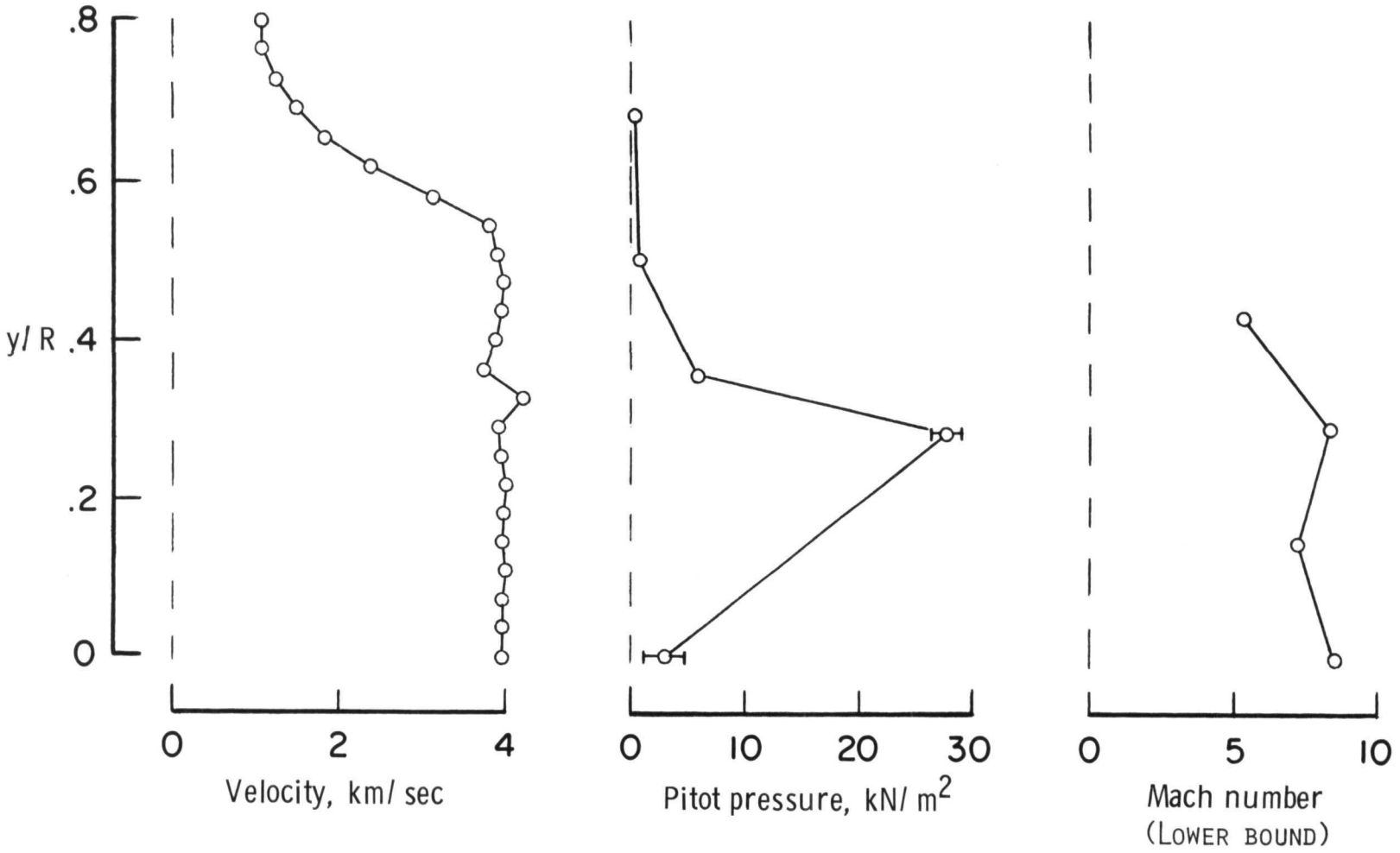

(a) Measured quantities.

Figure 13.- Measured and derived results at $\Delta t_1 = 100$ μsec. No nozzle diaphragm.

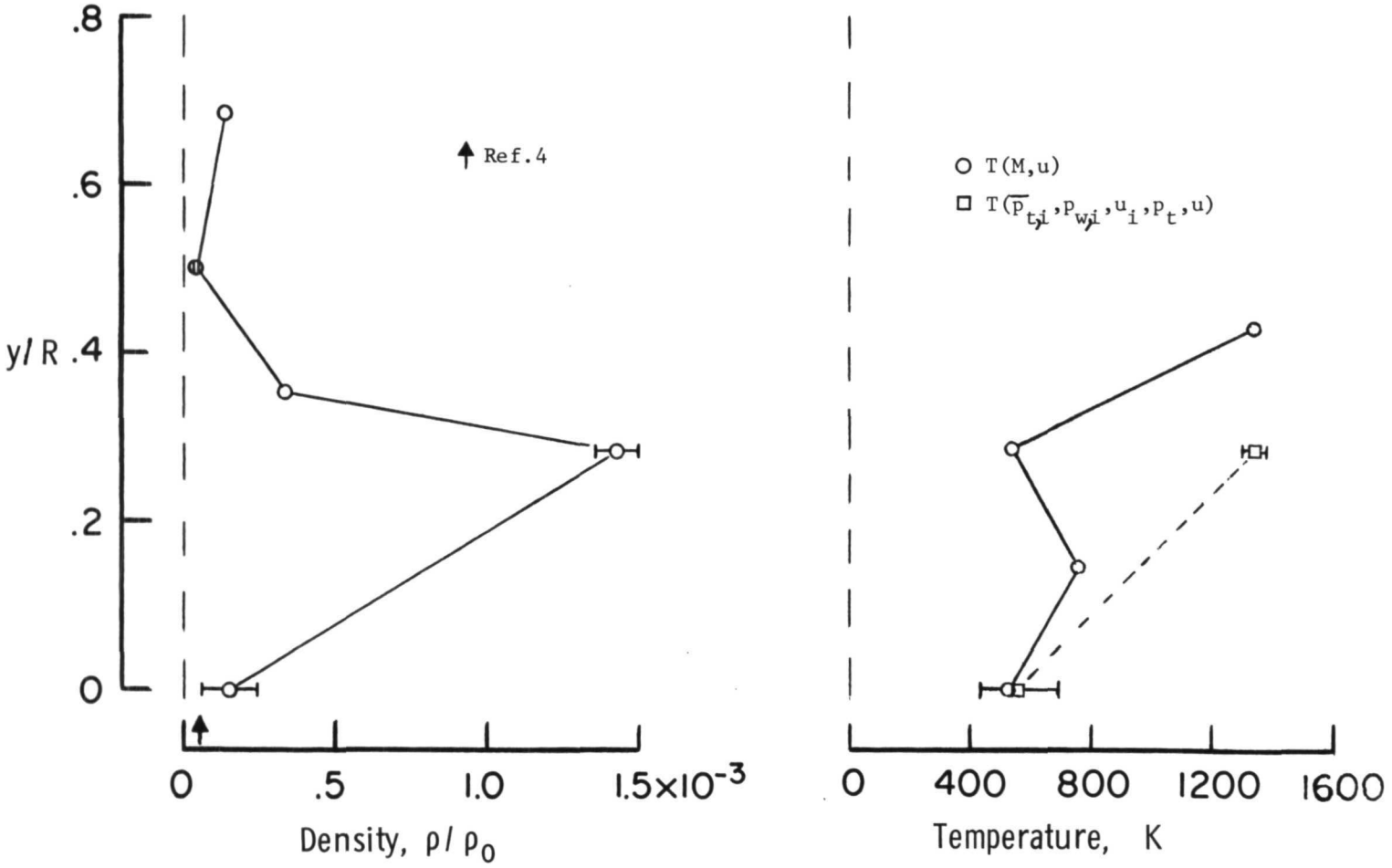

(b) Derived quantities.

Figure 13.- Concluded.

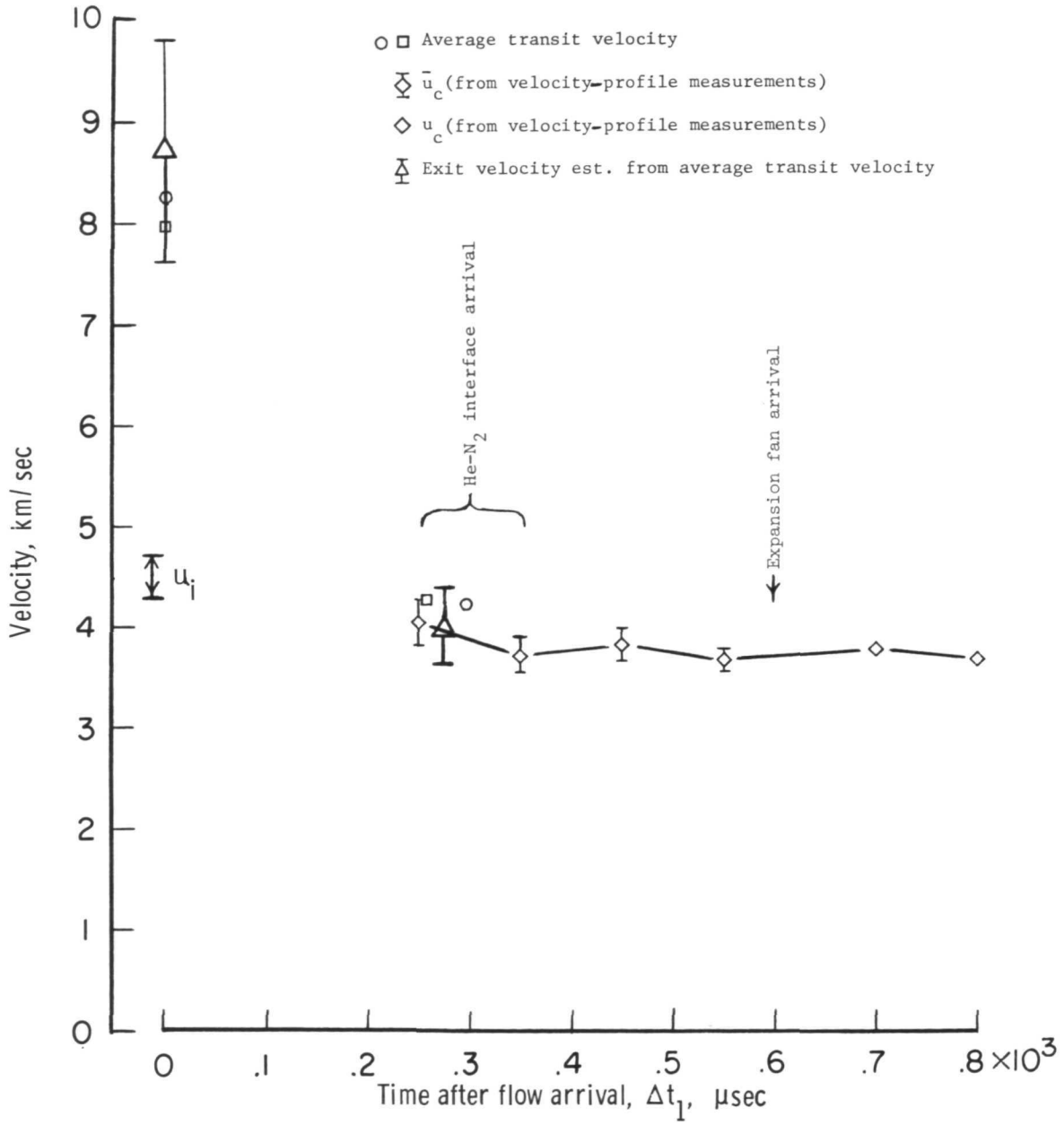

Figure 14.- Flow velocity on tunnel center line. Evacuated nozzle.

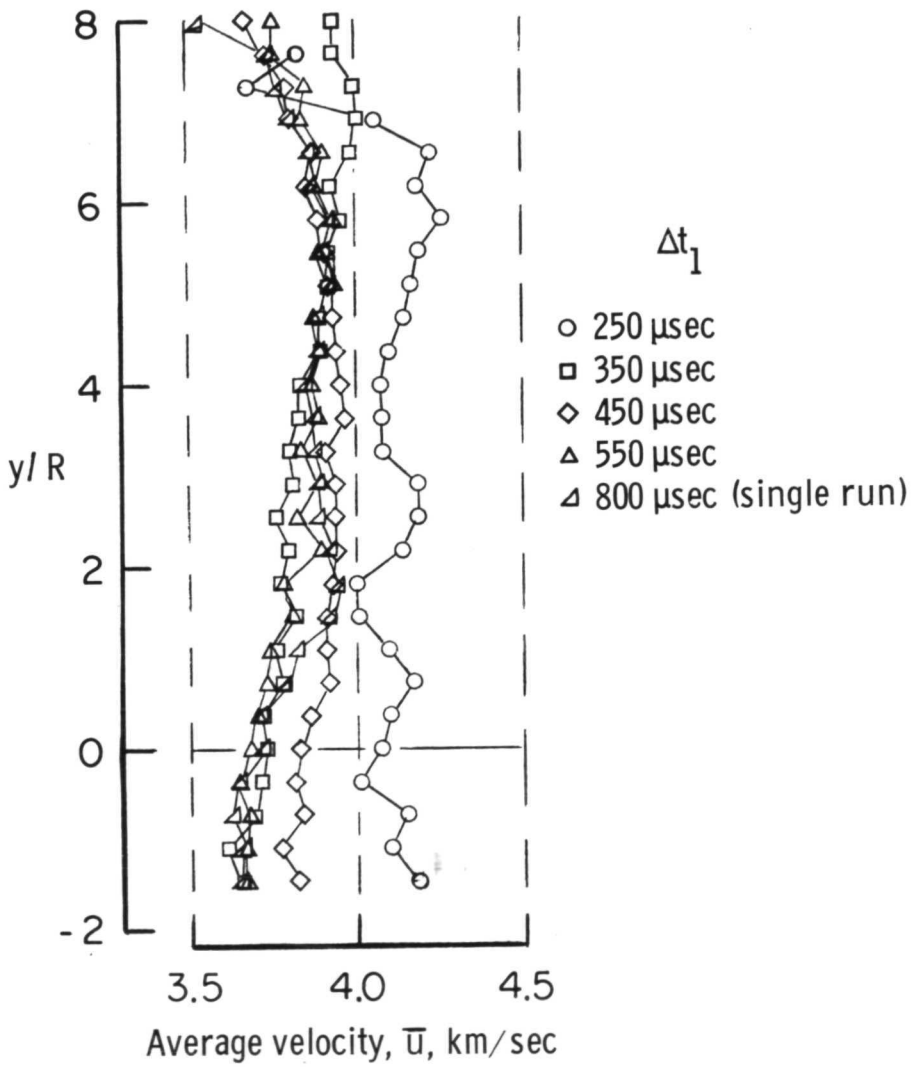

(a) Average velocity profiles.

Figure 15.- Profiles of flow velocity. Evacuated nozzle.

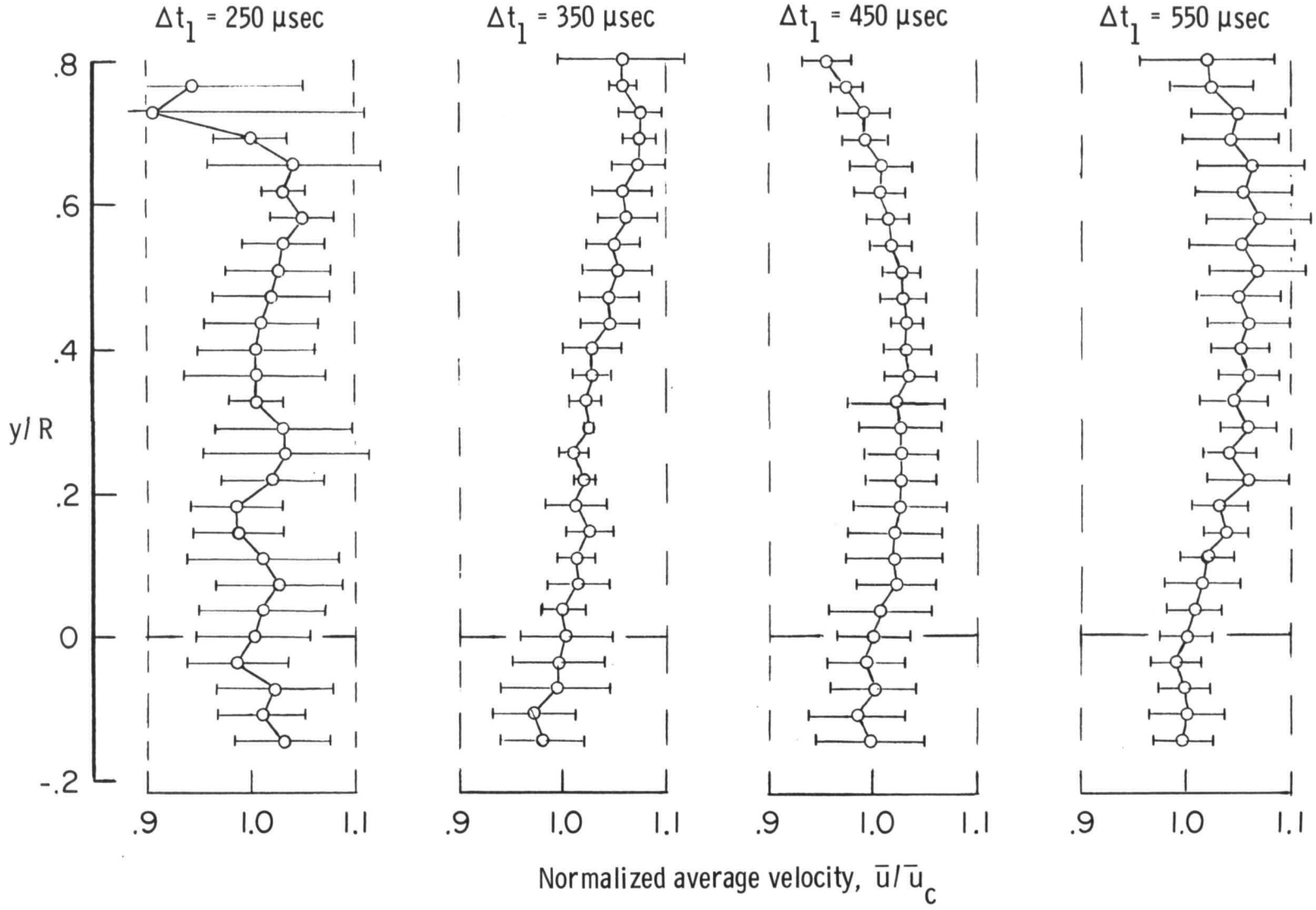

(b) Average velocity profiles with standard deviation from the mean.

Figure 15.- Continued.

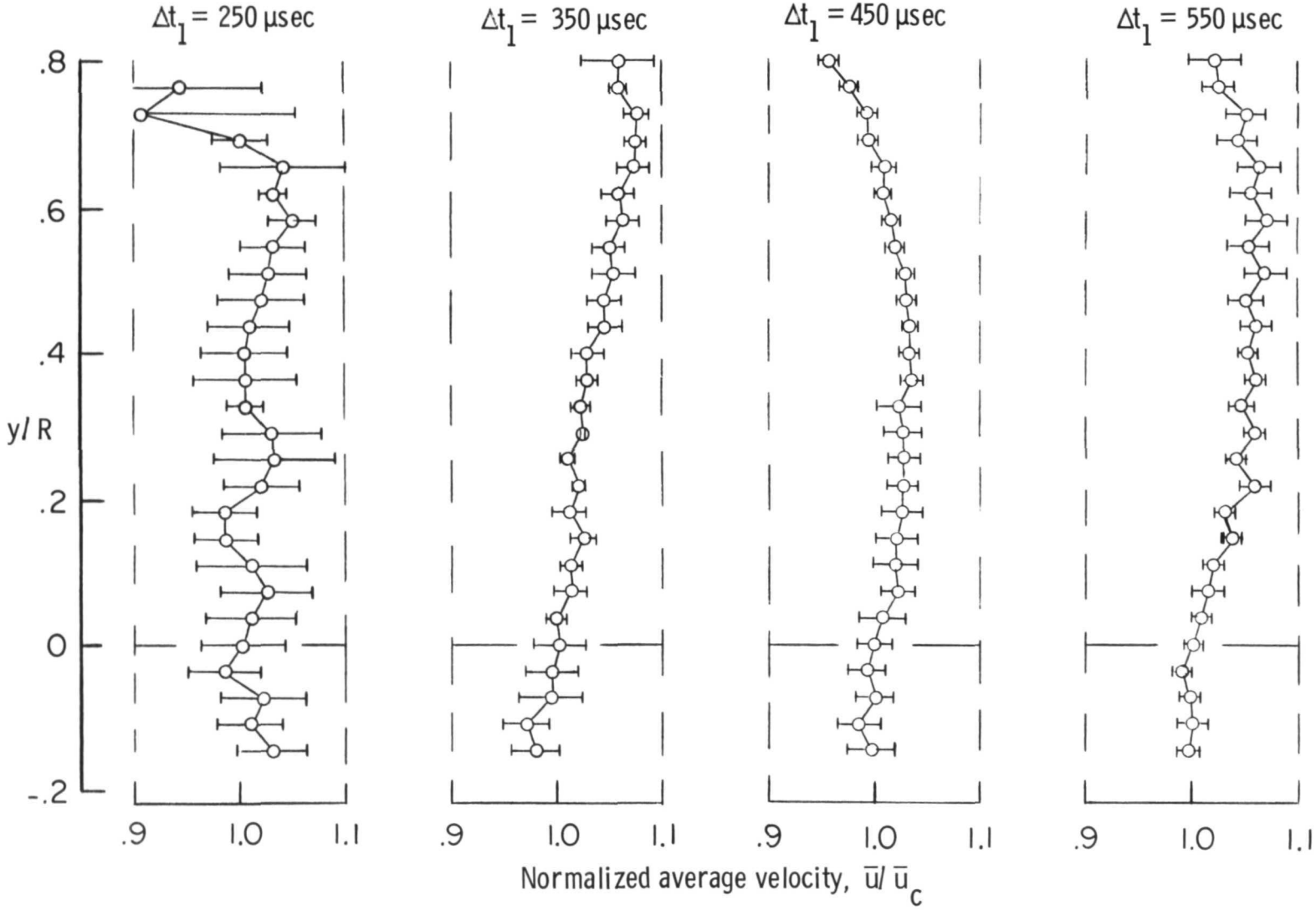

(c) Average velocity profiles with estimated variance of the mean.

Figure 15.- Continued.

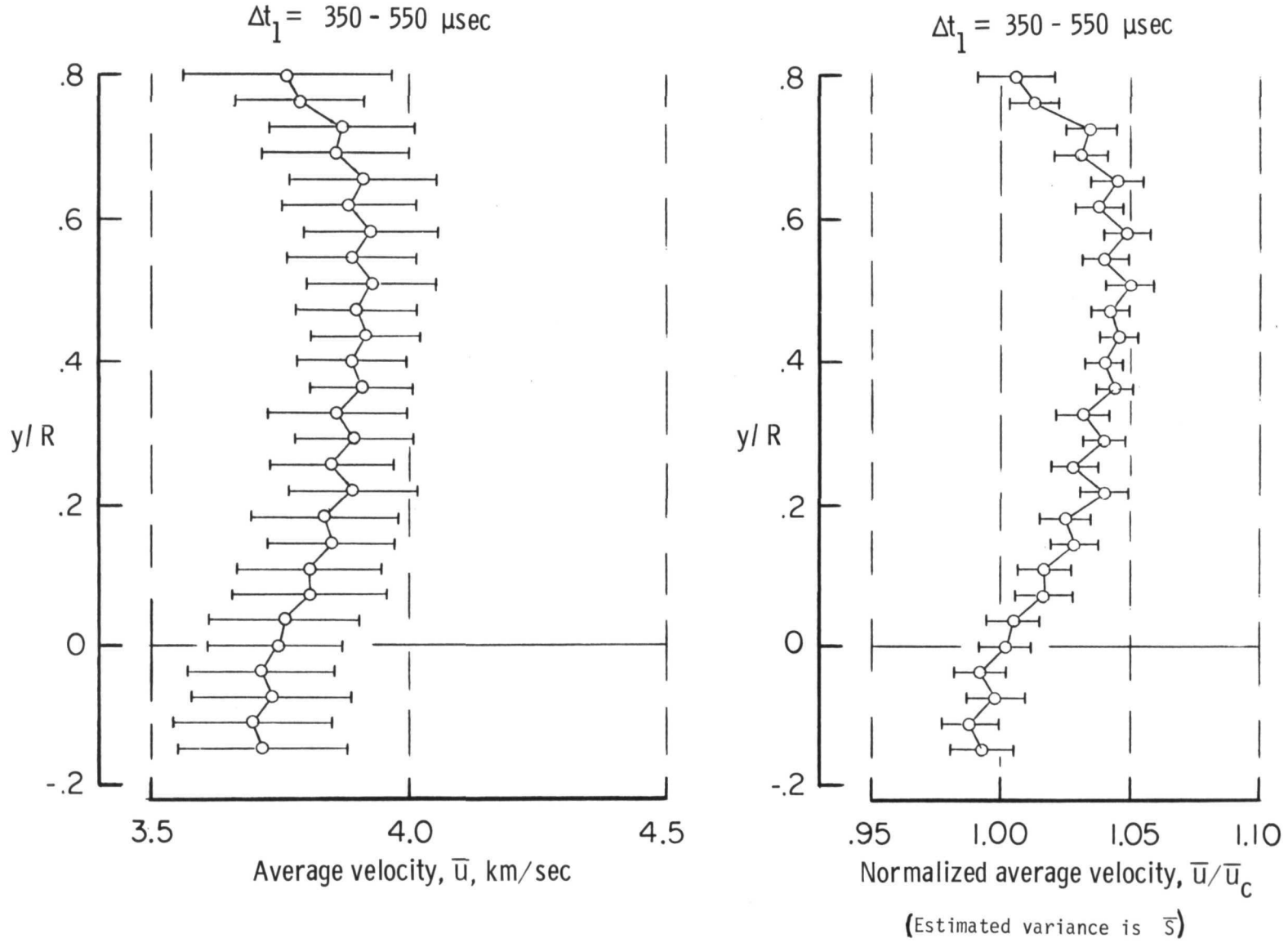

(d) Profiles of average velocity of 14 runs.

Figure 15.- Continued.

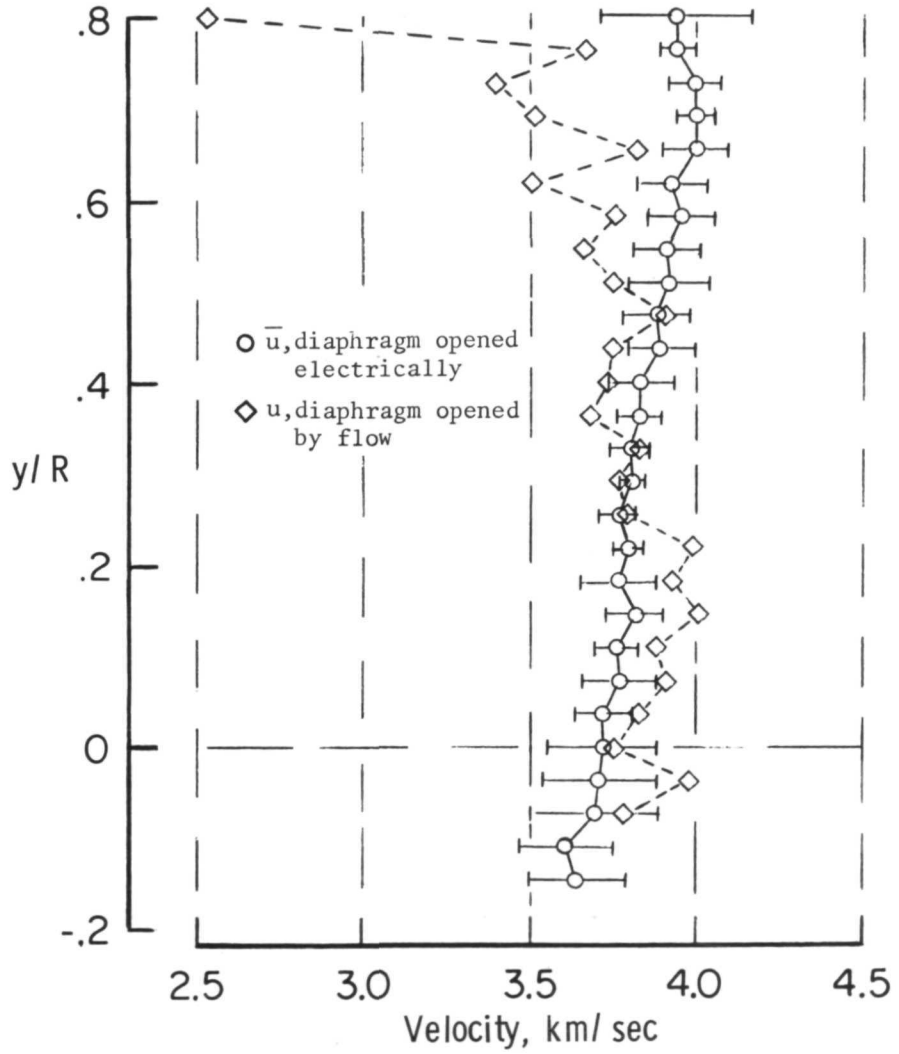

(e) Velocity profiles for nozzle diaphragm opened by flow and diaphragm electrically opened. $\Delta t_1 = 350$ μsec.

Figure 15.- Concluded.

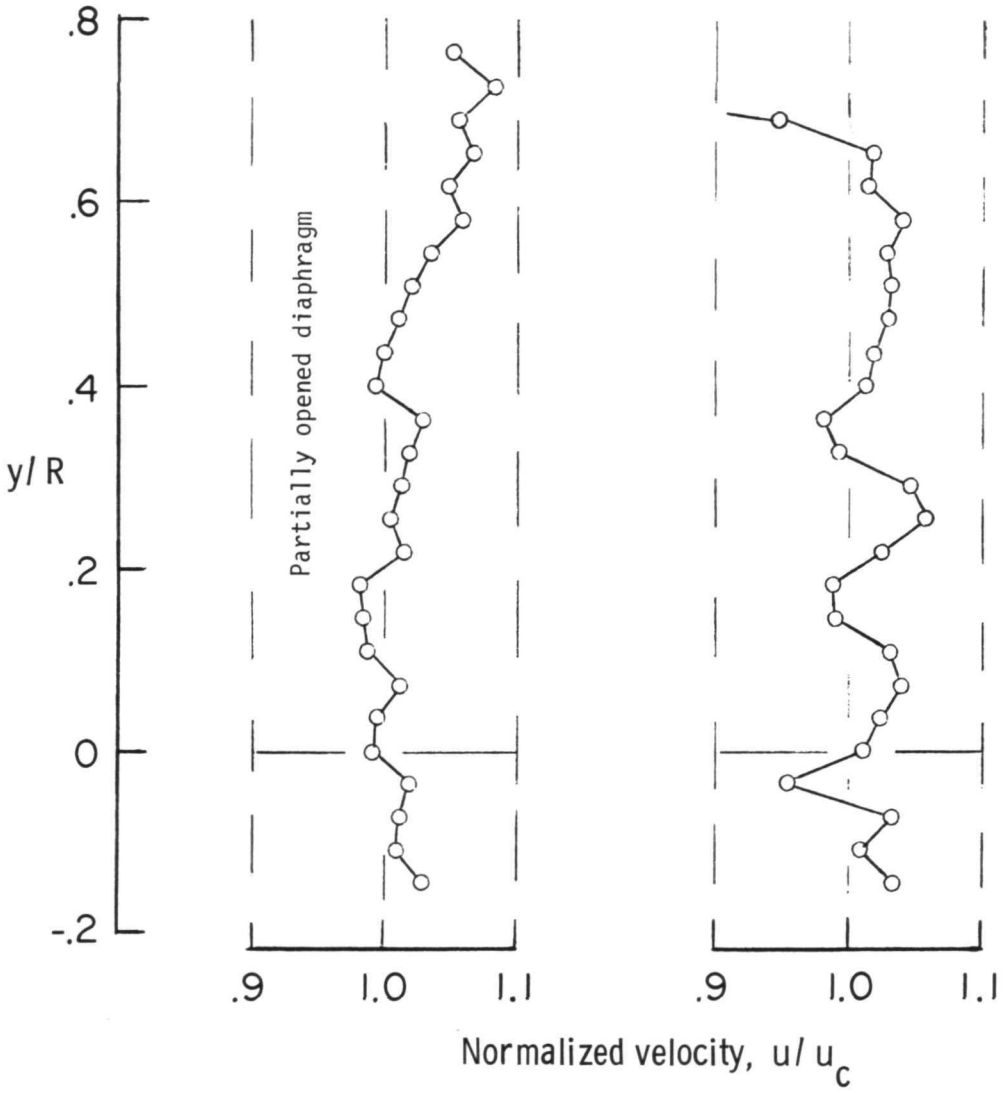

(a) $\Delta t_1 = 250$ μsec.

Figure 16.- Flow velocity profiles. Evacuated nozzle.

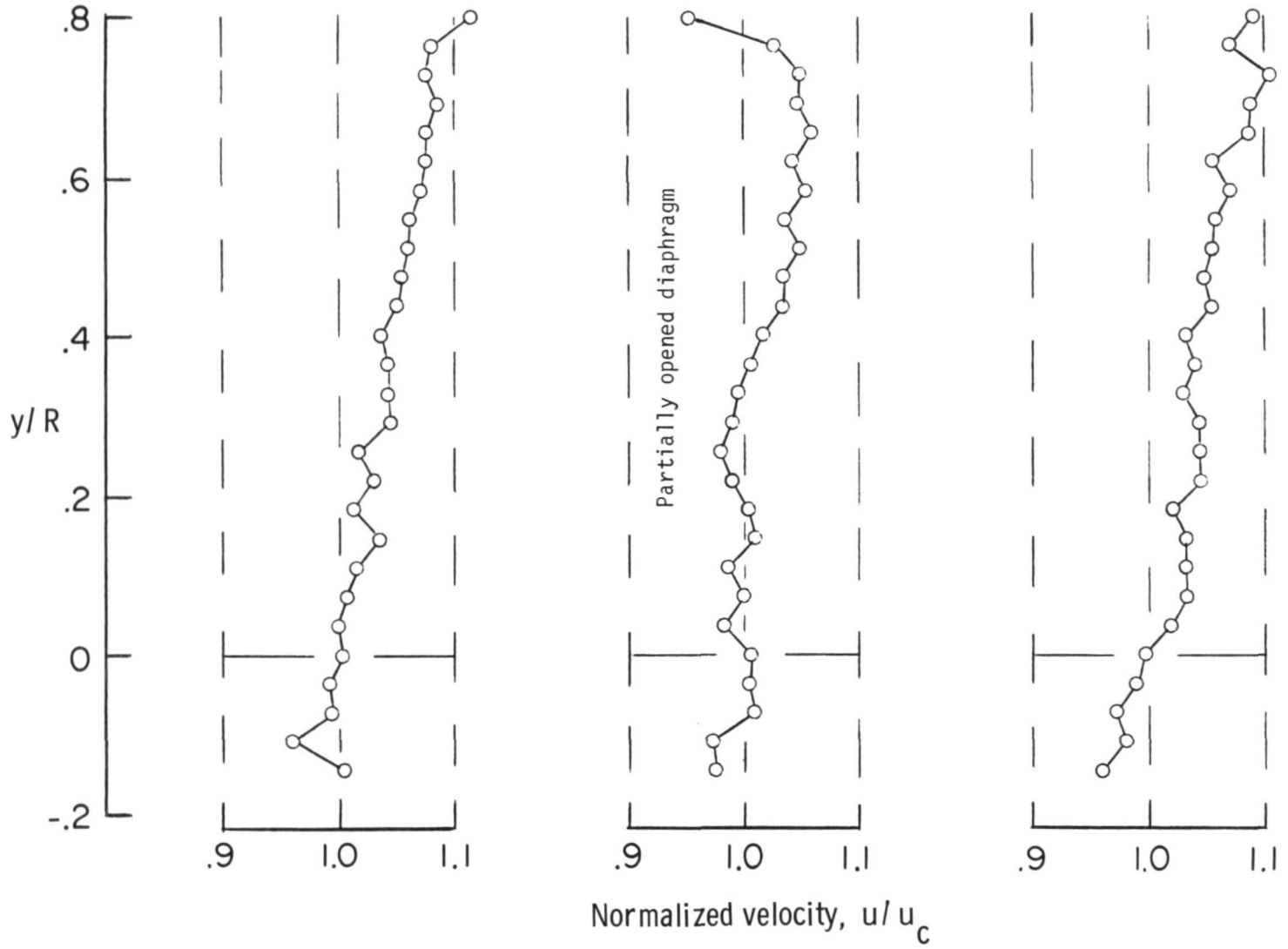

(b) $\Delta t_1 = 350$ μsec.

Figure 16.- Continued.

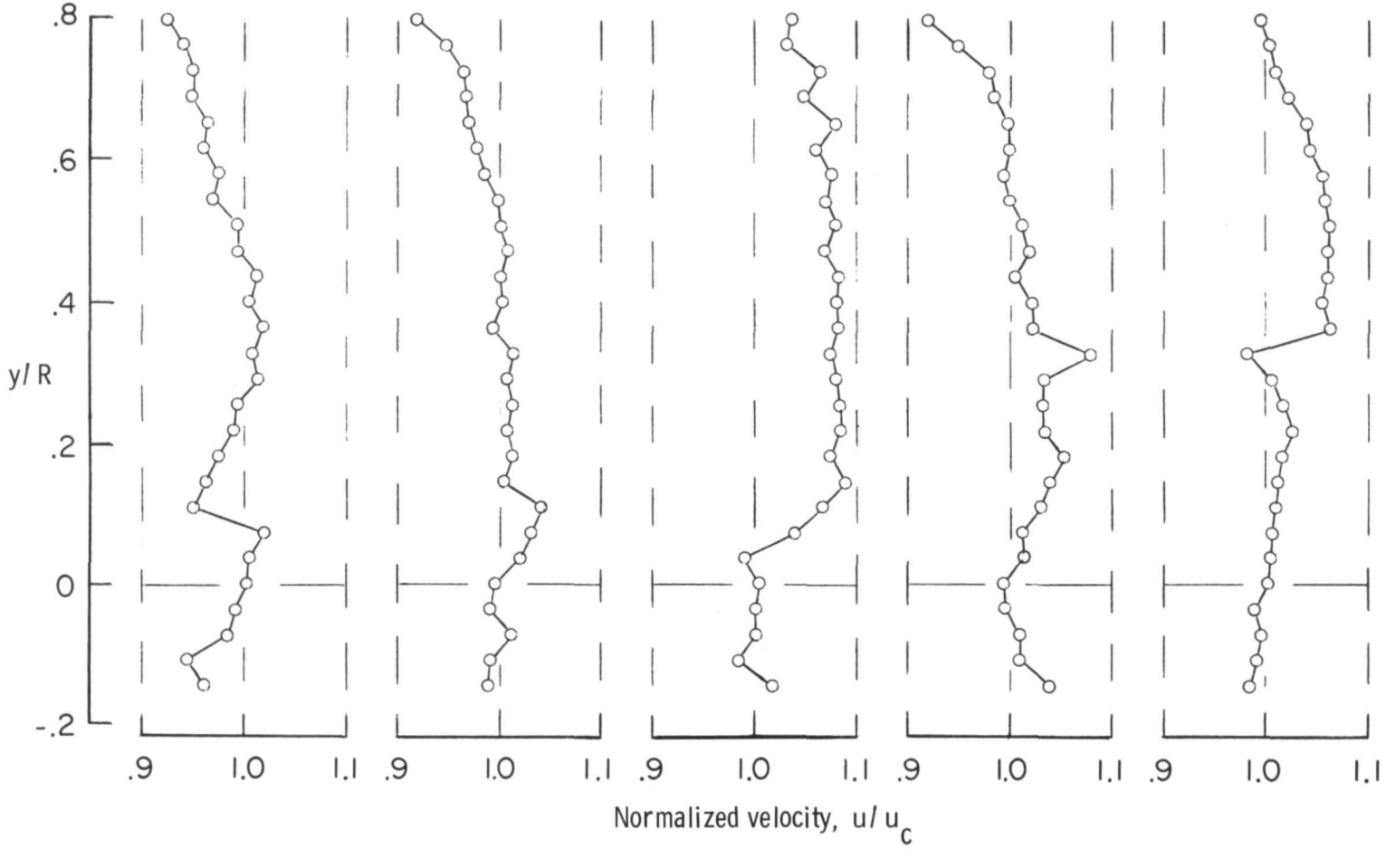

(c) Δt_1 = 450 μsec.

Figure 16.- Continued.

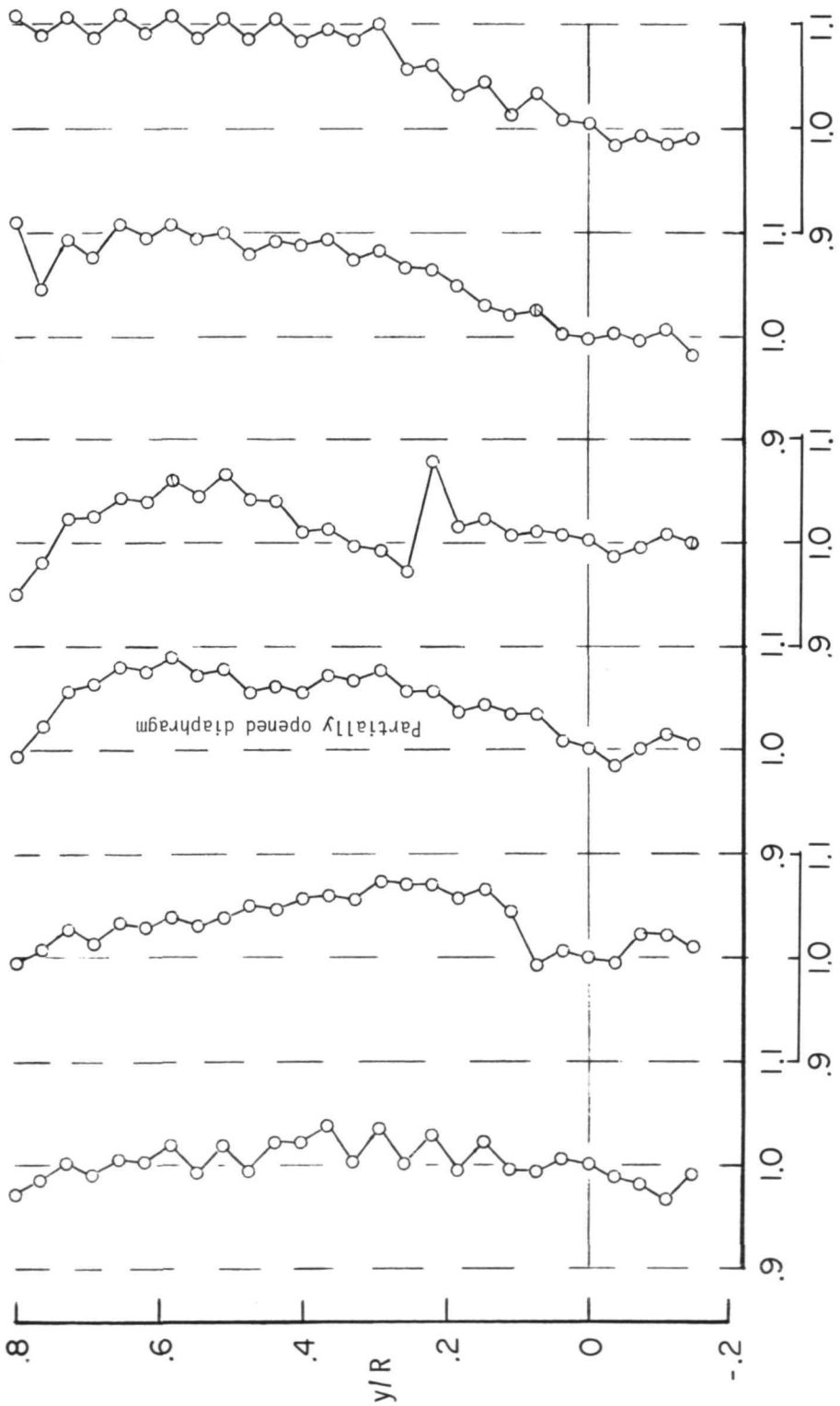

(d) Δt_1 = 550 μsec.

Figure 16.- Continued.

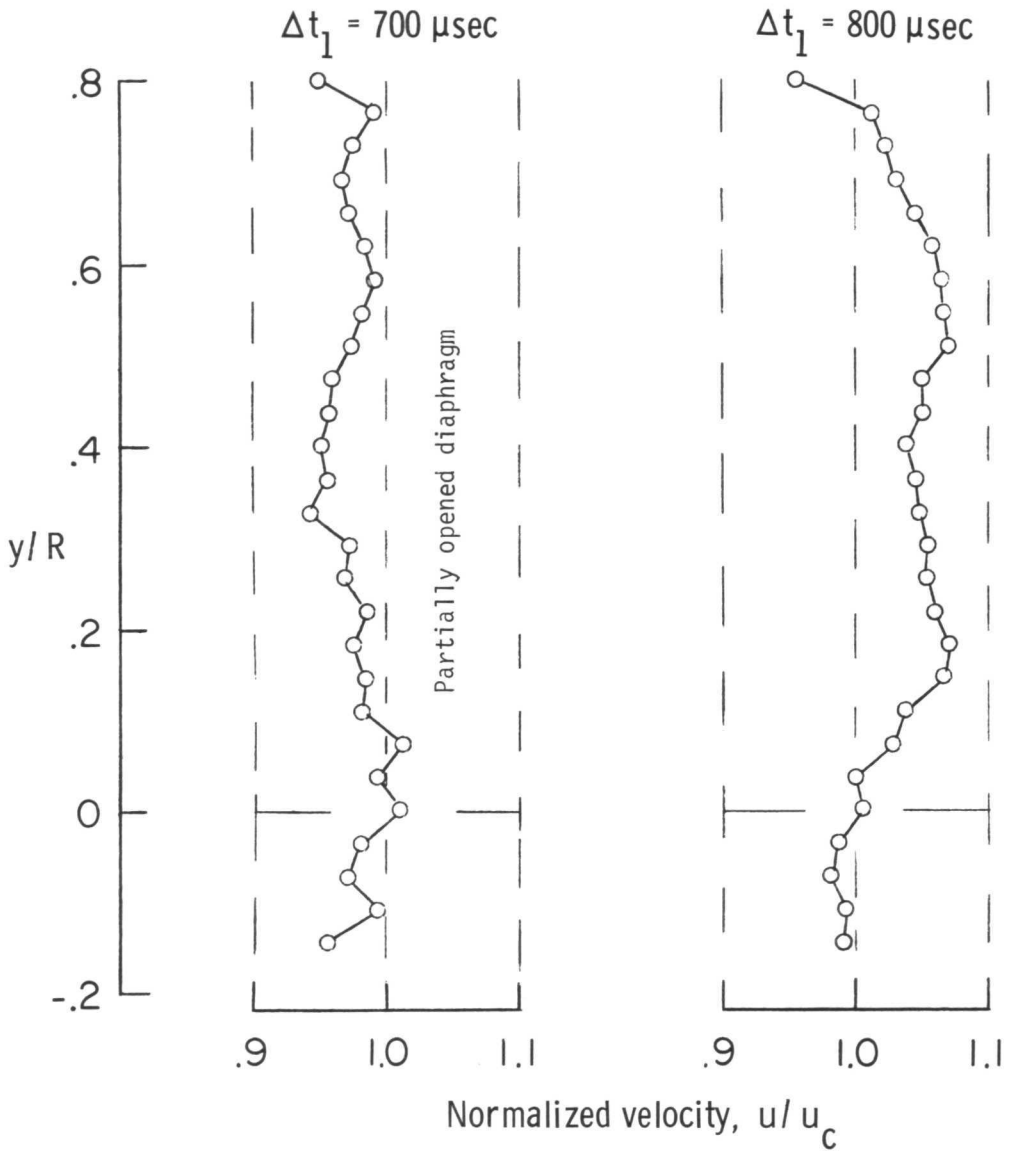

(e) Δt_1 = 700 and 800 μsec.

Figure 16.- Concluded.

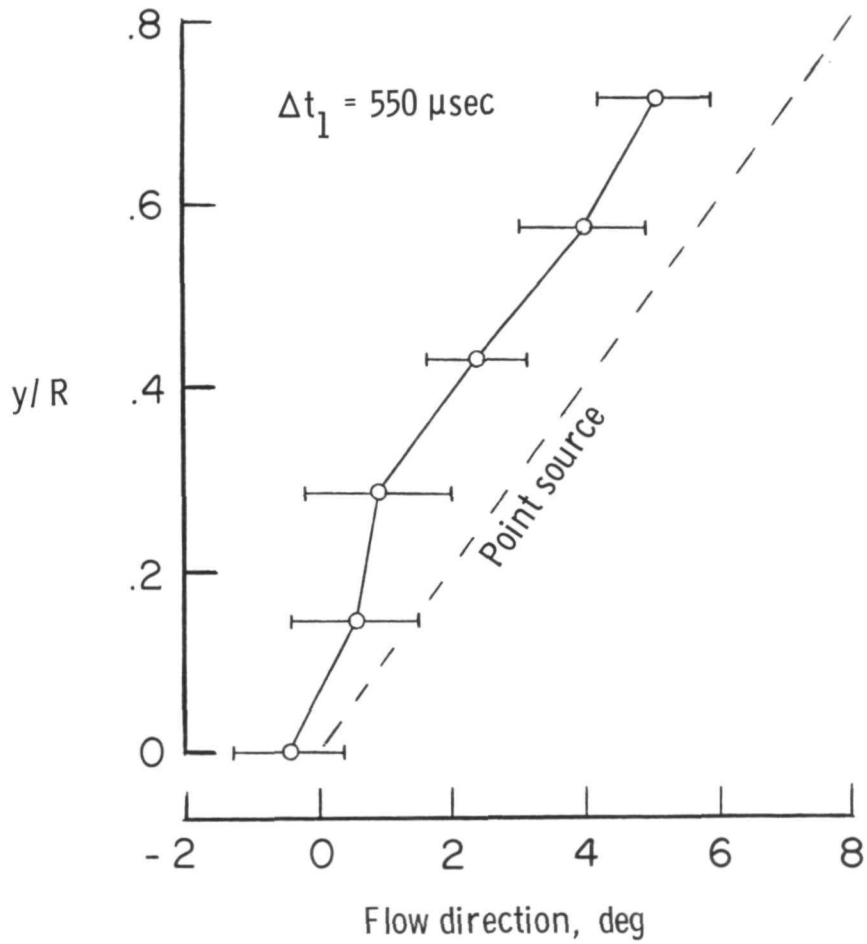

Figure 17.- Flow direction. Evacuated nozzle.

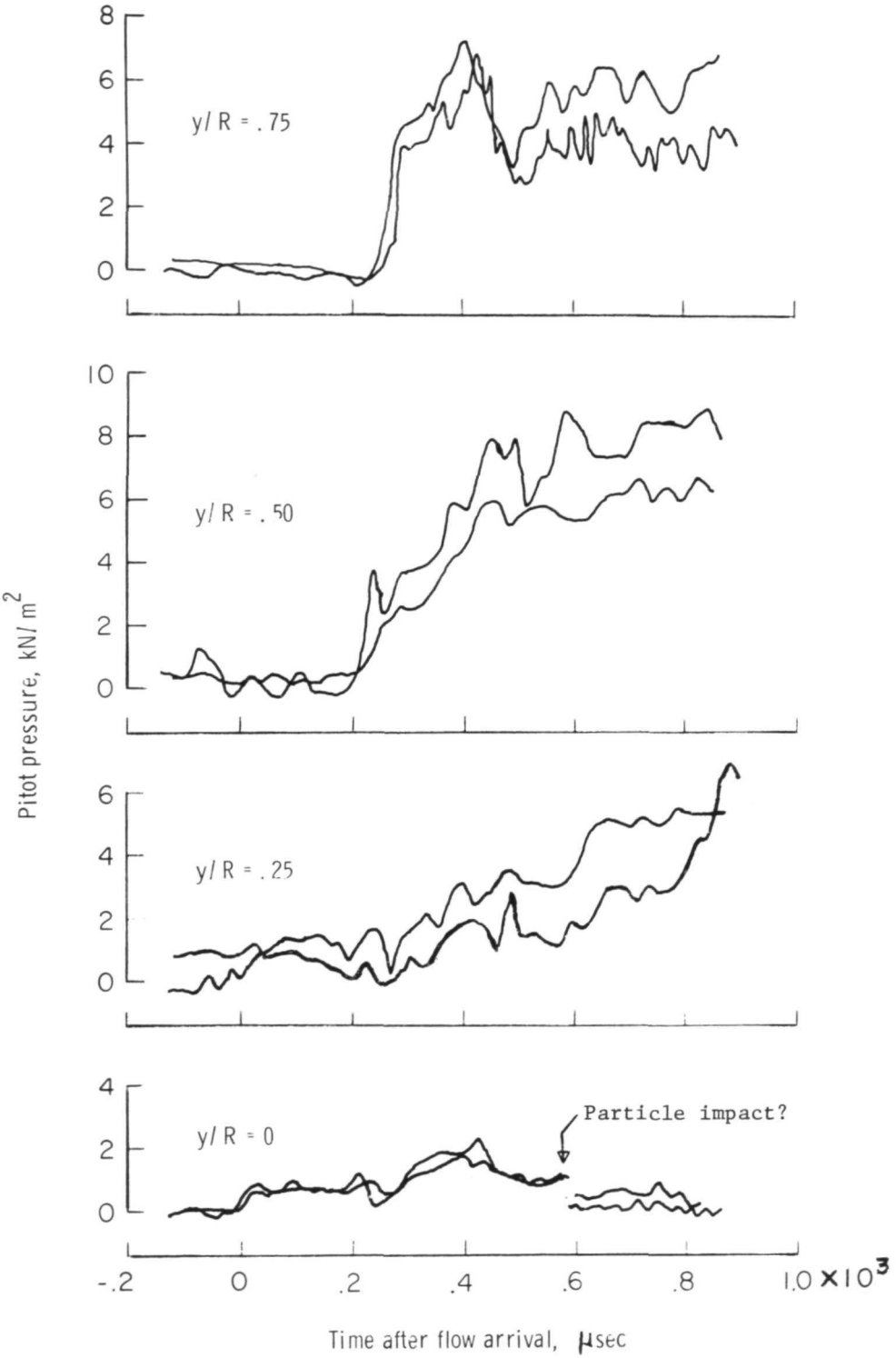

(a) Rake (bare gages).

Figure 18.- Pitot pressure. Evacuated nozzle.

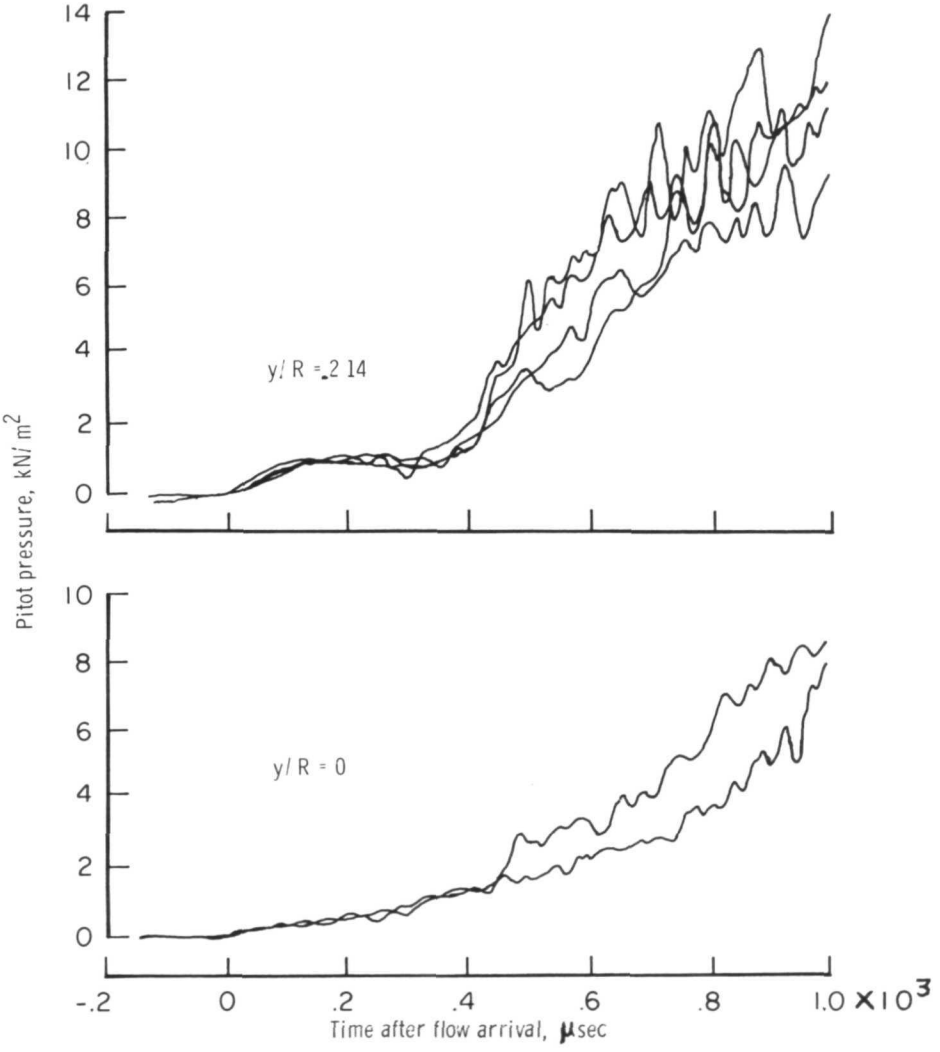

(b) Single probes.

Figure 18.- Concluded.

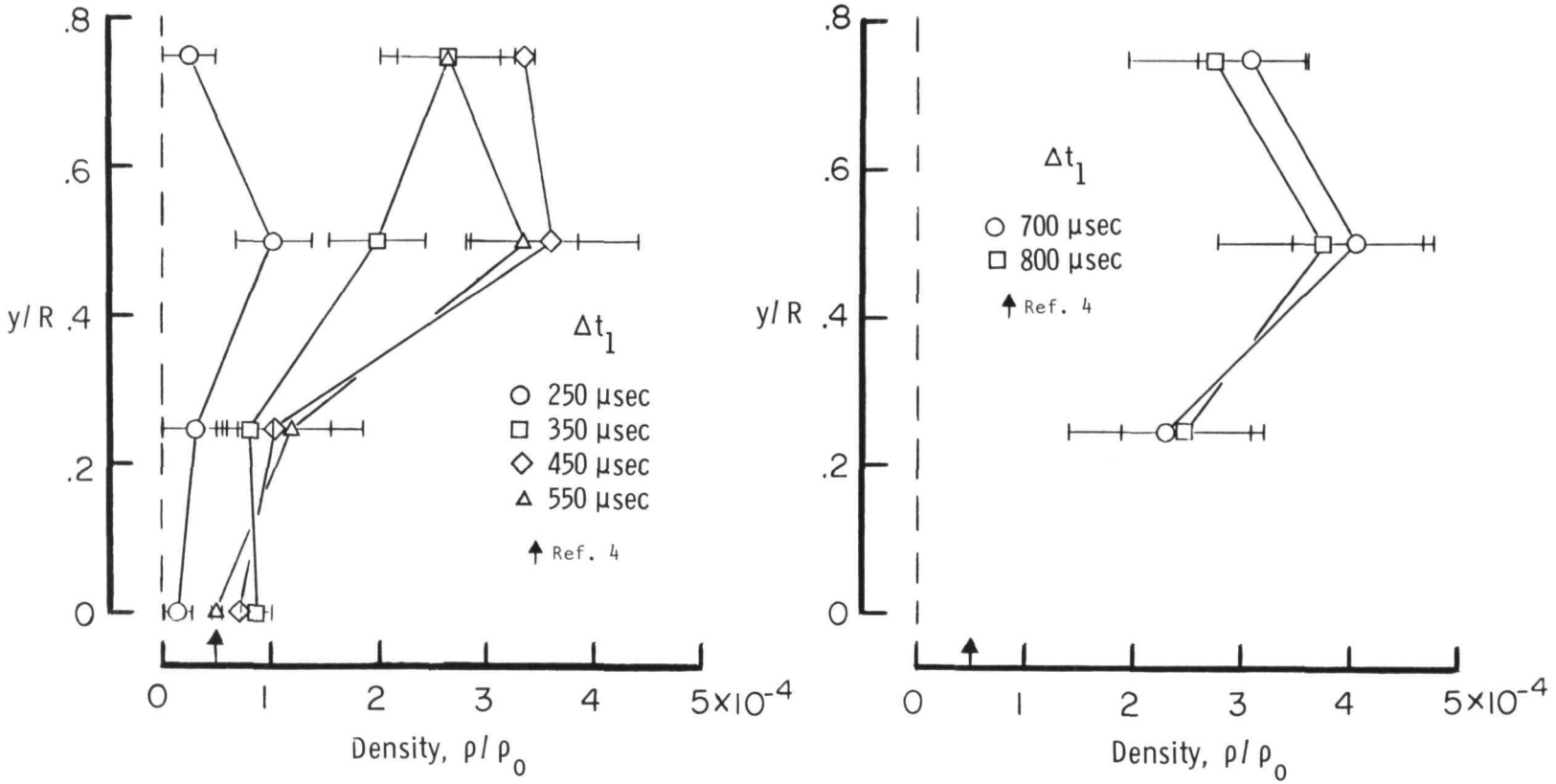

(a) Derived from bare-gage-rake data.

Figure 19.- Density. Evacuated nozzle.

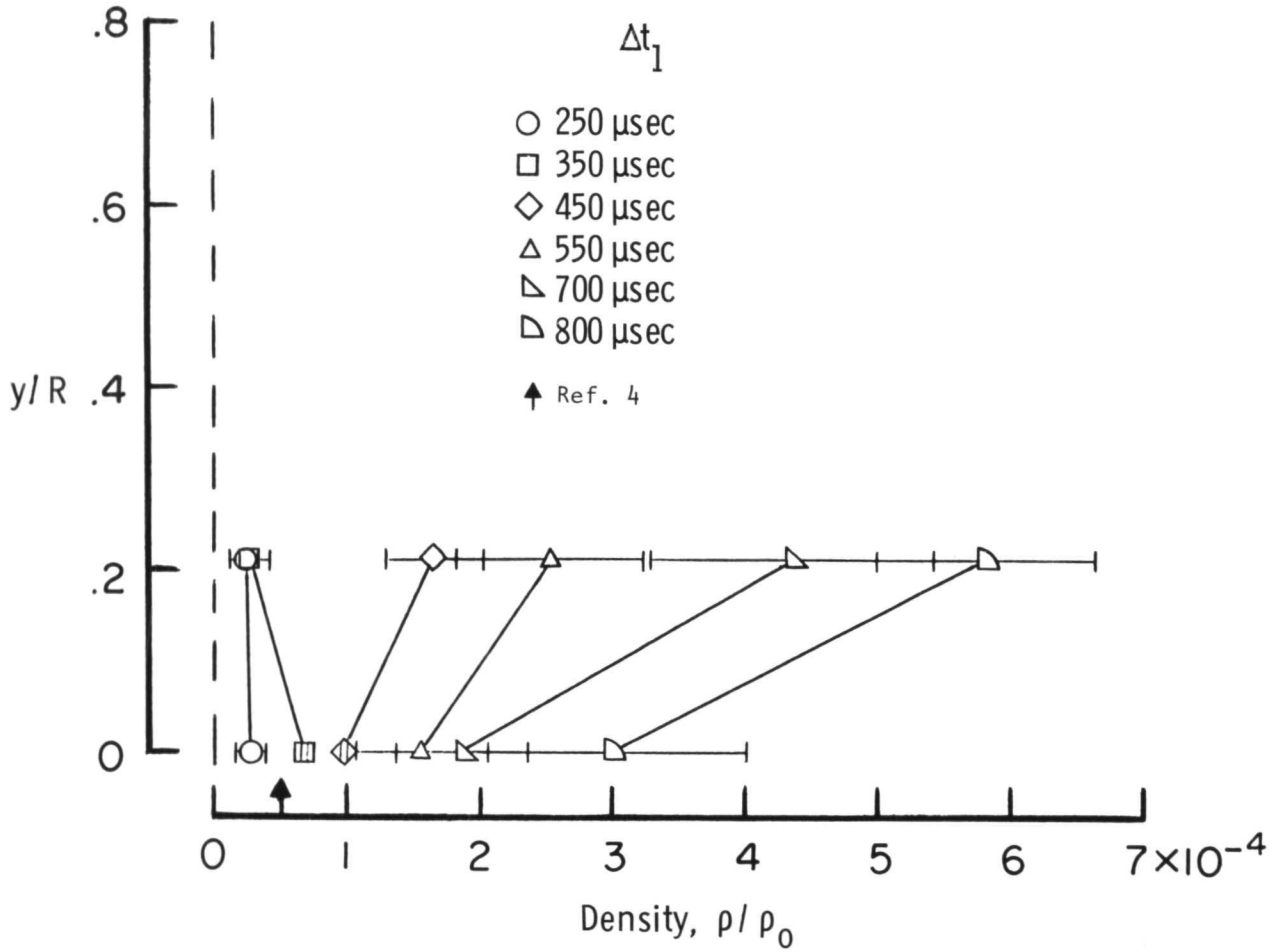

(b) Derived from single-probe data.

Figure 19.- Concluded.

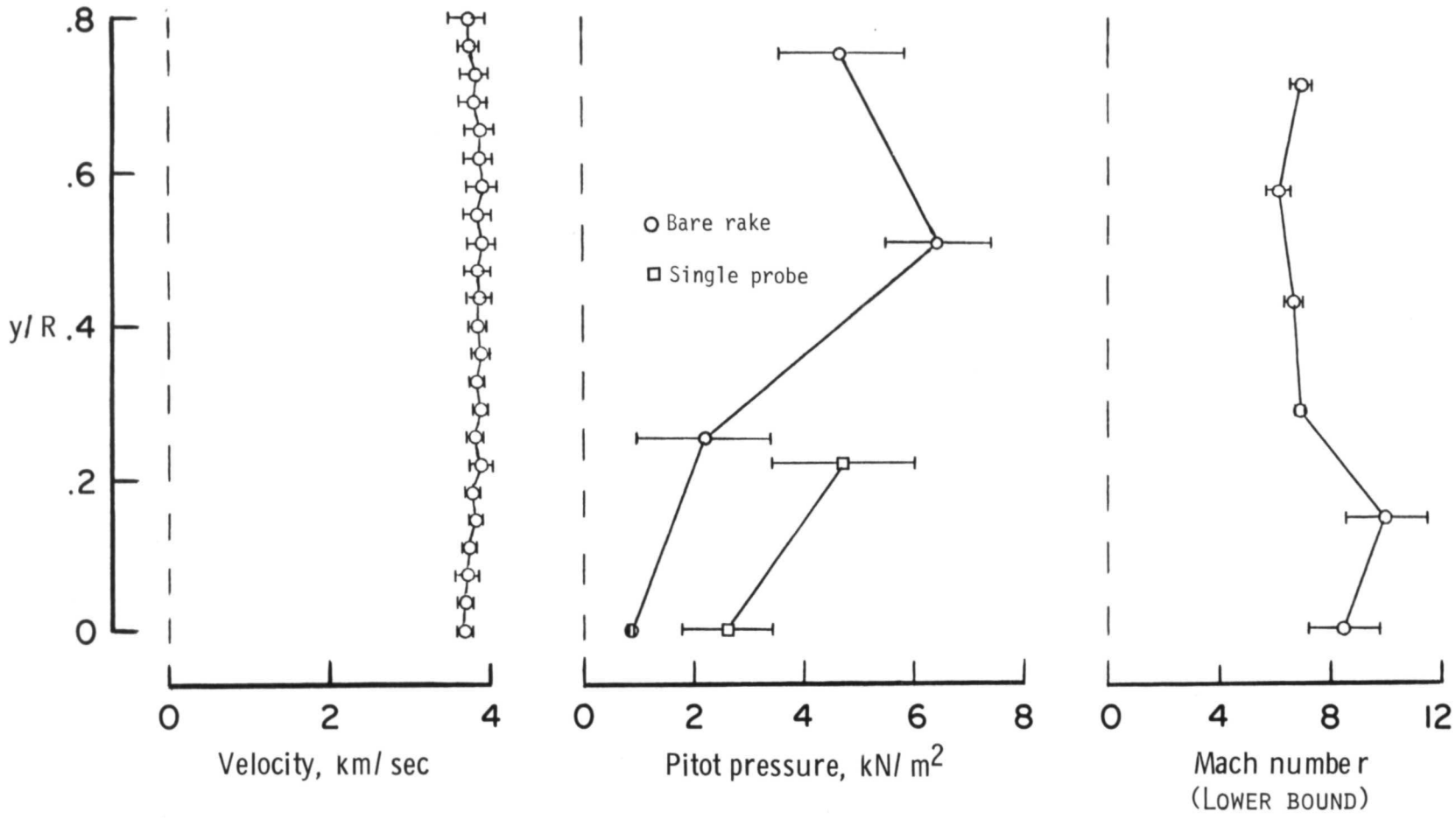

(a) Measured quantities.

Figure 20.- Measured and derived results at Δt_1 = 550 μsec. Evacuated nozzle.

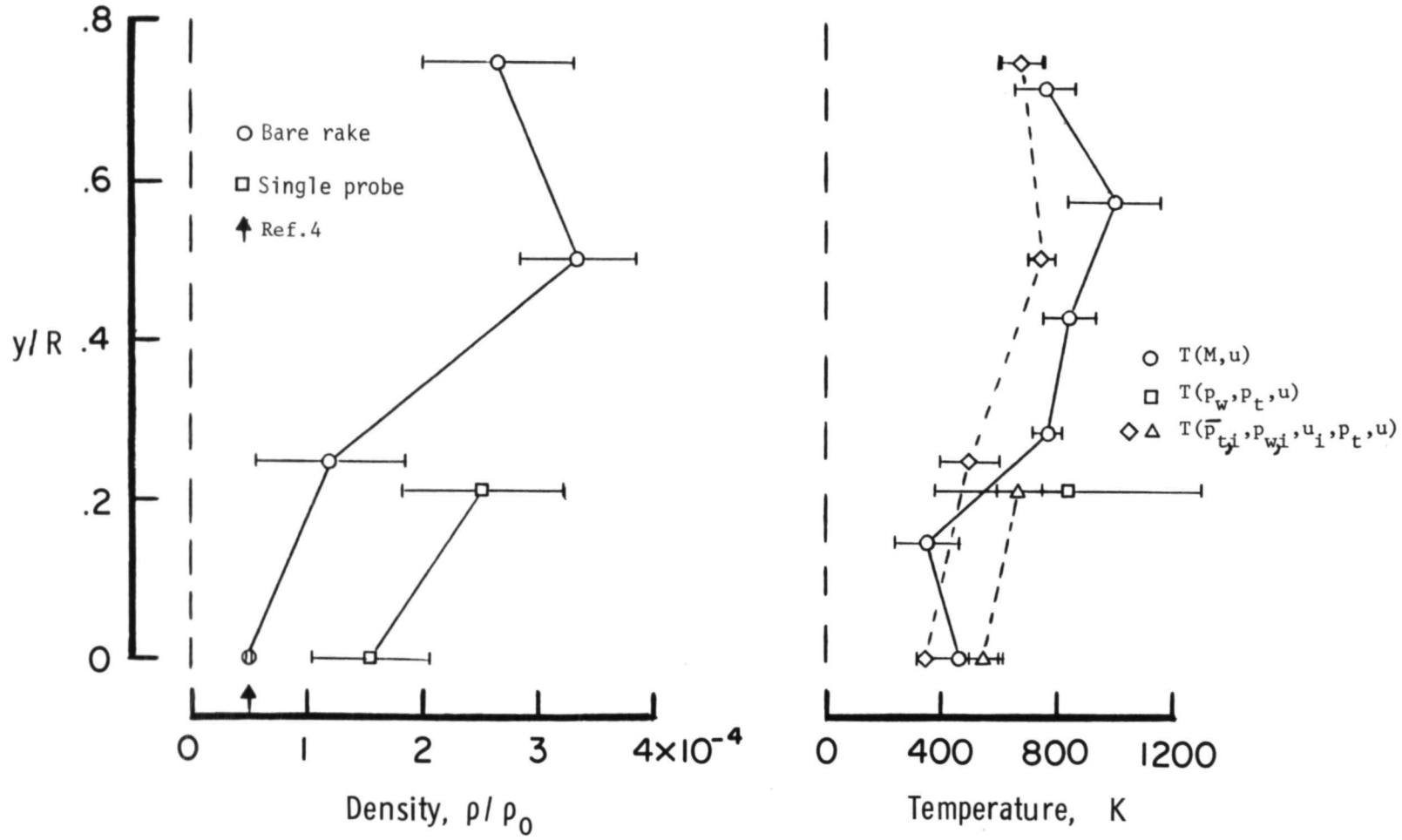

(b) Derived quantities.

Figure 20.- Concluded.

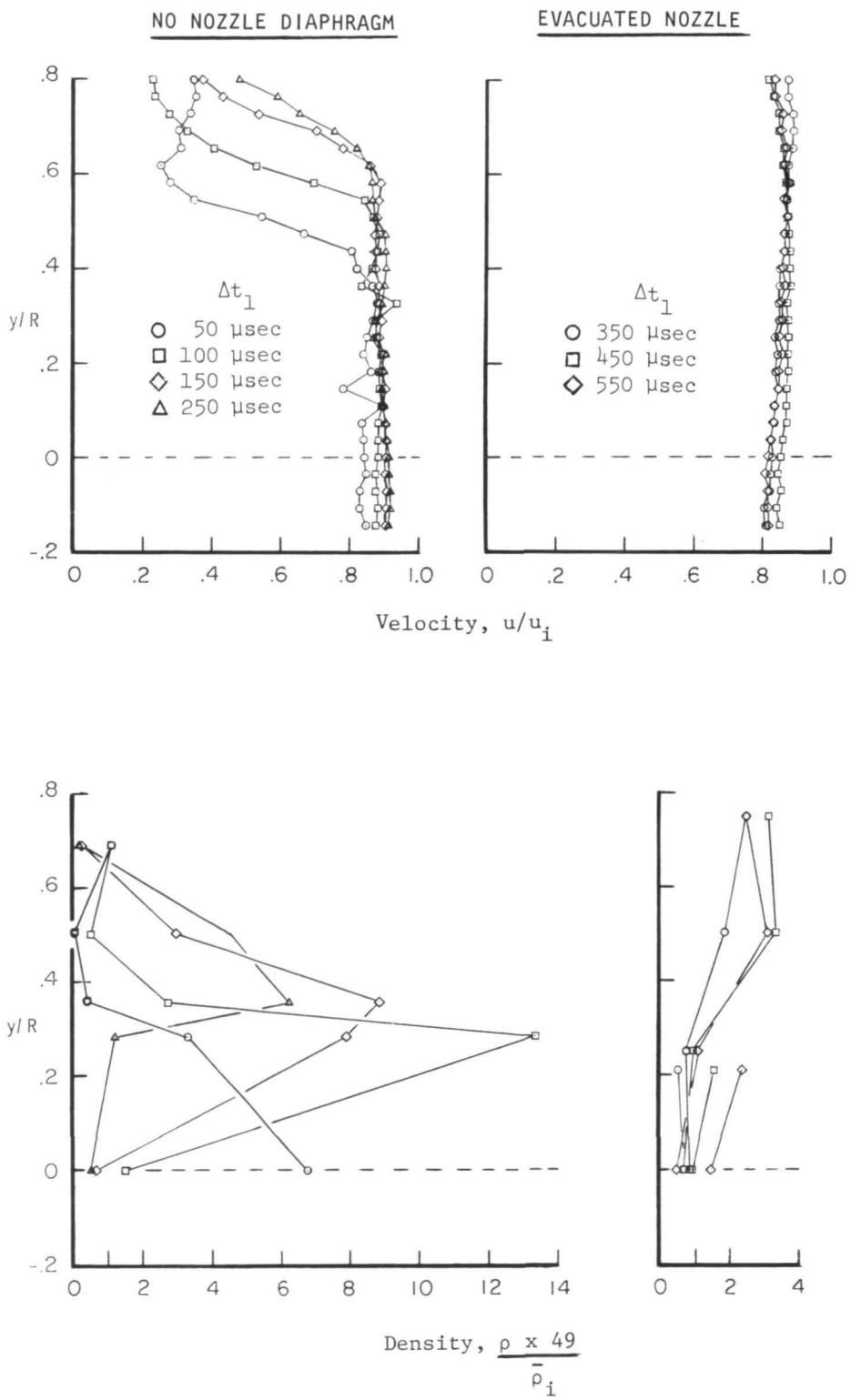

Figure 21.- Velocity and density profiles for the two initial nozzle conditions.

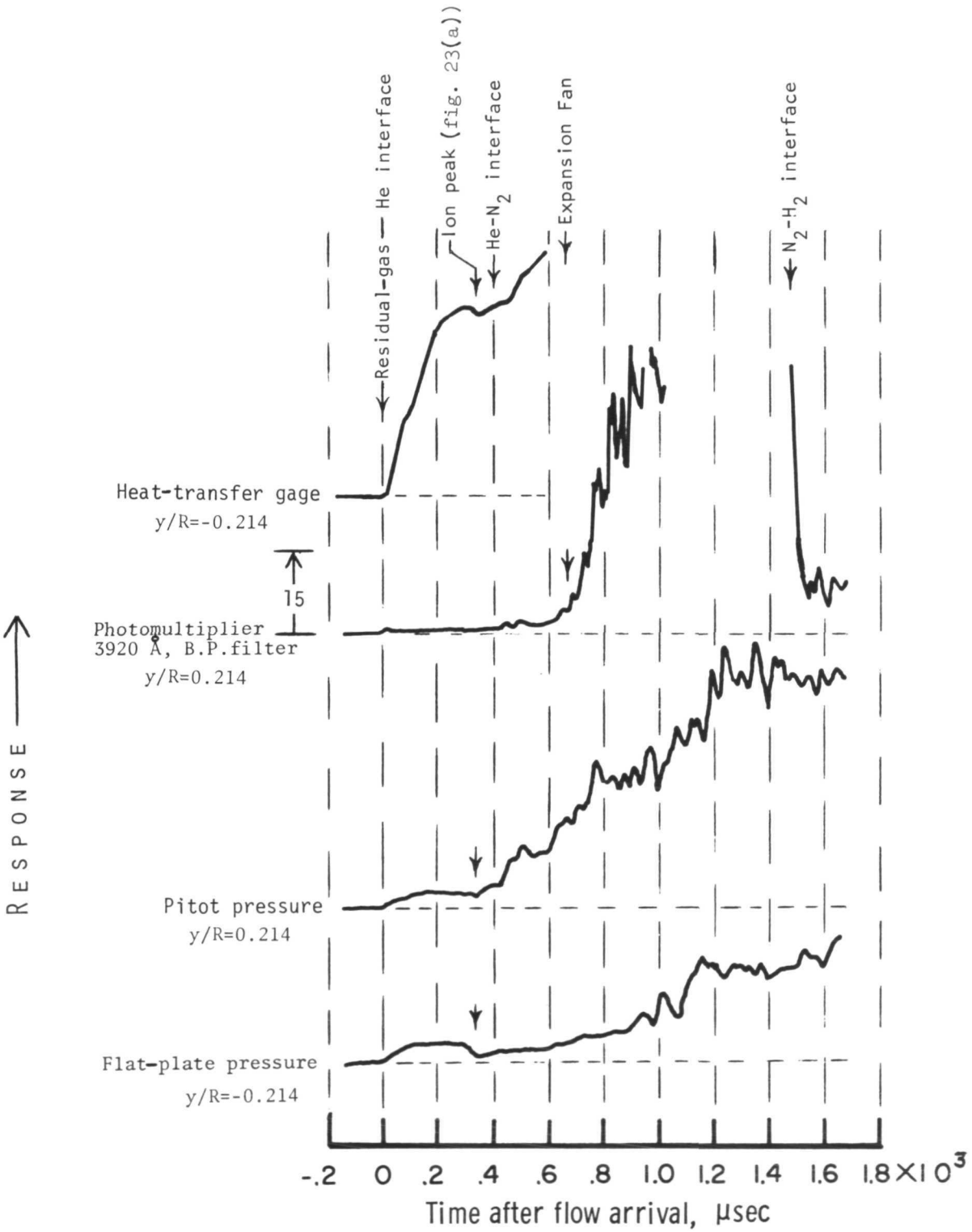

(a) Four probe responses for same tunnel run.

Figure 22.- Probe responses at nozzle exit. Evacuated nozzle.

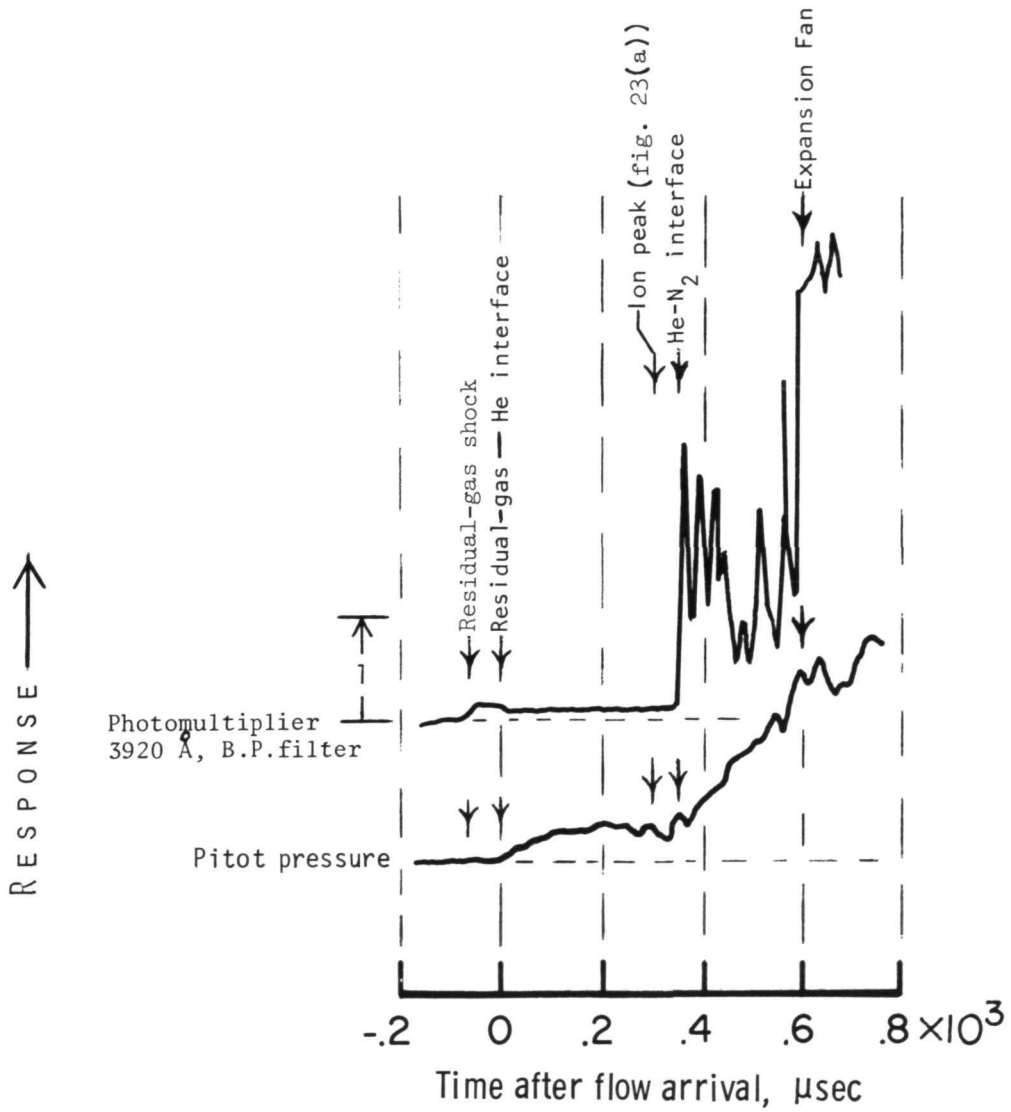

(b) Probe responses at y/R = 0.214; photomultiplier with filter.

Figure 22.- Continued.

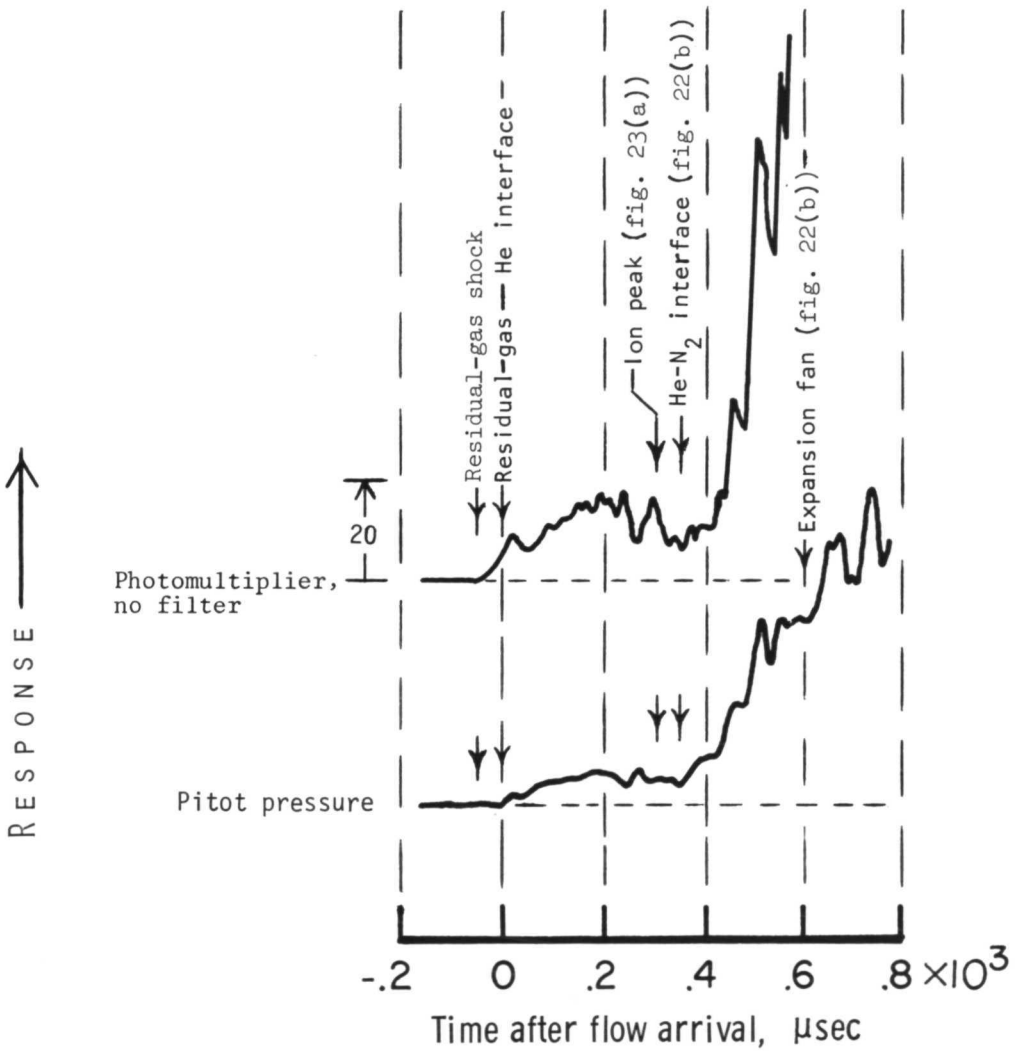

(c) Probe responses at y/R = 0.214; photomultiplier without filter.

Figure 22.- Concluded.

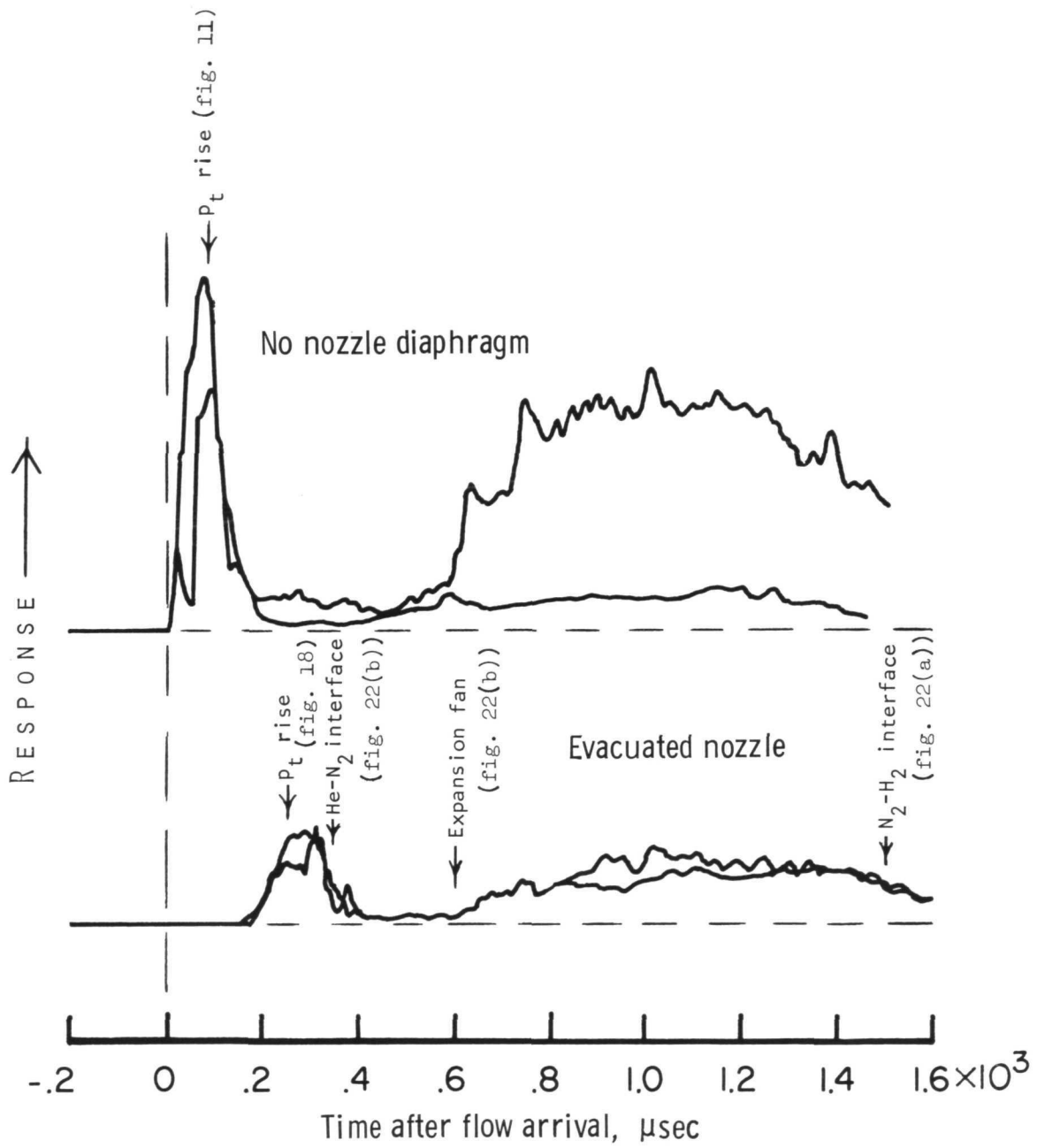

(a) Ion probe.

Figure 23.- Probe responses at y/R = -0.44.

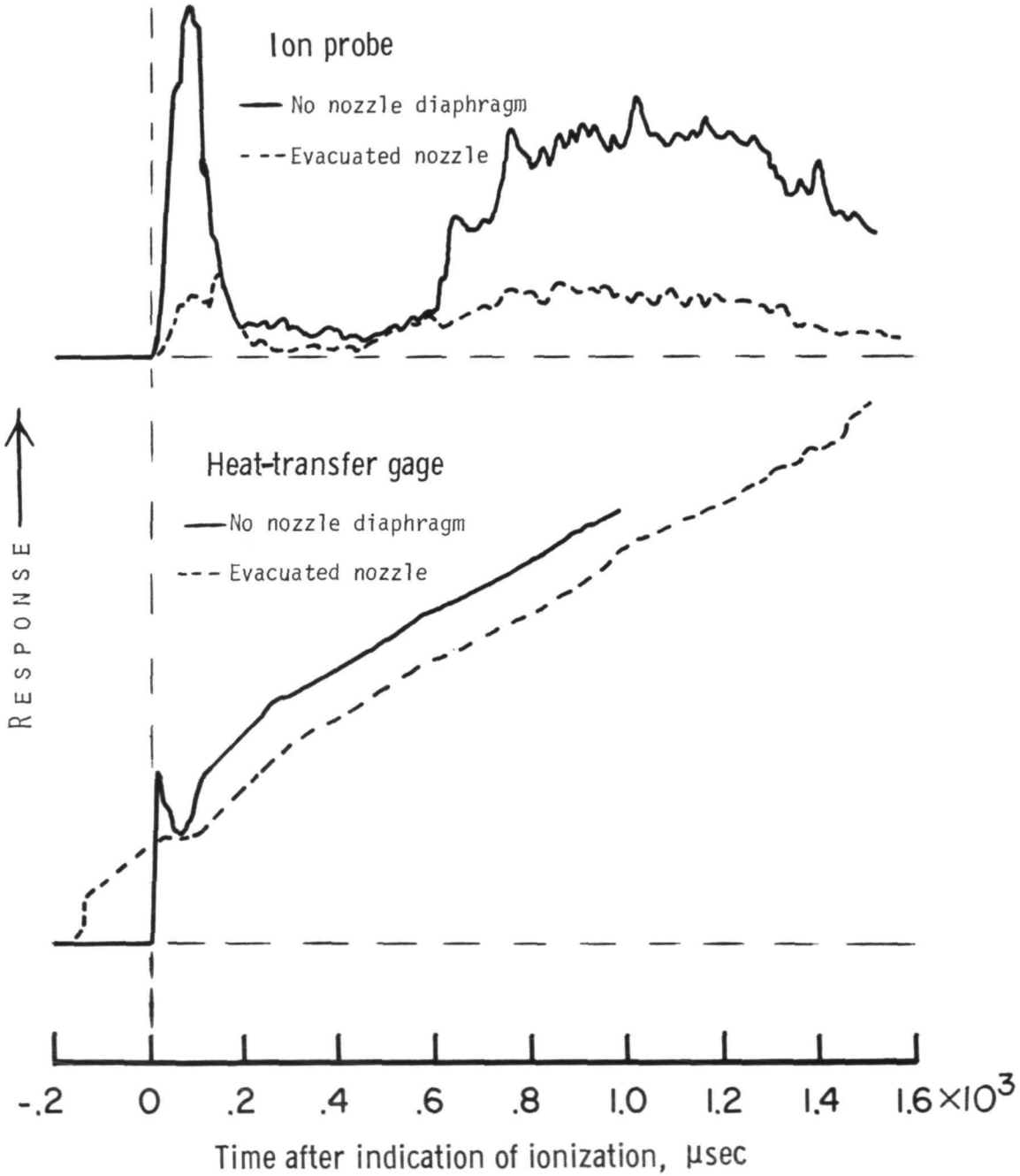

(b) Heat-transfer gage and ion probe.

Figure 23.- Concluded.

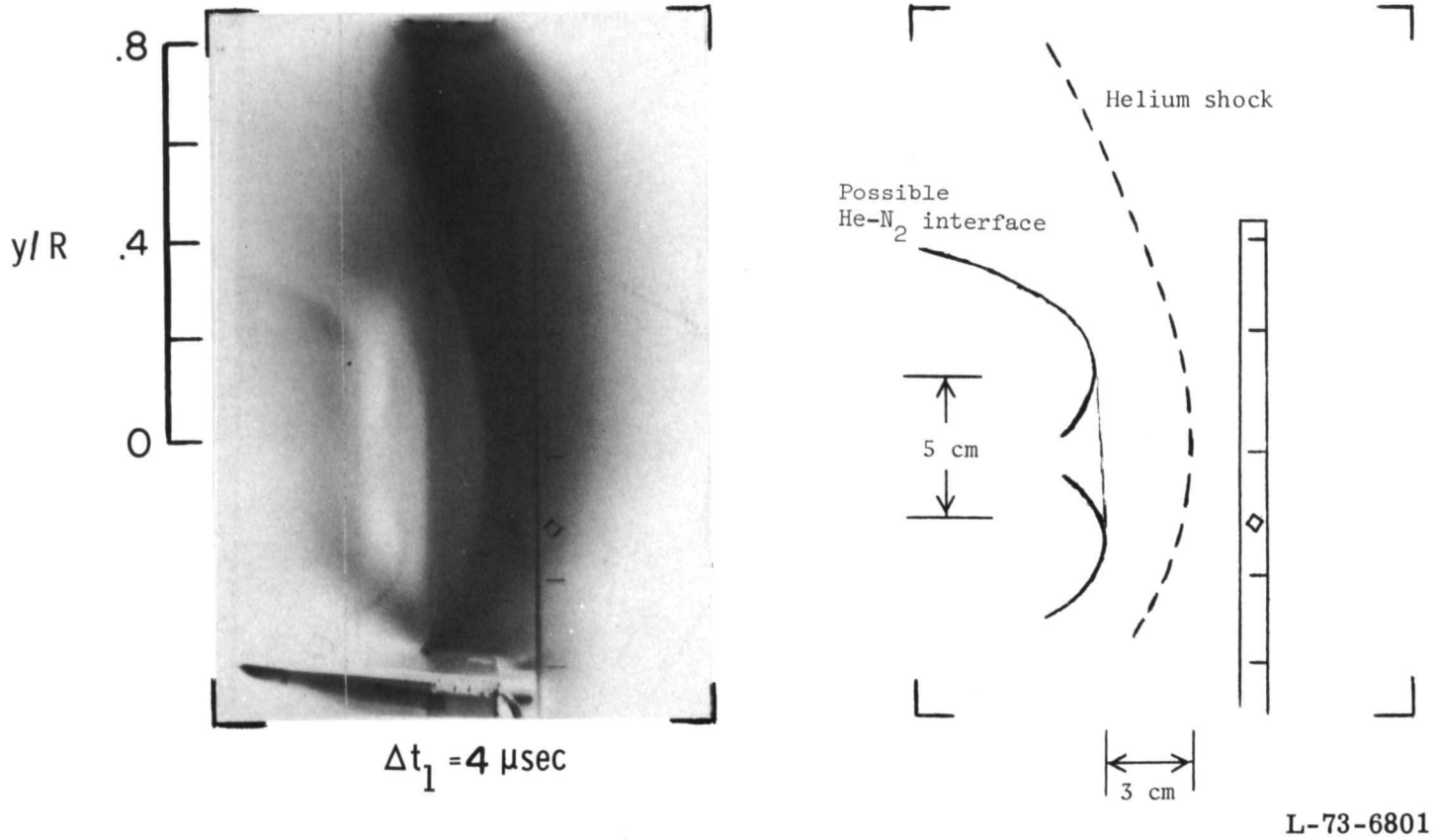

Figure 24.- Shape of emerging helium shock and possible interface. No nozzle diaphragm.

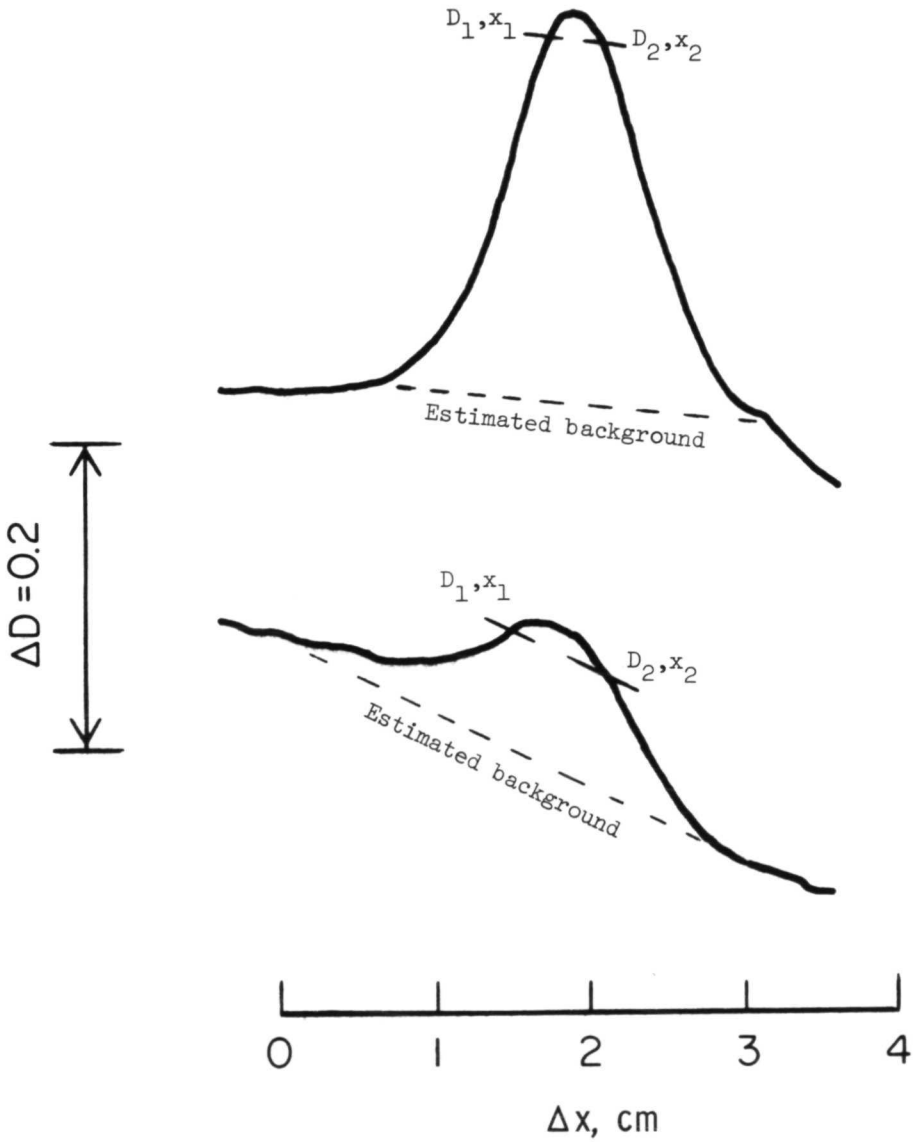

Figure 25.- Sample densitometer scan traces.

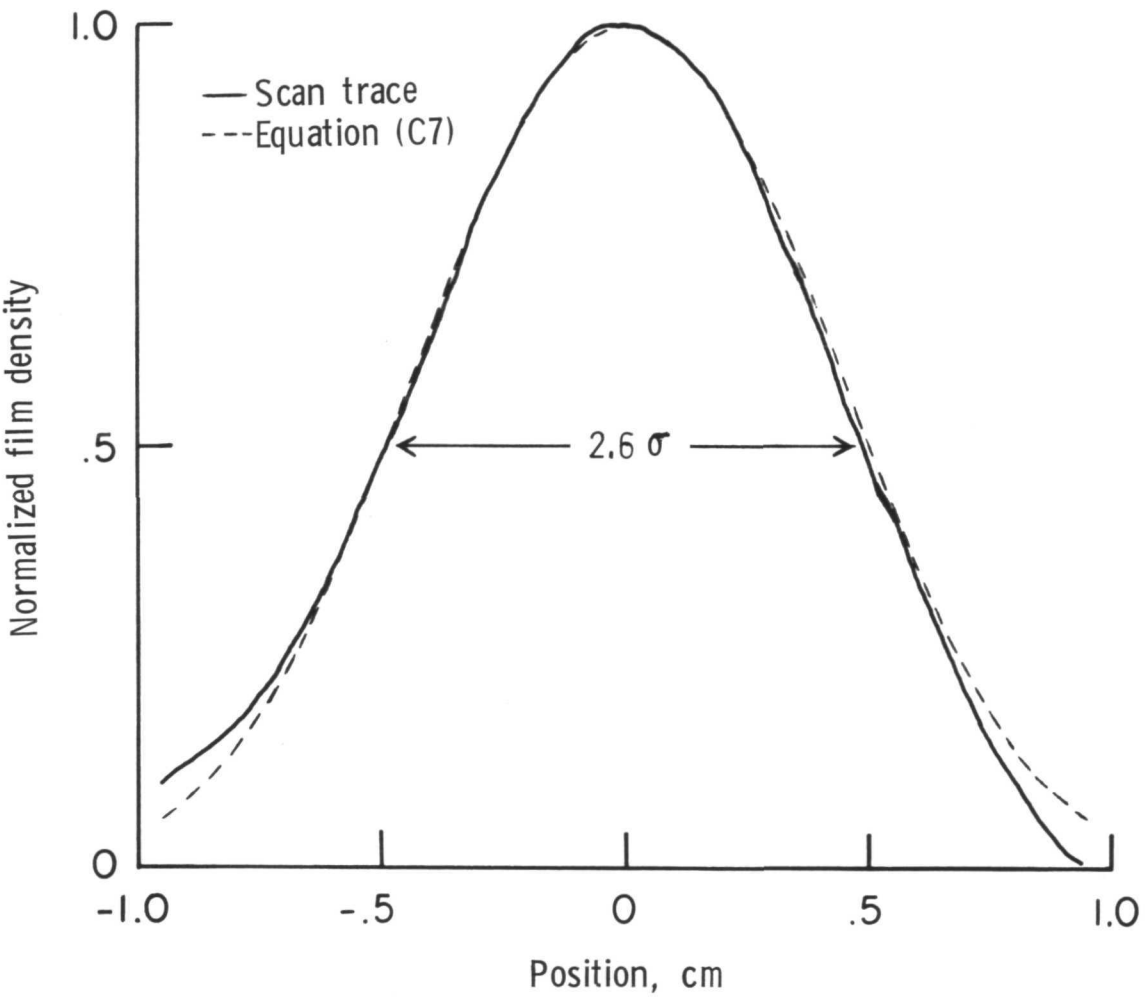

Figure 26.- Comparison of scan trace and curve obtained from equation (C7).

NATIONAL AERONAUTICS AND SPACE ADMINISTRATION
WASHINGTON, D.C. 20546

OFFICIAL BUSINESS
PENALTY FOR PRIVATE USE $300

SPECIAL FOURTH-CLASS RATE
BOOK

POSTAGE AND FEES PAID
NATIONAL AERONAUTICS AND
SPACE ADMINISTRATION
451

U.S.MAIL

POSTMASTER: If Undeliverable (Section 158 Postal Manual) Do Not Return

"The aeronautical and space activities of the United States shall be conducted so as to contribute . . . to the expansion of human knowledge of phenomena in the atmosphere and space. The Administration shall provide for the widest practicable and appropriate dissemination of information concerning its activities and the results thereof."

—NATIONAL AERONAUTICS AND SPACE ACT OF 1958

NASA SCIENTIFIC AND TECHNICAL PUBLICATIONS

TECHNICAL REPORTS: Scientific and technical information considered important, complete, and a lasting contribution to existing knowledge.

TECHNICAL NOTES: Information less broad in scope but nevertheless of importance as a contribution to existing knowledge.

TECHNICAL MEMORANDUMS: Information receiving limited distribution because of preliminary data, security classification, or other reasons. Also includes conference proceedings with either limited or unlimited distribution.

CONTRACTOR REPORTS: Scientific and technical information generated under a NASA contract or grant and considered an important contribution to existing knowledge.

TECHNICAL TRANSLATIONS: Information published in a foreign language considered to merit NASA distribution in English.

SPECIAL PUBLICATIONS: Information derived from or of value to NASA activities. Publications include final reports of major projects, monographs, data compilations, handbooks, sourcebooks, and special bibliographies.

TECHNOLOGY UTILIZATION PUBLICATIONS: Information on technology used by NASA that may be of particular interest in commercial and other non-aerospace applications. Publications include Tech Briefs, Technology Utilization Reports and Technology Surveys.

Details on the availability of these publications may be obtained from:

SCIENTIFIC AND TECHNICAL INFORMATION OFFICE

NATIONAL AERONAUTICS AND SPACE ADMINISTRATION

Washington, D.C. 20546